



8th South African Conference on Photonic Materials

6 - 10 May 2019

**Kariega Game Reserve
South Africa**



Programme and Abstracts

Tamashi

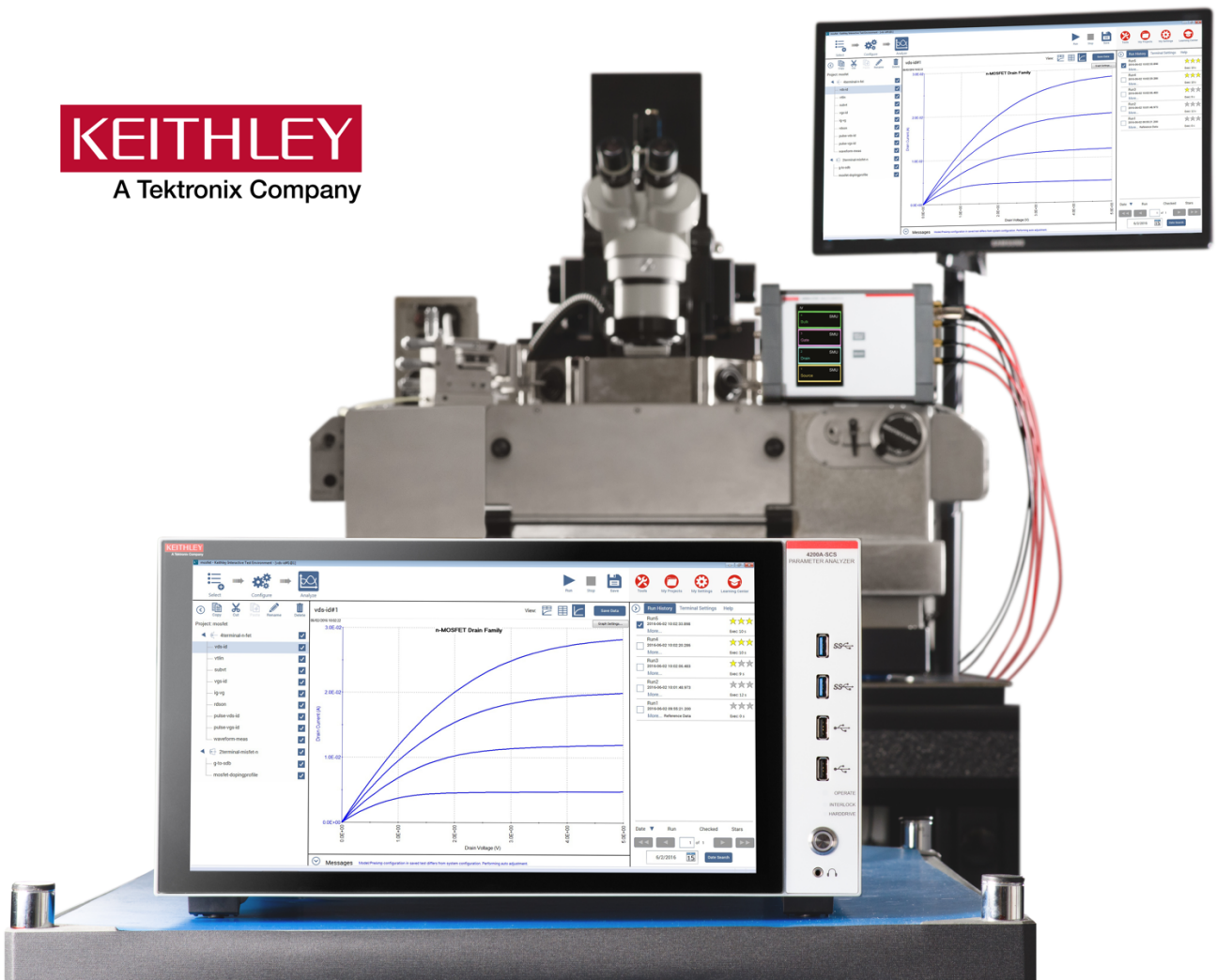
TECHNOLOGY INVESTMENTS (PTY) LTD.

'Fighting Spirit'

Keithley 4200A Parameter analyser

- Mosfet, BJT Transistors
- Non-Volatile Memory Devices
- NBTI/PBTI
- Failure Analysis
- Diodes & PN Junctions
- Sensors
- Electrochemistry
- LED & OLED
- Materials Characterization
- Resistivity & Hall Effect Measurements
- III-V Devices
- Nanoscale Devices
- Solar Cells
- MEMS Devices

KEITHLEY
A Tektronix Company



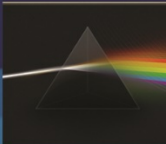

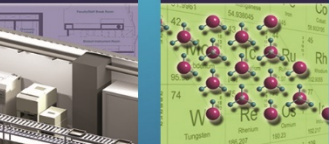
Tel: +27 11 668-1939/1938
Email: sales@tamashi.co.za

Table of Contents

Organising Committee.....	ii
List of Sponsors.....	ii
Message from SAIP President.....	iii
Message from the Dean of the Faculty of Science at Nelson Mandela University.....	iv
Invited Speakers.....	v
Marco Bettinelli.....	v
Vanya Darakchieva.....	vi
Vladimir Dyakonov.....	vii
Chris van de Walle.....	viii
Lasse Vines.....	ix
Olga Shenderova.....	x
Otwin Breitenstein.....	xi
Wieslaw Strek.....	xii
Oscar L. Malta.....	xiii
Programme Overview.....	xv
Scientific Programme and Abstracts.....	1
Tuesday 7 May.....	1
Wednesday 8 May.....	17
Thursday 9 May.....	32
Posters.....	47

wirsam SCIENTIFIC

Since 1968 Leaders in Technology & Support

<p>Analytical</p> 	<p>Microscopy</p> 	<p>Material Testing</p> 	<p>Petrochemical</p> 
<p>General Laboratory</p> 	<p>Sample Preparation</p> 	<p>Turn Key Solutions</p> 	<p>Analytical X-Ray</p> 

www.wirsam.com

JOHANNESBURG
T : +27 11 482 1060
wirsamjb@wirsam.com

CAPE TOWN
T : +27 21 386 9020
wirsamct@wirsam.com

DURBAN
T : +27 31 709 0199
wirsamdb@wirsam.com

PORT ELIZABETH
T : +27 41 365 2060
wirsampe@wirsam.com

VAAL TRIANGLE
T : +27 16 931 1731
wirsamvt@wirsam.com

Mass spectrometers for vacuum, gas, plasma and surface science



Instruments for Advanced Science

Residual Gas Analysis

- ▶ RGA at UHV/HHV
- ▶ High pressure RGA
- ▶ Molecular beams
- ▶ High mass RGA
- ▶ Temperature programmed desorption
- ▶ Electron/photon stimulated desorption



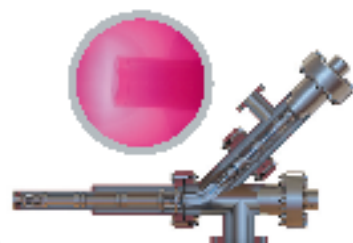
Thin Film Surface Analysis

- ▶ Static and dynamic SIMS
- ▶ Chemical composition & depth profiling
- ▶ SIMS for FB including bolt-on modules & integrated SIMS-on-a-Flange
- ▶ Choice of primary ions
- ▶ Complete SIMS workstations



Plasma Characterisation

- ▶ EQP ion mass and energy analyser
- ▶ RF, DC, ECR and pulsed plasma
- ▶ Neutrals and neutral radicals
- ▶ Time resolved analysis
- ▶ HPR-60 extends analyses to atmospheric pressure processes



www.HidenAnalytical.com

info@hiden.co.uk

Organising Committee

Prof Danie Auret	UP	Additional Member
Prof Reinhart Botha	NMU	Abstracts convenor / Editorial office / Proceedings guest editor
Prof Japie Engelbrecht	NMU	Editorial office / Proceedings guest editor
Dr Richard Harris	UFS	KIC Application
Mr Johan Janse v Rensburg	UP	Editorial office / Proceedings guest editor
Prof Ted Kroon	UFS	Website and Indico / Editorial office / Proceedings guest editor / KIC Application
Prof Walter Meyer	UP	Additional Member
Prof Setumo Motloung	NMU	Sponsors
Prof Jackie Nel	UP	Programme convenor
Prof Martin Ntwaeaborwa	Wits	Additional Member
Prof Hendrik Swart	UFS	Additional Member
Prof Ernest van Dyk	NMU	Conference Co-chair / Finance
Prof André Venter	NMU	Conference Chair
Dr Freddie Vorster	NMU	Venue, Accommodation and Registration, Accompanying persons program
Mrs Chanie Neveling	NMU	Secretary, Venue, Accommodation and Registration

NMU: Nelson Mandela University

UFS: University of the Free State

UP: University of Pretoria

Wits: University of the Witwatersrand

The committee was assisted by the Office of the South African Institute of Physics, particularly Mr Brian Masara (logistics and finances) as well as Mr Tebogo Mokhine (IT Support)

Sponsors

Sponsor: Dean of the Faculty of Science, Nelson Mandela University (NMU)	www.science.mandela.ac.za
Sponsor: Communication & Stakeholder Liaison (NMU)	www.mandela.ac.za
Exhibitor: Tamashi	https://www.tamashi.co.za/
Sponsor: Tektronix	https://www.tek.com/
Sponsor: Hiden Analytical	https://www.hidenanalytical.com/
Sponsor: WIRSAM	https://www.wirsam.com/
Sponsor: Dean of the Faculty of Science and Agriculture, University of the Free State (UFS)	https://www.ufs.ac.za/natagri

Message from the SAIP President

Dear Colleagues,

I am delighted to welcome you to the 8th South African Conference on Photonic Materials (SACPM 2019) hosted by the University of the Free State, the University of Pretoria and Nelson Mandela University, under the auspices of the Division for Condensed Matter Physics and Materials, and the Division of Applied Physics, of the South African Institute of Physics. The organisers have selected a wonderful venue for this conference, the Kariega Game Reserve in the Eastern Cape Province; a unique location that allows the scientific program to be integrated with a social activities that reflect the uniquely South African setting of the conference.

The South African Institute of Physics (SAIP), through its Division for Condensed Matter Physics and Materials, and its Division of Applied Physics, is very proud to be associated with this conference series. Both divisions of the SAIP are very active and regularly organise international conferences on Photonic Materials. SACPM 2019 is the 8th conference in this successful conference series dating back to 2004, when the first meeting of the SACPM was held, also at Kariega Game Reserve. I want to my express my sincere gratitude to the conference chair, Prof Andre Venter, and all the members of the organising committee, for putting together a very exciting program, featuring an excellent mix of South African and international experts in the field of Photonic Materials. I particularly appreciate the call out to senior students (PhD) and emerging researchers (postdocs) to participate in this conference through a reduced registration fee.

A special welcome to the international invited speakers, who travelled from all across the globe (USA, Italy, Sweden, Germany, Poland, Brazil and Norway) to present their latest research highlights in the field of Photonic Materials. I encourage all, especially the students and emerging researchers, to engage in discussions with these world-renowned experts. Thank you for joining our vibrant research community this week, and for sharing your scientific expertise with the students and the emerging researchers.

On behalf of the South African Institute of Physics, it is my distinct pleasure to welcome you to the 8th South African Conference on Photonic Materials. I wish you all a very successful conference and hope that the networking and discussions at this conference - both during the formal program as well as during the social program - will be the start of many long lasting collaborations.

Patrick Woudt
SAIP President

Message from the Dean of the Faculty of Science, Nelson Mandela University

Dear Delegate,

It is indeed a great pleasure and honour for me as the Executive Dean of the Faculty of Science at the Nelson Mandela University, to welcome you all to the 8th biennial South African Conference on Photonics Materials (SACPM 2019). The conference, as you may know, is co-organised by the University of Pretoria, the University of the Free State and the Nelson Mandela University, under the auspices of the Division for Physics of Condensed Matter and the Applied Physics Division of the South African Institute of Physics (SAIP). The location for this conference is unique and I cannot think of a more relaxed and naturally more beautiful location in which to discuss and advance Photonics related matters.

The continued search for better and more efficient way of generating and harnessing light and other forms of radiation will undoubtedly continue to stimulate the development of novel technologies needed to facilitate the demands of the 4th and 5th industrial revolution. Advances in consumer electronics, telecommunications, the health manufacturing industry, defence and security, and entertainment, are but a few examples. It is therefore no surprise then that all around the world, scientists, engineers and technicians eagerly engage in progressive research in Photonics. South Africa is no exception in this regard, as many of our researchers are playing an active leading role in Photonic materials research. A brief overview of the programme for SACPM 2019 suggests an exciting range of oral and poster presentations on very relevant and current issues related to the properties and development of advanced Photonic materials and its applications.

I sincerely hope that you will find the conference academically stimulating, and that the beautiful surroundings and the overwhelming natural beauty of the Eastern Cape, will contribute to the SACPM 2019 Conference being forever engraved in your “fondest memories” folder. A special word of welcome also to all our invited guests and international participants. Thank you for being willing to travel far, even across the globe for some, to share your expertise with us. This is sincerely appreciated. I encourage our students to take this opportunity to interact with our international delegates.

On behalf of the Nelson Mandela University, the Faculty of Science, welcomes you to this momentous event.

Azwinndini Muronga
Executive Dean,
Faculty of Science
Nelson Mandela University

Invited speakers



Marco Bettinelli

Professor of Inorganic Chemistry, Luminescent Materials Laboratory, Department of Biotechnology University of Verona.

Prof Bettinelli's scientific interests deal with numerous aspects of luminescent materials, and in particular with the synthesis, characterization and spectroscopic (luminescence and upconversion) properties of crystalline, nanocrystalline and amorphous systems containing lanthanide and transition metal ions.

Abstract: A further look at $Tb^{3+} \rightarrow Eu^{3+}$ energy transfer processes in luminescent materials

Energy transfer processes in condensed matter have been studied for a long time and a huge number of studies have appeared in the literature. However, they remain today very interesting phenomena, especially when they involve trivalent lanthanide ions. In fact, energy transfer is important for the development of phosphors, scintillators, materials for solar cells, nanothermometers, materials for optical bioimaging and many other light emitting materials. I will present and discuss recent results based on these processes in the case of the $Tb^{3+} \rightarrow Eu^{3+}$ transfer in inorganic hosts. As a matter of fact, very different types of behaviour can be observed in different materials, depending on their structural peculiarities. The $Tb^{3+} \rightarrow Eu^{3+}$ transfer processes have also potential applications in the field of luminescent devices.



Vanya Darakchieva

Professor of Materials, Linköping University, Sweden.

Prof Darakchieva is working on the development of novel semiconductor and nanoscale materials, and spectroscopic metrology for ultra-fast electronics and optoelectronics that will greatly improve computation and communication capabilities.

Abstract: Free Charge Carriers and Phonon-Plasmon Coupling in Ultrawide Bandgap Semiconductors

Ultra-high bandgap semiconductors, such as high-Al content wurtzite AlGa_N and monoclinic β -Ga₂O₃ have gained substantial interest most recently for their potential use in high voltage electronic applications. Correct and accurate characterization of free charge carrier properties in bulk and heteroepitaxial layer structures is a crucial step in successful design of semiconductor heterostructure devices. Long-wavelength (infrared and far infrared) optical spectroscopy, in particular ellipsometry, is a traditional tool to investigate the effect of free charge carriers onto the optical response of semiconductor materials, even if part of complex layer structures. At long wavelengths, specifically in materials with polar lattice resonances, collective free charge carrier excitations, plasmons, couple with the lattice vibration modes.

In this work, a set of n-type single crystals of monoclinic symmetry β -Ga₂O₃ and crack-free high-Al content AlGa_N epitaxial films with different free electron concentration values were investigated by generalized far infrared and infrared spectroscopic ellipsometry. For the case of AlGa_N, coupling of longitudinal optical (LO) phonons with collective plasma oscillations occurs along high-symmetry directions of the lattice. The coupled modes, while changing their frequencies with increasing free charge carrier density maintain the polarization direction of the LO phonons at zero free charge carrier density [1]. In the case of monoclinic β -Ga₂O₃ as predicted by our model [2,3], all modes change amplitude and frequency with the free electron concentration [4]. In excellent agreement with our model prediction, we find that longitudinal-phonon-plasmon coupled modes are polarized either within the monoclinic plane or perpendicular to the monoclinic plane. The most important observation is that all longitudinal-phonon-plasmon coupled modes polarized within the monoclinic plane continuously change their direction as a function of free electron concentration.



Vladimir Dyakonov

Chair of Experimental Physics VI, Julius-Maximilian University of Würzburg, Germany.

Prof Dyakonov holds the Chair of Experimental Physics (Energy research) in the Faculty of Physics and Astronomy of Julius-Maximilian University of Würzburg, Germany since 2004 and he is the Scientific Director of the Bavarian Centre of Applied Energy Research (ZAE Bayern) since 2005. His main research interests are in the fields of thin-film photovoltaics, semiconductor spectroscopy and functional energy materials, in general.

Abstract: Defects in wide gap silicon carbide for quantum applications

Atom-scale colour centres in silicon carbide (SiC) are promising candidates for quantum application at room temperature. [1,2] This spin system has many attributes similar to the NV centres in diamond, e.g. it shows high spin polarization and can be initialized and read out by means of magnetic resonance. On the other hand, spin defects in SiC offer many unique advantages: These are intrinsic lattice defects and since there are many different SiC polytypes, a variety of colour centre types such as silicon vacancies, divacancies, carbon antisite carbon vacancy pairs are identified in this technologically mature wide gap semiconductor and can therefore be considered for different application scenarios. The challenge is to achieve a long electron spin coherence with the natural isotope abundance as well as the controlled generation of quantum centres in SiC in the nanostructures.

Here I will mainly focus on silicon vacancies (VSi). VSi are intrinsic lattice defects with semi-integer spin ($S = 3/2$) [3], which makes them immune to non-axial strains and enables high-precision vector magnetometry and thermometry. [4] We investigate the coherence properties of VSi in a commercial 4H-SiC wafer with natural isotope abundance using the pulsed-ODMR technique. [5] Applying Rabi, Ramsey-, spin-echo- and CPMG pulse sequences, the characteristic times of spin-lattice (T_1) and spin spin-spin (T_2) relaxation in the temperature range from 10 to 300 K and at magnetic field strengths of up to 30 mT were determined. It is remarkable that long spin-spin relaxation times in the millisecond range are achieved by dynamic decoupling of the electron spin system from the nuclear spin baths. In addition, the technologically advanced SiC enabled us to realize single p-n junctions and to demonstrate that the ensemble of VSi defects can be electrically driven, leading to efficient electroluminescence. [6]

Finally, we will discuss the generation of optically active VSi in a controlled manner. Using electron and neutron irradiation it is possible to control the defect density over eight orders of magnitude within an accuracy down to a single defect level. [7] However, in order to position the defects more deterministically and in 3D, we have introduced a simple, maskless method for write VSi centres in SiC nanostructures with focused proton beam. [8]



Chris van de Walle

Professor of Materials, University of California, Santa Barbara, USA.

Prof van de Walle's research interests include first-principles calculations for materials, defects and doping in semiconductors and oxides, surfaces and interfaces, and the physics of hydrogen in materials.

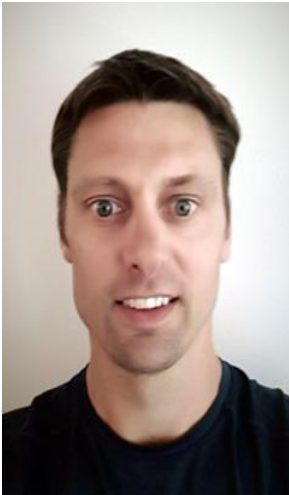
Abstract: First-principles studies of loss mechanisms in light emitters

Nitride semiconductors are the key materials for solid-state lighting; however, their efficiency is still limited, caused by loss mechanisms that are experimentally difficult to probe. I will discuss the theoretical advances that are enabling us to quantitatively evaluate the rate of nonradiative processes such as Auger recombination [1] and defect-assisted carrier recombination

[2]. Our approach allows us to suggest specific strategies for increasing the efficiency of nitride light emitters, and is also transferable to other materials systems.

In this talk, I will focus on point-defect-assisted recombination, often referred to as Shockley-Read-Hall recombination. The recombination centers could be point defects, but unintentional impurities often play an equally important role. For instance, carbon that is unavoidably incorporated during metal-organic chemical vapor deposition can act as a source of yellow luminescence [3], and we have found iron to be a strong nonradiative recombination center in GaN [4]. Theoretical advances now enable us to calculate the energetics as well as electronic and optical properties of point defects with unprecedented accuracy [5]. We have developed a first-principles methodology to determine nonradiative carrier capture coefficients. Accurate calculations of electron-phonon coupling, combined with results for defect formation energies and charge-state transition levels, enable the calculation of nonradiative capture rates for electrons and holes [6] and the evaluation of Shockley-Read-Hall coefficients [2,7]. This approach allows us to identify specific defects that play a key role in limiting the efficiency of nitride semiconductor devices.

Work performed in collaboration with A. Alkauskas, C. Dreyer, A. Janotti, E. Kioupakis, G. Kresse, J. Lyons, J. Shen, J. Speck, J. Varley, D. Wickramaratne, and Q. Yan, and supported by DOE and NSF.



Lasse Vines

Associate Professor at the Department of Semiconductor Physics, University of Oslo, Norway.

Prof Vine has an interest in semiconductor physics and materials physics in bulk, thin films and nanostructures, especially point defects, doping and diffusion in semiconductors. His research interests include thin-film solar cells based on $\text{Cu}_2\text{ZnSn}(\text{S},\text{Se})_4$ and $\text{Cu}_2\text{Zn}(\text{Sn},\text{Ge},\text{Si})\text{S}_4$ and wide bandgap semiconductors and transparent conductive oxides (especially, ZnO, SiC and ITO).

Abstract: Electrically Active Defects in $\beta\text{-Ga}_2\text{O}_3$

The physics of gallium oxide (Ga_2O_3) – an interesting wide bandgap semiconductor – is currently under intensive investigations within a broad research community. This interest is due to the intriguing fundamental properties of Ga_2O_3 , with potential use in a range of other applications, e.g. in power electronics, solar blind photodetectors, scintillators for medical diagnostics, transparent and passivating layers in solar cells, detectors tolerating high radiation/temperature, etc. The most stable phase at ambient conditions, $\beta\text{-Ga}_2\text{O}_3$, has wide band gap of $E_g \sim 4.8$ eV, and a high breakdown field, estimated at ~ 8 MV/cm, which is a major advantage in power electronics. Already, a significant progress has been made with depletion mode and enhancement-mode devices attaining off-state breakdown voltages of over 750 V and 600 V, respectively.

One of the issues slowing down the development of Ga_2O_3 is the lack of fundamental understanding and difficulties in controlling electrically active point defects and defect complexes. Indeed, starting from “simplest” point defects, due to the low symmetry of typically used monoclinic $\beta\text{-Ga}_2\text{O}_3$, there are two different configurations of Ga in the unit cell (tetragonal and octagonal, Ga_T and Ga_O , respectively) and three different environments in the O sub-lattice in $\beta\text{-Ga}_2\text{O}_3$. Such complexity results in equally many different vacancy configurations and sites for extrinsic impurities to reside, provoking a number of electronic states in the bandgap. Further, taking into consideration potential extrinsic impurities and corresponding defect complexes, the result is a plethora of potential localized electronic states.

Here, the present status of understanding electrically active defects in $\beta\text{-Ga}_2\text{O}_3$ will be reviewed, and recent results will be discussed related to the formation and thermal behavior of irradiation induced defects centers. Indeed, deep level transient spectroscopy (DLTS) and steady state phot capacitance spectroscopy (SSPC) show that several electrically active defect levels are present in as grown material, or arise after processing. In particular, recent results combining DLTS with secondary ion mass spectrometry (SIMS) and ion irradiation on a range of different samples will be shown. The results reveal both intrinsic and extrinsic defects present in the samples, and give insight into the nature new and previously reported energy levels. For example, iron is shown to be an important impurity in bulk samples with an energy level position around 0.78 eV below the conduction band edge, acting as a deep compensating center, while irradiation demonstrate the appearance of a nearby intrinsic defect level, and the results are further supported by density functional calculations. Further, a reorganization occur after irradiation at temperatures below 300°C, indicating a high diffusivity among some of the prominent defects.



Olga Shenderova

President of Adámas Nanotechnologies Inc., Raleigh, USA.

Prof Shenderova received her Ph.D. in Materials Science from the St. Petersburg State Technical University, Russia (1991). She did atomistic modeling studies of nanocarbon structures at North Carolina State University (1995-2001) initially as a postdoctoral researcher and then as a Research Assistant Professor. Since 2001 she has worked at International Technology Center, Raleigh, NC on applied research projects in the areas of nanodiamonds. She started Adámas Nanotechnologies Inc. for the commercialization of nanodiamond particles and related technologies. She has given more than 100 invited talks and authored over 190 papers. She has more than 20 patents/patent applications on nanodiamond. She received

the Nerken Award, 2014 for scientific and technological developments of nanodiamond from the American Vacuum Society.

Abstract: Fluorescent Diamond Particles: Synthesis, Properties, and Applications

Diamond particles containing color centers, the crystallographic defects embedded within the diamond lattice, outperform other classes of fluorophores by providing a combination of outstanding photostability, magneto-optical properties and intrinsic biocompatibility. Within the N-related family of optical defects, the nitrogen-vacancy defect (NV) has received the greatest consideration due to numerous applications in both emerging and mature technologies: background-free and long-term cell imaging in the red/near infrared spectral region, super-resolution imaging, correlative and multiphoton microscopy. The spin properties of NV centers in nanodiamonds promise exciting applications in ultrasensitive metrology at the nanoscale detecting changes in magnetic and electric fields, temperature and pressure. A breakthrough recent discovery that ^{13}C polarization can be strongly enhanced in diamond at room temperature based on optical pumping of NV centers advocates nanodiamonds as a new paradigm for optical hyperpolarization in magnetic resonance (MRI) clinical imaging. Recently, our group succeeded in large-scale production of fluorescent diamond particles (FDP) containing NV centers in hundred-gram per batch scales using irradiation with 2-3 MeV electrons. Major factors influencing the efficiency of color centers production in diamond particles as well as compromises between brightness and particles size will be discussed. One limitation in FND production has been the narrow fluorescent color palette while one of the important requirements for fluorescent bioprobes is multicolor emission for multiplexed imaging of few markers in a single study. Our recent achievements in production of multicolor diamonds (from blue to NIR emission) will be reported as well as our efforts toward their adaptation for use in the biological science community will be reviewed.

Acknowledgment: NIH NHLBI SBIR Phase I and Phase II Contract HHSN268201500010C; NIH NCI Phase I SBIR grant R43CA232901.



Otwin Breitenstein

Researcher, Max Planck Institute; Associate Professor, University Halle

As an Associate Professor at Halle University he lectures on the physics of solar cells. He is the author of a book on Lock-in Thermography and has published more than 200 contributions about his research in scientific journals and at international conferences. Since 1999 he is using lock-in thermography for detecting internal shunts in silicon solar cells. Since 2001 he has introduced this technique on a microscopic scale for isolating faults in ICs.

Abstract: The Role of Inhomogeneities for Understanding Current-Voltage Characteristics of Solar Cells

All solar cells show inhomogeneous electronic properties. These inhomogeneities degrade the conversion efficiency of the cells. This holds in particular for multicrystalline (mc) silicon cells, where local differences of the lifetime of more than an order of magnitude exist. This contribution summarizes our research in this field in the last two decades. It explains how these inhomogeneities can be imaged and quantified, and the physical origins and the efficiency degradation potential of J01, J02, and ohmic current inhomogeneities are reviewed. Recent STEM investigations have revealed that the dominant defect-induced recombination in mc material is due to so-called Lomer dislocations, dominating the recombination in small-angle grain boundaries. J02 currents are flowing in positions where extended defects like scratches or the cell edge are crossing the pn-junction. Therefore J02 currents are always highly localized, in contrast to J01 currents. Also the nature of ohmic currents, which are also always localized, is reviewed. Hence, for describing most of the area of silicon solar cells, a one-diode model is sufficient, but J02 and ohmic currents reduce the efficiency in particular at low illumination intensity. Examples for quantitatively estimating the degradation potential of local J01, J02, and ohmic currents are given for two typical solar cells under two illumination intensities. Finally, different pre-breakdown mechanisms are reviewed. Except of the three previously known mechanisms, one new mechanism is described, which is dominant for monocrystalline cells.



Wieslaw Strék

Institute of Low Temperature and Structure Research, Polish Academy of Sciences, Wrocław.

The scope of Prof Strék's research activities encompasses optical properties of rare earth compounds and transition metals, electron relaxation theory (radiative, non-radial transitions, cooperative reactions), laser spectroscopy, optical sensor and biosensors, laser materials, photodynamic therapy, technologies of luminescent materials (nanophosphors), transparent ceramics, porous thermoinsulation materials, nanoceramic materials for fuel cells, cryotherapy.

Abstract: Emission spectra of RE doped nanocrystals under high density excitation

The Stokes and anti-Stokes emission spectra of RE doped nanocrystals were investigated under irradiation with focused beam of CW laser diodes. It was found that apart of f-f transitions there appeared the intense broadband white emission the intense broad band white emission under high density excitation in IR as well as UV range. The intensity of broadband white emission was characterized by excitation density threshold. It increases exponentially with excitation power. It was observed decreasing of f-f transitions with simultaneous increasing white emission. In particular the effect of excitation density and concentration of RE³⁺ ions were investigated. In particular the efficient photocurrent co-occurs with appearance of white emission was investigated. It increased exponentially with excitation power density. The mechanism of white light emission is discussed in terms of intervalence charge transfer (IVCT) within the (RE²⁺,RE³⁺) ion pair. The possibilities of application of white light emission for optoelectronic devices are presented.



Oscar L. Malta

Professor at the Department of Fundamental Chemistry of the Federal University of Pernambuco (UFPE), Brazil.

Over the course of four decades, Prof Malta has made important contributions to the research on lanthanides, both in the fundamental and applied fields. In 2015, Malta received the Ricardo Ferreira Award for Scientific Merit, recently created by the Foundation for Science and Technology of Pernambuco, Facepe. In 2014, he received the Professor Paulo José Duarte Medal from the Brazilian Chemistry Association.

Abstract: Modelling the Luminescence due to 4f – 4f transitions in rare earth based materials: Recent advances

An overview of our recent work on the nature and behavior of the intraconfigurational 4f – 4f transitions in chemical environments of controllable characteristics, as well as on non-radiative energy transfer processes involving trivalent rare earth ions (both ion-to-ion and intramolecular) and their emission quantum yields, is presented. Perspectives and challenges on this fascinating subject is discussed.

Programme Overview

	Monday	Tuesday	Wednesday	Thursday	Friday
	6 May	7 May	8 May	9 May	10 May
					GAME DRIVE (Option 2)
7:00		BREAKFAST	BREAKFAST	BREAKFAST	BREAKFAST
		Chair 1: Hendrik Swart	Chair: Walter Meyer	Chair: Ernest van Dyk	
8:00		<i>Invited Speaker: Marco Bettinelli</i>	<i>Invited Speaker: Chris van de Walle</i>	<i>Invited Speaker Otwin Breitenstein</i>	Checkout & Departure
8:20		J Miranda De Carvalho	A W Barnard	I Kwembur	
8:40		L Erasmus	I G Ivanov	S Werta	
9:00		GB Nair	S M Tunhuma	D Kumi	
9:20		S Motloung	<i>Invited Speaker: Lasse Vines</i>	R Mhlongo	
9:40		R Wiglusz		D Hile	
10:00		TEA	TEA	TEA	
10:20					
		Chair 2: André Venter	Chair: Setumo Motloung	Chair: Martin Ntwaeaborwa	
10:40		<i>Invited Speaker: Vanya Darakchieva</i>	<i>Invited Speaker: Olga Shenderova</i>	<i>Invited Speaker: Wieslaw Strek</i>	
11:00		H Zhang	N Suliali	Z Tshabalala	
11:20		Ul Hassan	P Kuehne	D Oosthuizen	
11:40		Z Urgessa	L Brandt	B Jaffar	
12:00		R Yakimova	M Ntwaeaborwa	CONFERENCE PHOTO	
12:20		M Diale	E Hasabeldaim		
12:40		LUNCH	LUNCH	LUNCH	
13:00					
		Chair: Frederik Vorster	Chair: Japie Engelbrecht	Chair: Ted Kroon	
14:00	Arrival, Registration & Room Allocation	<i>Invited Speaker: Vladimir Dyakonov</i>	D Poelman	<i>Invited Speaker: Oscar L. Malta</i>	
14:20			NAM Saeed		
14:20			J Engelbrecht	J Hölsä	R Verstraete
15:00			J Du	TEA	E Lee
15:20			TEA	TEA POSTER SESSION 2	TEA
15:40					
16:00			GAME DRIVE (Option 1)		
16:20					
16:40					
17:00					
17:30		Sunset	Sunset	Sunset	
18:00	WELCOME DINNER	POSTER SESSION 1 with finger supper	DINNER	CONFERENCE DINNER	
20:30					

Scientific Programme and Abstracts
Tuesday 7 May 2019

07:00		BREAKFAST	
Oral Session 1 – Session Chair: Hendrik Swart			
08:00	Pg 2	Invited Speaker: Marco Bettinelli	A further look on the Tb ³⁺ →Eu ³⁺ energy transfer processes in luminescent materials
08:40	Pg 3	Jose Miranda De Carvalho	Microwave-assisted solid-state synthesis for improved dopant homogeneity and high performance of Sr ₂ MgSi ₂ O ₇ :Eu ²⁺ , Dy ³⁺ persistent phosphors
09:00	Pg 4	Lucas Erasmus	Development of a phosphor material for application in luminescent solar concentrators
09:20	Pg 5	Govind Nair	Improved steady-state photoluminescence derived from the compensation of the charge-imbalance in Ca ₃ Mg ₃ (PO ₄) ₄ :Eu ³⁺ phosphor
09:40	Pg 6	Setumo Motlounq	Effects of varying Tb ³⁺ concentration on the structural and luminescence properties of Mg _{1.5} Al ₂ O _{4.5} :x% Tb ³⁺ (0 ≤ x ≤ 2) nanophosphor prepared by citrate sol-gel technique
10:00	Pg 7	Rafael Wiglusz	Modulation of spectroscopic properties in the yttrium orthophosphates YXO ₄ (where X = P ⁵⁺ , As ⁵⁺ , V ⁵⁺) doped with Eu ³⁺
10:20		TEA	
Oral Session 2 – Session Chair: André Venter			
10:40	Pg 8	Invited Speaker: Vanya Darakchieva	Free charge carriers and phonon-plasmon coupling in ultra-wide-bandgap semiconductors
11:20	Pg 9	Hengfang Zhang	A comprehensive study of AlN nucleation layers grown onto on-axis and 4° off-axis SiC (0001 ⁻) substrates and its influence on GaN growth
11:40	Pg 10	Jawad Ul Hassan	Isotopically enriched V-doped Si on-axis layers of 4H-SiC: Substrates for III-nitrides based HEMT devices
12:00	Pg 11	Zelalem Urgessa	Effects of Hexamethylenetetramine on the optical and structural properties of ZnO Nanorods grown by Chemical Bath Deposition
12:20	Pg 12	Rositsa Yakimova	Raman activity of silver-graphene/SiC system
12:40	Pg 13	Mmantsae Diale	Review of SiC defects
13:00		LUNCH	
Oral Session 3 – Session Chair: Frederik Vorster			
14:00	Pg 14	Invited Speaker: Vladimir Dyakonov	Defects in wide gap silicon carbide for quantum applications
14:40	Pg 15	Japie Engelbrecht	Comments on the refractive index of InSb _x As _{1-x}
15:00	Pg 16	Jiaren Du	Toward near-infrared persistent luminescence of Mn ⁴⁺ activated phosphors
15:20		TEA	
18:00		Poster Session 1	

A further look at $Tb^{3+} \rightarrow Eu^{3+}$ energy transfer processes in luminescent materials

Marco Bettinelli

Luminescent Materials Laboratory, Department of Biotechnology, University of Verona, and INSTM, UDR Verona, Strada Le Grazie 15, 37134 Verona, Italy; email marco.bettinelli@univr.it

Energy transfer processes in condensed matter have been studied for a long time and a huge number of studies have appeared in the literature. However, these phenomena are still very interesting, especially when they involve trivalent lanthanide ions. In fact, energy transfer is important for the development of phosphors, scintillators, materials for solar cells, nanothermometers, materials for optical bioimaging and many other light emitting materials. I will present and discuss recent results based on these processes in the case of the $Tb^{3+} \rightarrow Eu^{3+}$ transfer in inorganic hosts containing large quantities of terbium ions, in particular phosphates, silicates and germanates. As a matter of fact, different types of behaviour are observed in different materials, depending on their structural peculiarities. The $Tb^{3+} \rightarrow Eu^{3+}$ transfer processes have also potential applications in the field of luminescent devices.

Microwave-assisted solid-state synthesis for improved dopant homogeneity and high performance of $\text{Sr}_2\text{MgSi}_2\text{O}_7:\text{Eu}^{2+},\text{Dy}^{3+}$ persistent phosphors

José M. Carvalho^{1,2,*}, David Van der Heggen¹, Lisa I. D. J. Martin¹, Philippe F. Smet¹

¹ Lumilab, Department of Solid-State Sciences, Ghent University, Krijgslaan 281 S1, 9000 Gent, Belgium

² Institute of Physics, University of São Paulo, BR-05508-900, São Paulo-SP, Brazil

*e-mail: jose.mirandacarvalhojunior@ugent.be

1. Introduction

Conventional solid-state (CSS) synthesis is the most common method nowadays to obtain a variety of advanced materials such as persistent and LED phosphors. However, the CSS process suffers from low diffusion of the ions as well as increased temperature gradients in particles during the heating. These drawbacks can lead to potentially inhomogeneous materials, showing deviating optical properties. In order to overcome the diffusion limits in the synthesis and the temperature gradients during the heating, microwave-assisted solid-state (MASS) synthesis is proposed. MASS synthesis is based on dielectric heating, which is a selective heating and depends on the dielectric properties of the materials such as the dielectric constant (ϵ) and the tangent loss (δ). Due to the direct interaction of the solid particles with incident electromagnetic radiation, MASS synthesis is characterized by increased diffusion of ions that travel long distances within the crystals [1]. In this work, we study systematically the dopants' homogeneity and phase purity in the MASS method through cathodoluminescence imaging in a scanning electron microscope (SEM-CL), quantum yield, and photon counting techniques in order to achieve high-quality materials with improved performance. Comparisons for both CSS-obtained and available commercial materials are also presented.

2. Results

The materials obtained by both CSS and MASS methods have a melilite-type tetragonal structure ($P\bar{4}2_1m$) composed of sheets of corner-linked tetrahedra (Si_2O_7 and MgO_4) connected by an interlayer of Sr^{2+} cations. All doped materials have a broad emission band centered at 470 nm when excited by UV-blue light, attributed to $\text{Eu}^{2+} 4f^65d^1 \rightarrow 4f^7$ transitions. Regarding the emission performance, the experimental quantum efficiency of the MASS-obtained material ($\Phi_{\text{MASS}} = 27\%$) is higher when compared to the CSS one ($\Phi_{\text{CSS}} = 17\%$). The SEM-CL analysis indicates that the MASS material has a more homogeneous dopant distribution among different sets of grains as well as better overall compositional purity, leading to increased emission homogeneity at the microscopic level (Figure). However, the reduction of Eu^{3+} to Eu^{2+} seems to be more efficient in the CSS method. After an additional reduction step, the storage capacity [2] of the MASS ($N_\gamma: 4.84 \times 10^{17}$ photons/g) material achieved higher values than the CSS (7.18×10^{14} photons/g) and even the commercial $\text{Sr}_2\text{MgSi}_2\text{O}_7$ phosphor (6.52×10^{16} photons/g).

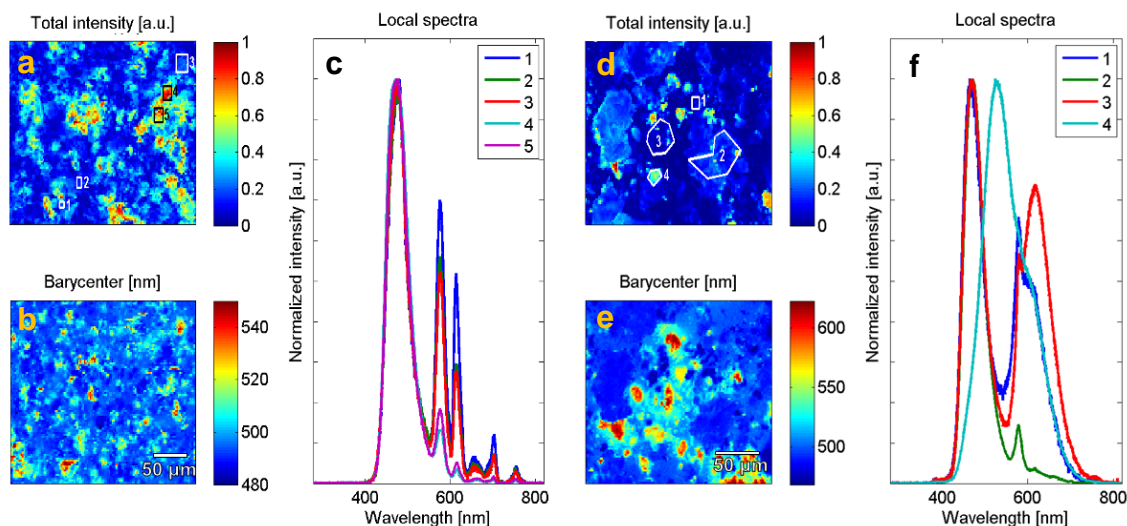


Figure. SEM-CL hyperspectral images of the $\text{Sr}_2\text{MgSi}_2\text{O}_7:\text{Eu}^{2+},\text{Dy}^{3+}$ materials obtained by MASS (a, b) and CSS (d, e) method. The numbers in the images (a, and d) correspond to the area of the local spectra extracted for the MASS (c) and CSS (f) materials.

3. References

[1] A.G. Whittaker, *Chem. Mater.* **17** (2005) 3426–3432.

[2] D. Van der Heggen, J.J. Joos, D.C. Rodríguez Burbano, J.A. Capobianco, P.F. Smet, *Materials* **10** (2017) 1–13.

Development of a phosphor material for application in luminescent solar concentrators

L.J.B. Erasmus^{1,2}, H.C. Swart¹, D. Poelman², J.J. Terblans¹, P.F. Smet²

¹Department of Physics, University of the Free State, Bloemfontein, South Africa

²Department of Solid State Sciences, Ghent University, Ghent, Belgium

Corresponding author e-mail address: erasmuslb@ufs.ac.za

In the field of photovoltaics, a luminescent solar concentrator (LSC) refers to a device that is used as a large area solar radiation collector, which then converts and emits radiation and directs it to solar cells that are located at the small side area of the LSC. However, a transparent luminescent solar concentrator (TLSC) is a new approach for collecting only solar radiation that is invisible to the human eye and utilizing it for energy generation as illustrated in Figure 1. This approach is an attractive solution to address the energy demands of buildings and mobile electronics without affecting their appearance [1]. As illustrated in Figure 1 the basic design of TLSC is a luminescent material that is embedded into a transparent waveguide. A portion of the solar spectrum is absorbed by the luminescent material and this energy is then emitted at a different wavelength. Some of this emitted radiation is then trapped inside the waveguide due to internal reflection and is directed towards the edges of the TLSC where the energy can be converted into electric power by the use of solar cells [1].

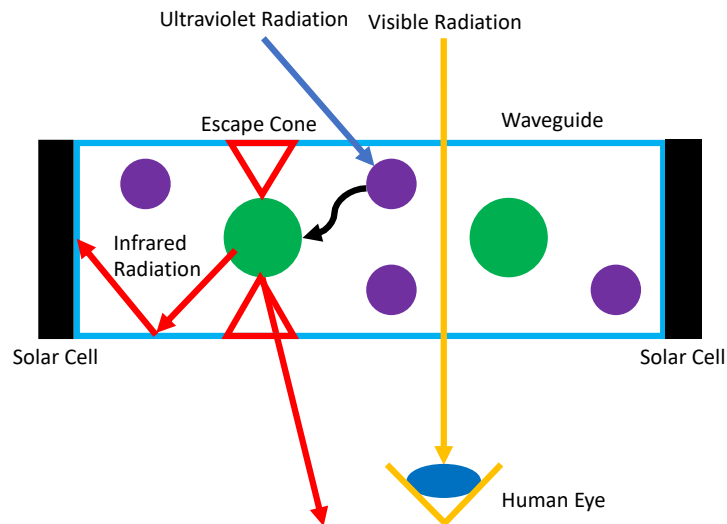


Fig. 1: Schematic explaining the basic principle of a TLSC. Radiation from the visible region passes through the material without being absorbed, while radiation from the ultraviolet region is absorbed by the material. This energy is then transferred, down converted/shifted and emitted in the infrared region. Some of this radiation is guided towards the edges of the material where solar cells are used for energy conversion while some of the radiation is lost through the escape cones.

In order to maximize the overall power conversion efficiency of an TLSC device there are challenges that need to be addressed. These include the reflection from the front of the waveguide, the spectrum absorption efficiency of the luminescent material, the quantum efficiency of the luminescent material, the waveguide's efficiency to trap emitted photons and the ability of the luminescent material to suppress reabsorption [1]. All these parameters must be taken in consideration when choosing a suitable material for a TLSC device. Rare-earth doped phosphor materials are especially of interest for this study because of their relatively narrow emission bands (5-20 nm) and the inorganic hosts, which are more chemically- and photo-stable than their organic counterparts [2]. Another important criterium is that there must be a complete spectral separation between emission and absorption bands of the phosphor material. In this contribution a suitable rare earth doped phosphor material was identified and the results for the synthesis process of this material will be given.

References

- [1] C. Yang and R. R. Lunt, "Limits of Visibly Transparent Luminescent Solar Concentrators," *Adv. Opt. Mater.*, 5(8) (2017) 1600851.
- [2] M. Vasiliev, K. Alameh, M. Badshah, S.-M. Kim, and M. Nur-E-Alam, "Semi-Transparent Energy-Harvesting Solar Concentrator Windows Employing Infrared Transmission-Enhanced Glass and Large-Area Microstructured Diffractive Elements," *Photonics*, 5(3) (2018) 25.

Improved steady-state photoluminescence derived from the compensation of the charge-imbalance in $\text{Ca}_3\text{Mg}_3(\text{PO}_4)_4:\text{Eu}^{3+}$ phosphor

Govind B. Nair¹, Ashwini Kumar¹, H.C. Swart¹, S. J. Dhoble²

¹Department of Physics, University of the Free State, P. O. Box 339, Bloemfontein 9300, South Africa.

²Department of Physics, R.T.M. Nagpur University, Nagpur, India- 440033.

Corresponding author e-mail address: govind1291@yahoo.com

1. Introduction

Phosphate lattices doped with Eu^{3+} ions form one of the most important inorganic luminescent materials due to their ability to exhibit optical properties relevant to several scientific analysis and applications. One of the unique properties of Eu^{3+} ions is that it has a non-degenerate ground state ($^7\text{F}_0$) and the emitting excited state ($^5\text{D}_0$) that do not undergo crystal-field splitting. Subsequently, several biomedical and biochemical applications employ Eu^{3+} -activated hosts as luminescent probes. Doping of trivalent lanthanide ions like Eu^{3+} often lead to charge-imbalance in the host lattice, if they are unable to locate a favourable trivalent site within the host. Unfortunately, a majority of the phosphate lattices provide only a divalent site for accommodating trivalent lanthanide ions [1,2]. Under such a circumstance, the extra charge of the trivalent ion remains uncompensated and it acts as a luminescence quencher within the host by promoting non-radiative transitions. Reports suggest that compensation of this extra charge can improve the luminescence emission effectively. This can be achieved by codoping a suitable monovalent alkali ion or by introducing a divalent ion-vacancy into the host.

This work focuses on the charge-compensation effects produced by different monovalent alkali ions, *viz.* Li^+ , Na^+ , K^+ , and the vacancy defects in the Eu^{3+} -activated $\text{Ca}_3\text{Mg}_3(\text{PO}_4)_4$ host. To compensate the extra charge produced due to doping of Eu^{3+} ions in the Ca^{2+} site, two approaches were adopted. In the first approach, a Ca^{2+} vacancy (\square^+) was deliberately created in such a way that three Ca^{2+} ions were removed for doping of every two Eu^{3+} ions. In the second case, a monovalent alkali ion (Li^+ , Na^+ or K^+) was incorporated along with one Eu^{3+} ion to replace two Ca^{2+} sites in the host. Sol-gel/Pechini method was employed for the synthesis of $\text{Ca}_3\text{Mg}_3(\text{PO}_4)_4:\text{Eu}^{3+},\text{M}$ ($\text{M} = \square^+, \text{Li}^+, \text{Na}^+$ and K^+) phosphor. The photoluminescence properties were compared between the uncompensated and the charge-compensated samples of $\text{Ca}_3\text{Mg}_3(\text{PO}_4)_4:\text{Eu}^{3+}$ phosphor. The luminescence emissions of $\text{Ca}_3\text{Mg}_3(\text{PO}_4)_4:\text{Eu}^{3+}$ phosphor significantly improved with the introduction of charge-compensators. The remarkable enhancement in the emission intensity of the charge-compensated samples was accompanied by noteworthy improvement in the color purity of their emissions.

2. Results

Fig. 1 shows the PL emission spectra, respectively, for the charge-compensated $\text{Ca}_3\text{Mg}_3(\text{PO}_4)_4:0.1\text{Eu}^{3+}, \text{M}$ (where, $\text{M} = \square^+, \text{Li}^+, \text{Na}^+$ and K^+) phosphors and the uncompensated $\text{Ca}_3\text{Mg}_3(\text{PO}_4)_4:0.1\text{Eu}^{3+}$ phosphor. The PL emission intensity enhanced significantly with the introduction of charge-compensators. The photoluminescence emission showed maximum improvement in case of Na^+ doped sample.

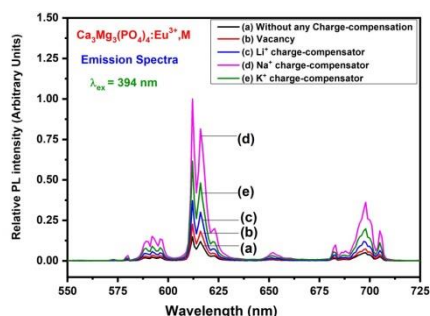


Fig. 1: Photoluminescence emission spectra of uncompensated and charge-compensated $\text{Ca}_3\text{Mg}_3(\text{PO}_4)_4:0.1\text{Eu}^{3+}, \text{M}$ (where, $\text{M} = \square^+, \text{Li}^+, \text{Na}^+$ and K^+) phosphors excited at 394 nm.

3. References

[1] G. B. Nair and S. J. Dhoble. *Luminescence*. **32** (2017) 125.

[2] Y. Peng, W. Shi, C. Han, Y. Kang, Y. Wang and Z. Zhang, *Spectrochim. Acta Part a Mol. Biomol. Spectrosc.* **145** (2015) 194.

Effects of varying Tb^{3+} concentration on the structural and luminescence properties of $Mg_{1.5}Al_2O_{4.5}:x\% Tb^{3+}$ ($0 \leq x \leq 2$) nanophosphor prepared by citrate sol-gel technique

V.M. Maphiri¹, F.B. Dejene², T.D. Malevu³, T.C. Mokhena⁴, S.V. Motloung^{1,5}

¹Department of Physics, Sefako Makgatho Health Sciences University, P.O. Box 94, Medunsa, 0204, South Africa

²Department of Physics, University of the Free State (Qwaqwa Campus), Private Bag X13, Phuthaditjhaba, 9866, South Africa

³School of Chemistry and Physics, University of KwaZulu-Natal (Westville campus), Private bag X54001, Durban 4000, South Africa

⁴Department of Chemistry, Nelson Mandela Metropolitan University (NMMU), P. O. Box 77000, Port Elizabeth 6031, South Africa

⁵Department of Physics, Nelson Mandela Metropolitan University (NMMU), P. O. Box 77000, Port Elizabeth 6031, South Africa
Corresponding author e-mail address: cchataa@gmail.com

1. Introduction

In recent years, alkaline earth aluminates materials have been extensively studied as one of the most important advanced phosphor materials. Magnesium aluminate phosphor ($MgAl_2O_4$) is one of the most promising alkaline earth aluminates with a possible application as blue light emitting [1]. This study presents the effect of varying Tb^{3+} concentration on the structural and luminescence properties of $Mg_{1.5}Al_2O_{4.5}:x\% Tb^{3+}$ ($0 \leq x \leq 2$) nanophosphor prepared by citrate sol-gel technique. The proposed excitation and emission channels are outlined in details. The main aim of this study is to provide an alternative phosphor material for practical application such as in light emitting diodes (LEDs).

2. Results

Highly crystalline $Mg_{1.5}Al_2O_{4.5}:x\% Tb^{3+}$ ($0 \leq x \leq 2$) nano-powders were successfully synthesized via citrate sol-gel method. The X-ray diffraction (XRD) data revealed that $Mg_{1.5}Al_2O_{4.5}:x\% Tb^{3+}$ could be indexed to the single cubic phase of $MgAl_2O_4$. The energy dispersive X-ray spectroscopy (EDS) confirmed the presents of all expected elements (Mg, Al, O and Tb). The scanning electron microscope (SEM) showed that varying the Tb^{3+} concentration insignificantly influences the morphology of the prepared samples. When the samples were excited at 273 nm as shown in Fig. 1, the photoluminescence (PL) results showed that the host has emissions at 384, 401, 550 and 690 nm that are attributed to intrinsic defects within the host material. The Tb^{3+} doped samples showed extra emissions located at 490, 541, 588 and 620 nm which attributed to the Tb^{3+} transition $^5D_4 \rightarrow ^7F_6$, $^5D_4 \rightarrow ^7F_5$, $^5D_4 \rightarrow ^7F_4$ and $^5D_4 \rightarrow ^7F_3$, respectively [2]. The International Commission on Illumination (CIE) colour chromaticity showed a shift from blue to green when varying Tb^{3+} concentration and visa verse when varying the excitation wavelength on $x = 0.8\%$ sample.

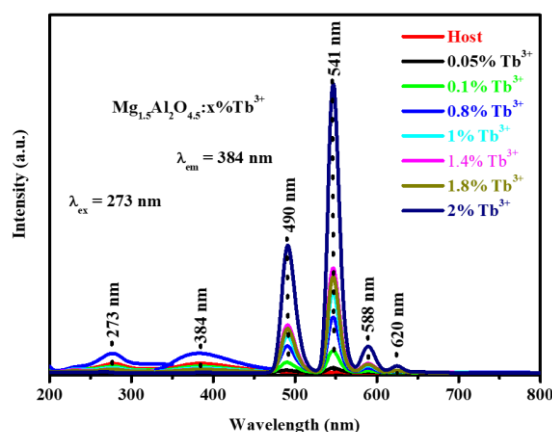


Fig. 2: The excitation and emission spectra of the $Mg_{1.5}Al_2O_{4.5}:x\% Tb^{3+}$ ($0 \leq x \leq 2$) series.

3. References

- [1] S.V. Motloung, F.B. Dejene, E.M. Sithole, L.F. Koao, O.M. Ntwaeaborwa, H.C. Swart, T.E. Motaung and M.J. Hato, *J. Electron. Mater.* **45** (2016) 4796.
- [2] E.A. Raja, B. Dhabekar, S. Menon, S.P. More, T.K.G. Rao and R.K. Kher, *Indian Journal of Pure and Applied Physics* **47** (6) (2009) 420

Modulation of spectroscopic properties in the yttrium orthooxides YXO_4 (where $\text{X} = \text{P}^{5+}, \text{As}^{5+}, \text{V}^{5+}$) doped with Eu^{3+} ions

A. Watras¹, Ph. Boutinaud², M. Bettinelli³, K. Szyszka¹, M. Wujczyk¹ and R.J. Wiglusz^{1,*}

¹Institute of Low Temperature and Structure Research PAS, Okolna 2 str. 50-422 Wroclaw, Poland

²Université Clermont Auvergne, SIGMA Clermont, Institut de Chimie de Clermont-Ferrand, BP 10448, F-63000 Clermont-Ferrand, France

³Luminescent Materials Laboratory, Dept. of Biotechnology, University of Verona, Strada Le Grazie 15, 37134 Verona, Italy

*Corresponding author e-mail address: r.wiglusz@intibs.pl

1. Introduction

From the beginning of phosphor research history, up to the present time, we still do not know how to efficiently search for novel phosphors with superior spectroscopic properties. Development of phosphor with desirable properties reminds more roaming around instead heading straight to the target. This situation takes place because we still do not know how some factors ie: how crystal structure impact on material spectroscopic properties. Nowadays no one could predict with high certainty which material will have high absorption cross-section values or high luminescence quantum efficiency. Systematic studies are needed to receive base information and dependencies between material structure and spectroscopic properties. In this paper we would like to present results of our preliminary studies in this area.

The study of yttrium orthooxides YXO_4 ($\text{X} = \text{P}, \text{As}$ and V) is a subject of increasing interest within the scientific community due to their structural properties and potential applications as host materials for optically active ions [1,2,3]. They crystallize in two different structural types (zircon or monazite) depending on the trivalent metal and the X element. In particular, YPO_4 , YAsO_4 and YVO_4 have an isomorphic crystal zircon structure and belong to the tetragonal space group $I4_1/amd$ with four formula units per unit-cell ($Z = 4$) (see Table 1).

Table 1. Crystallographic data for orthophosphates YXO_4

	YVO_4	YPO_4	YAsO_4
cryst. syst.	zircon tetragonal	zircon tetragonal	zircon tetragonal
space group	$I4_1/amd$ (no.141)	$I4_1/amd$ (no.141)	$I4_1/amd$ (no.141)
a (Å)	7.1183(1)	6.8947(6)	6.9040(1)
c (Å)	6.2893(1)	6.0276(6)	6.2820(1)
α (°)	90	90	90
point-group symmetry	D_{4h}	D_{4h}	D_{4h}
coordination no.	Y(8); V(4); O(3)	Y(8); P(4); O(3)	Y(8); As(4); O(3)

2. Results

The luminescence thermal quenching measurements were performed for all samples. In Fig. 1 the integrated intensity of 2 mol% $\text{Eu}^{3+}:\text{YXO}_4$ is presented in function of ambient temperature. The most interesting is case of 2 mol% $\text{Eu}^{3+}:\text{YVO}_4$ sample, where from 80 to 450 K emission intensity remains stable, while above this temperature it starts do increase very fast achieving its maximum at 725 K and then quickly decrease. Emission intensity at 80 K has only 5% of maximum value at 725 K.

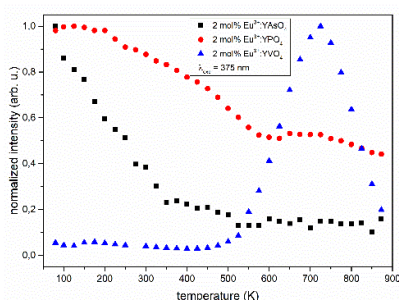


Fig. 3. Representative emission intensity of the $^5\text{D}_0$ level of 2 mol% $\text{Eu}^{3+}:\text{YXO}_4$ sintered at 1000°C and under excitation at 375 nm.

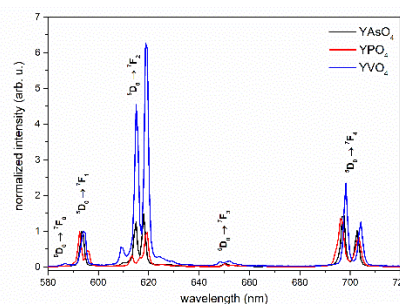


Fig. 2. Representative emission spectra of 2 mol% $\text{Eu}^{3+}:\text{YXO}_4$ sintered at 1000°C and measured at 300 K, under excitation at 395 nm.

3. References

- [1] R. J. Wiglusz, A. Bednarkiewicz, and W. Streck *Inorg. Chem.* **51** (2012) 1180.
- [2] T. Grzyb, R.J. Wiglusz, A. Gruszczyńska and S. Lis, *Dalton Trans.* **43** (2014) 17255.
- [3] A. Strzyp, A. Watras, K.Zawisza, P. Boutinaud, R.J. Wiglusz, *Inorg. Chem.* **56** (2017) 10914.
- [4] R. J. Finch and J. M. Hanchar, *Rev. Mineral. Geochem.* **53** (2003) 1

Free Charge Carriers and Phonon-Plasmon Coupling in Ultrawide Bandgap Semiconductors

Mathias Schubert^{1,2,3}, Alysa Mock^{1,2}, Rafal Korlacki³, Sean Knight³, Stefan Schöche³, Anelia Kakanakova-Georgieva^{1,4}, Ken Goto⁵, Zbigniew Galazka⁶, Vanya Darackchieva^{1,2}

¹Center for III-Nitride Technology, C3NiT-Janžén, Linköping University, 581 83 Linköping, Sweden

²THz Materials Analysis Center (THEMAC), Linköping University, 581 83 Linköping, Sweden

³Department of Electrical and Computer Engineering, University of Nebraska-Lincoln, Lincoln, NE 68588, USA

⁴Department of Physics, Chemistry, and Biology, Linköping University, 581 83 Linköping, Sweden

⁵Novel Crystal Technology, Inc., Saitama-ken 350-1328, Japan

⁶Leibniz-Institut für Kristallzüchtung, Berlin, 12489, Germany

Corresponding author e-mail address: vanya.darackchieva@liu.se

Ultra-high bandgap semiconductors, such as high-Al content wurtzite AlGaN and monoclinic β -Ga₂O₃ have gained substantial interest most recently for their potential use in high voltage electronic applications. Correct and accurate characterization of free charge carrier properties in bulk and heteroepitaxial layer structures is a crucial step in successful design of semiconductor heterostructure devices. Long-wavelength (infrared and far infrared) optical spectroscopy, in particular ellipsometry, is a traditional tool to investigate the effect of free charge carriers onto the optical response of semiconductor materials, even if part of complex layer structures. At long wavelengths, specifically in materials with polar lattice resonances, collective free charge carrier excitations, plasmons, couple with the lattice vibration modes.

In this work, a set of n-type single crystals of monoclinic symmetry β -Ga₂O₃ and crack-free high-Al content AlGaN epitaxial films with different free electron concentration values were investigated by generalized far infrared and infrared spectroscopic ellipsometry. For the case of AlGaN, coupling of longitudinal optical (LO) phonons with collective plasma oscillations occurs along high-symmetry directions of the lattice. The coupled modes, while changing their frequencies with increasing free charge carrier density maintain the polarization direction of the LO phonons at zero free charge carrier density [1]. In the case of monoclinic β -Ga₂O₃ as predicted by our model [2,3], all modes change amplitude and frequency with the free electron concentration [4]. In excellent agreement with our model prediction, we find that longitudinal-phonon-plasmon coupled modes are polarized either within the monoclinic plane or perpendicular to the monoclinic plane. The most important observation is that all longitudinal-phonon-plasmon coupled modes polarized within the monoclinic plane continuously change their direction as a function of free electron concentration.

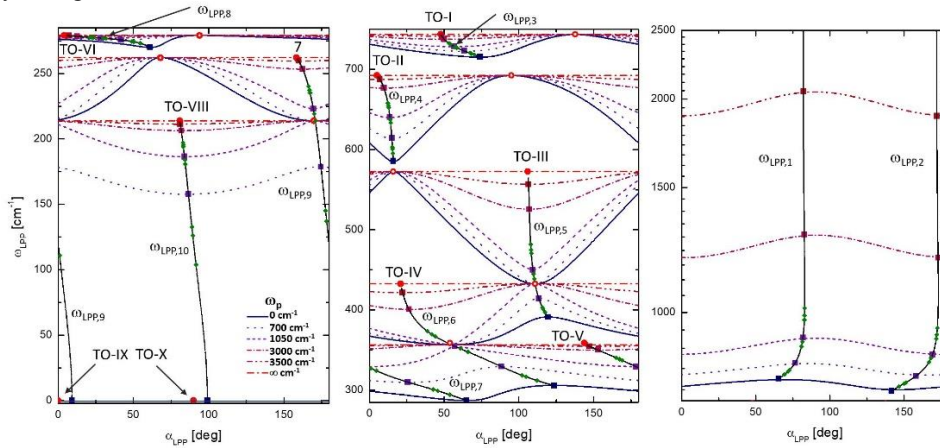


Figure 1. Colored lines with different styles: Bu-symmetry directional limiting frequencies, $\omega(\alpha)_{LPP,i}$, for β -Ga₂O₃ as a function of displacement direction, α , relative to axis a within the monoclinic plane, for selected plasma frequency parameters (see inset for labels). Black solid lines indicate the evolution of LPP modes as a continuous function of ω_p . Square symbols indicate Bu-symmetry LPP modes. Left panel: Modes $\omega(\alpha)_{LPP,8}$ - $\omega(\alpha)_{LPP,10}$, middle panel: modes $\omega(\alpha)_{LPP,3}$ - $\omega(\alpha)_{LPP,7}$, right panel: modes $\omega(\alpha)_{LPP,1}$ and $\omega(\alpha)_{LPP,2}$.

[1] S. Schöche et al., *J. Appl. Phys.* **121**, 205701 (2017).

[2] M. Schubert, et al., *Phys. Rev. B* **93**, 125209 (2016).

[3] M. Schubert, A. Mock, R. Korlacki, and V. Darackchieva, *Phys. Rev. B* **99**, 041201(R) (2019).

[4] M. Schubert, et al., *Appl. Phys. Lett* in press (2019).

A comprehensive study of AlN nucleation layers grown onto on-axis and 4° off-axis SiC (0001 $\bar{1}$) substrates and its influence on GaN growth

Hengfang Zhang,*¹ Ingemar Persson,³ Per Persson,³ Alyssa Mock,¹ Pitsiri Sukkaew,¹ Jr-Tai Chen^{1,2} and Vanya Darakchieva¹

¹Center for III-Nitride technology, C3NiT – Janzén, Linköping University, Linköping SE 581 83, Sweden

²SweGaN AB, Linköping SE 583 30, Sweden

³Thin Film Physics, IFM, Linköping University, Linköping SE 581 83, Sweden

*E-mail: hengfang.zhang@liu.se

1. Introduction

Group-III nitrides have been intensively investigated and widely employed in optoelectronic and electronic devices. Recently, nitrogen(N)-polar group-III nitrides have drawn much attention due to their unique characteristics compared with gallium(Ga)-polar nitrides in the application of high electron mobility transistors (HEMTs), such as the feasibility to fabricate low ohmic contacts, an enhanced carrier confinement with a natural back barrier, as well as high device scalability.

Growth of N-polar group-III nitrides layers are expected on C-face SiC substrates. However, according to previous studies, the initial AlN nucleation step is critical to the polarity control of AlN and GaN layers on SiC substrates. The presence of hexagonal hillocks onto the surface of N-polar GaN epilayers was identified as a common problem for the growth on on-axis substrates. The formation of hexagonal hillocks can be suppressed or eliminated by employing vicinal GaN, sapphire or SiC substrates with different misorientation angles. Much work has been focused on the experimental development of N-polar III-Nitride materials. Despite intense investigations, device-grade high-quality N-polar GaN epitaxial layers remain challenging.

2. Results

In this work, we study in a comparative manner epitaxial GaN layers grown onto on-axis and 4° off-axis SiC (0001 $\bar{1}$) substrates by hot-wall MOCVD. GaN epilayers are grown simultaneously on both substrates employing N-polar AlN nucleation layers (AlN-NLs). We investigate the difference in surface morphology and crystal quality of the GaN epilayers on the two substrates. Growth mechanisms leading to different polarities on the two types of substrates are discussed based on transmission electron microscopy (TEM) findings. ‘V’ shape inversion domain boundaries are observed between N-polar and Al-polar at AlN-NLs at on-axis substrate while metal rich Al-Al bonding layers are observed on off-axis substrates. The nature of AlN-NLs and its interfaces with the substrates and GaN epilayer is discussed. Atomic arrangement at the interface and possible bonding configurations are also analysed. Furthermore, the stain and free charge carriers of GaN layers are investigated by infrared spectroscopic ellipsometry.

Isotopically enriched V-doped SI on-axis layers of 4H-SiC: Substrates for III-nitrides based HEMT devices

Robin Karhu¹, Björn Lundqvist¹, Jr-Tai Chen^{1,2}, Einar Ö. Sveinbjörnsson^{1,3}, Björn Magnusson⁴, Ivan G. Ivanov¹, Örjan Danielsson¹, Olle Kordina^{1,2}, Erik Janzén¹ and Jawad Ul Hassan¹

¹Department of Physics, Chemistry and Biology (IFM), Linköping University, SE-581 83 Linköping, Sweden

²SweGaN AB, Teknikringen 8D, 583 30 Linköping, Sweden

³Science Institute, University of Iceland, IS-107, Reykjavik, Iceland

⁴Norstel AB, Ramshällsvägen 15 SE-602 38 Norrköping, Sweden
Jawad.ul-hassan@liu.se

1. Introduction

With the increasing demand for high-power capabilities, microwave devices are being pushed towards the limits where thermal management of devices becomes more critical. Conventionally, high purity semi-insulating (HPSI) 4H-SiC(0001) on-axis wafers are used as substrates for SiC/III-nitride based high electron mobility transistors (HEMT) structures for microwave applications [1]. Such substrates are quite difficult to grow and are extremely expensive. Also, it has been reported that HEMT devices based on SiC/III-nitride materials system have shown degradation of device characteristics due to an elevated temperature of the device active region [3]. In this study, we demonstrate the possibility to grow wafer-scale V-doped SI thick epilayers on standard low-cost n-type on-axis 4H-SiC(0001) substrates (widely used by the power electronics and LED industries). Such layers can be used as low-cost SI substrates for heteroepitaxial growth of III-nitrides based HEMT devices. We further demonstrate the possibility to grow such layers using isotopically enriched source gasses. Theoretically, it has been shown that isotopically enriched ²⁸Si¹²C can have about 30% higher thermal conductivity compared to natural SiC with a natural abundance of different isotopes of Si and C.

2. Results

For on-axis homoepitaxial growth, one of the major challenges has been to control the spontaneous formation of 3C-SiC inclusions on the Si-face of 4H-SiC substrates. The other issues involve inhomogeneous surface morphology and rough surface. The inhomogeneous surface morphology is mainly related to the lack of the control of the growth mechanism which is mainly dominant by the spiral growth mode around threading screw dislocations (TSDs). In this study, we have also developed on-axis growth process to obtain thick epilayers that are free of 3C polytype inclusions on 100 mm diameter 4H-SiC(0001) substrates. We have further developed the growth process to achieve control over the growth mode. Through the optimization of the growth process and in-situ surface preparation of the substrate, the growth mode was limited to the step-flow growth. This leads to more homogeneous surface morphology and the surface roughness is improved by an order of magnitude. In-situ doping of the epilayers with V was made to achieve SI properties. A room temperature resistivity better than $1 \times 10^9 \Omega\text{-cm}$ is estimated in the epilayers doped with an extremely low concentration of V ($2 \times 10^{16} \text{cm}^{-3}$). The crystalline quality of V-doped SI epilayers is confirmed to be much better than the conventional bulk grown HPSI substrates. For the growth of isotopically enriched epilayers, a new on-axis growth process was developed. A new on-axis growth process based on chlorinated chemistry was developed for the growth of V-doped isotopically enriched layer. The isotopic purity of ²⁸Si and ¹²C in the epilayers, measured by SIMS, is confirmed to be similar to the isotopic purity of the source gasses. Thermal conductivity measurements performed through thermo-reflectance technique show about 17% improvements in the thermal conductivity of the isotopically enriched epilayers compared to the natural layers.

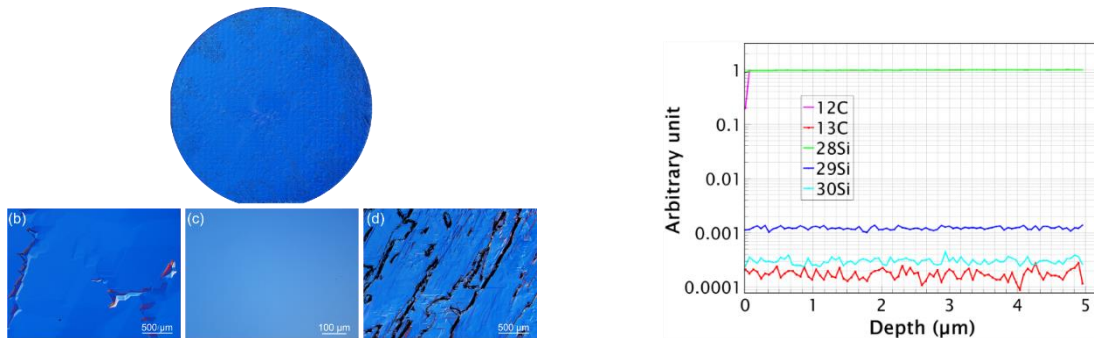


Fig. 1 (Left) optical image of a 100 mm diameter 4H-SiC wafer with 100 μm thick V-doped SI isotopically enriched epilayer, high magnification optical images at the bottom show regions grown through spiral growth, step-flow growth and the edge of the wafer with defects. (Right) SIMS analysis of isotopically enriched epilayer, the purity of ²⁸Si is 99.85 and ¹²C 99.98, similar to the isotopic purity of the source gasses.

Effects of Hexamethylenetetramine on the optical and structural properties of ZnO Nanorods grown by Chemical Bath Deposition

ZN Urgessa, NJ Suliali, JR Botha and A Venter

Department of Physics, Nelson Mandela University, P.O. Box 77000, Port Elizabeth 6031, South Africa
Corresponding author e-mail address: zelalem.urgessa@mandela.ac.za

1. Introduction

Over the last decade, solution based growth of ZnO nanostructure have been considered as a promising building block for a large number of electronic, optoelectronic, and photovoltaic devices [1]. In particular, because of its being cheap, low temperature and ability to produce high optical and crystal quality, the growth of ZnO nanostructures by chemical bath deposition (CBD) is of great potential for their integration into nanoscale devices [1-4]. CBD method of ZnO basically involves hydrothermal reaction of hexamethylenetetramine (HMTA) and zinc salts [3]. The main role of HMTA is accepted to be as a pH buffer and creates a steric interference [1,2]. However, its effect on the optical and structural properties of ZnO nanostructures, are still under debate. This present study gives a deeper insight into the multiple roles of HMTA on the structural and optical properties of ZnO nanorods grown by CBD. In addition, a comparison between HTMA and ammonia for the yield of high quality ZnO nanorods will be presented.

2. Results

Fig.1 (a) shows a low magnification scanning electron (SEM) micrograph of ZnO nanostructures grown by CBD with a [HMTA]/[Zn(NO₃)₂] ratio of : a) 0.25: 1, b) 0.33: 1, c) 0.5: 1 and d) 1:1. The insets are the corresponding higher magnification SEM images. As can be seen from these micrograph, a lower ratio of the HMTA ((a)) results in nanosheets with a thickness around 20 nm, whereas the 1:1 ratio produced nanorods, indicating the ratio clearly control the morphology of the nanostructures. Increasing the molar concentration of HMTA found to affect the aspect ratio of the rods. Preliminary photoluminescence (PL) and x-ray diffraction (XRD) studies revealed that in spite of the differences in morphology, the optical and structural properties of these nanostructures are more or less similar.

Detailed results showing the effect of [HMTA]/[Zn(NO₃)₂] ratio and effect of replacing HTMA with ammonia on the optical and structural properties of the ZnO nanorods will be presented in the paper.

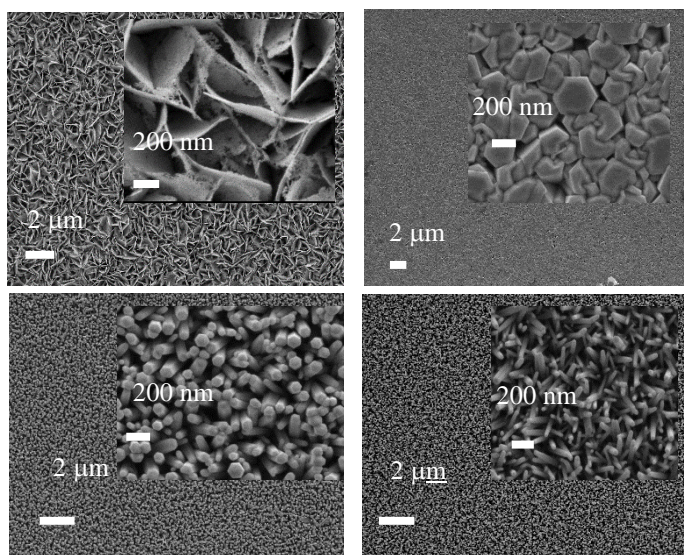


Fig. 1: Top-view low magnification SEM images of ZnO nanorods grown by CBD with a [HMTA]/[Zn(NO₃)₂] ratio of :
a) 0.25: 1,
b) 0.33: 1,
c) 0.5: 1,
d) 1:1.

The insets are the corresponding higher magnification SEM images.

3. References

- [1] R. Parize, J. Garnier, O. Chaix-Pluchery, C. Verrier, E. Appert, and V. Consonni. *J. Phys. Chem. C*, **120** (2016)5242–5250.
- [2] A. Saranya, T. Devasena, H. Sivaram and R. Jayavel, *Materials Science in Semiconductor Processing*, In press.
- [3] L. Vayssieres. *Adv. Mater.*, **15** (2003) 464.
- [4] Fang-I Lai, Jui-Fu Yang, and Shou-Yi Kuo *Materials*, **8** (2015) 8860.

Raman activity of silver-graphene/SiC system

**Rositsa Yakimova¹, Ivan Shteplyuk¹, Tihomir Iakimov¹, Kostas Sarakinos¹,
Bela Pecz², Filippo Giannazzo³, Ivan G. Ivanov¹**

¹ Department of Physics, Chemistry and Biology, Linköping University, SE-58183, Linköping, Sweden

² Institute for Technical Physics and Materials Science, Research Centre for Natural Sciences, Hungarian Academy of Sciences, P.O. Box 49, H-1525, Budapest, Hungary

³ Consiglio Nazionale delle Ricerche, Istituto per la Microelettronica e Microsistemi, Strada VIII, n. 5, Zona Industriale, 95121, Catania, Italy

Corresponding author e-mail address: rositsa.yakimova@liu.se

1. Introduction

Two-dimensional materials (2DMs) are recognized as promising components of next-generation miniaturized devices, and in the future [1], they will become even more important, playing a great role in the development of smart and biocompatible applications in biomedicine, sustainable electronics and environmental sensorics. Nowadays, 2DMs research activities are at the forefront of scientific attainments, promoting the discovery of unusual physical phenomena and offering avenues of novel technical concepts. Special focus is placed on the investigation of graphene as a main star of the 2DMs family [2], which potentially may become a multifunctional platform for on-demand design of different devices. In this regard, an integration of graphene with traditional semiconductors materials and metals may not only complement graphene for advanced technologies, but also may allow to design new hybrid materials with extraordinary performance in catalysis, sensing, optics and electronics. Here we present a representative example of such integration by combining the epitaxial graphene on SiC with silver nano-coatings.

2. Results

We have carried out a comprehensive investigation of the formation of ultra-thin Ag films deposited on epitaxial graphene/SiC by magnetron sputtering technique and their influence on the Raman spectra of graphene. Ag films were grown at room temperature with varying thicknesses from 2 nm to 30 nm. Morphology and structure of the metal nano-deposits were explored by SEM, XRD, C-AFM and HRTEM. In-depth Raman mapping analysis has been applied to reveal the effect of silver on shape, amplitude and position of the main characteristic vibrational modes of graphene (namely *G* and *2D*). A significant enhancement of the Raman signals of graphene is observed after silver deposition and can be explained in terms of electromagnetic mechanism of SERS. Average SERS enhancement factor for *G* mode increased with the increase of the Ag film thickness, reaching the maximum value for the 15 nm film (a factor of 73). By applying optical separation method, we investigate the strain and doping effects in graphene arising from silver decoration. The observed red-shift of *G* peak of graphene is originating from the charge transfer between silver and graphene, pointing to *n*-type doping. The presented hybrid system may find applications in optical sensing and Raman imaging, in which the analysis of molecules and biomaterials is facilitated by the surface enhanced Raman scattering (SERS) effect provided by the plasmonic silver nanoparticles. Furthermore, a formation of atomically thin silver films on graphene surface is a promising approach to reach uniform doping in graphene, which is highly demanded for transistor technologies.

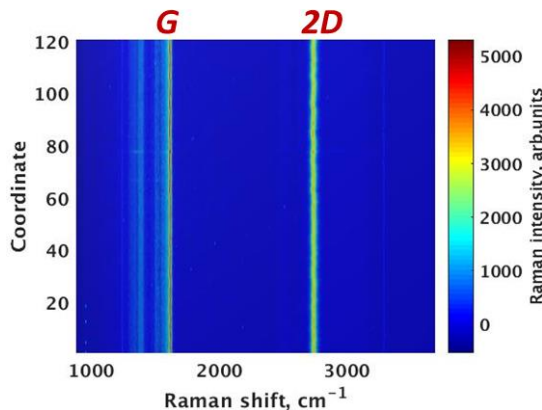


Fig. 4: 2D contour plot of Raman spectra of as-grown epitaxial graphene on 4H-SiC.

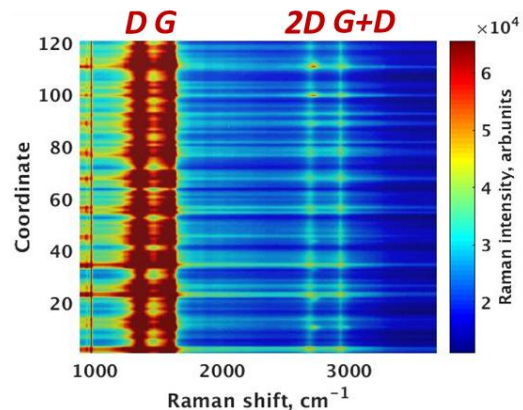


Fig. 2: 2D contour plot of Raman spectra of graphene after deposition of 15 nm Ag film.

3. References

- [1] N. Mounet, M. Gibertini, Philippe Schwaller, Davide Campi, A. Merkys, A. Marrazzo, T. Sohler, I. E. Castelli, A. Cepellott, G. Pizzi and N. Marzari, *Nature Nanotechnology* **13** (2018) 246–252
- [2] K. S. Novoselov, V. I. Fal'ko, L. Colombo, P. R. Gellert, M. G. Schwab & K. Kim, *Nature* **490** (2012) 192–200.

Review of SiC defects

Mmantsae Diale¹, Shandirai M Tunhuma¹ Alexander T Paradzah¹, Ezekiel Omotoso²

¹ University of Pretoria, Department of Physics, Private Bag X20, Hatfield.

² Department of Physics, Obafemi Awolowo University, Ile-Ife, 220005, Nigeria

Corresponding author e-mail address: mmantsae.diale@up.ac.za

1. Introduction

4H-SiC epitaxial layers were irradiated using various radioactive sources and particle accelerators. The electronic properties of induced defects were characterized by means of deep-level transient spectroscopy (DLTS) and Laplace DLTS. This paper is a review of various observations due to processing and various particles used in irradiation of 4H-SiC. From the results it was evident that the same defects were induced by various radiation sources. Irradiation induced the acceptor level of the Z_1 center and the donor level of the Z_2 center. The concentration of the native defects, which originate from impurities encountered in the growth process increased. DLTS spectra observed after irradiation were exhibited sitting on skewed baselines which in some instances inhibited accurate Laplace-DLTS resolution.

2. Results

DLTS spectra of the as-grown 4H-SiC is presented in figure 1, showing the Z_1 and Z_2 at $E_{0.11}$ and $E_{0.66}$. Due to other processes, other induced defects are presented in the figure.

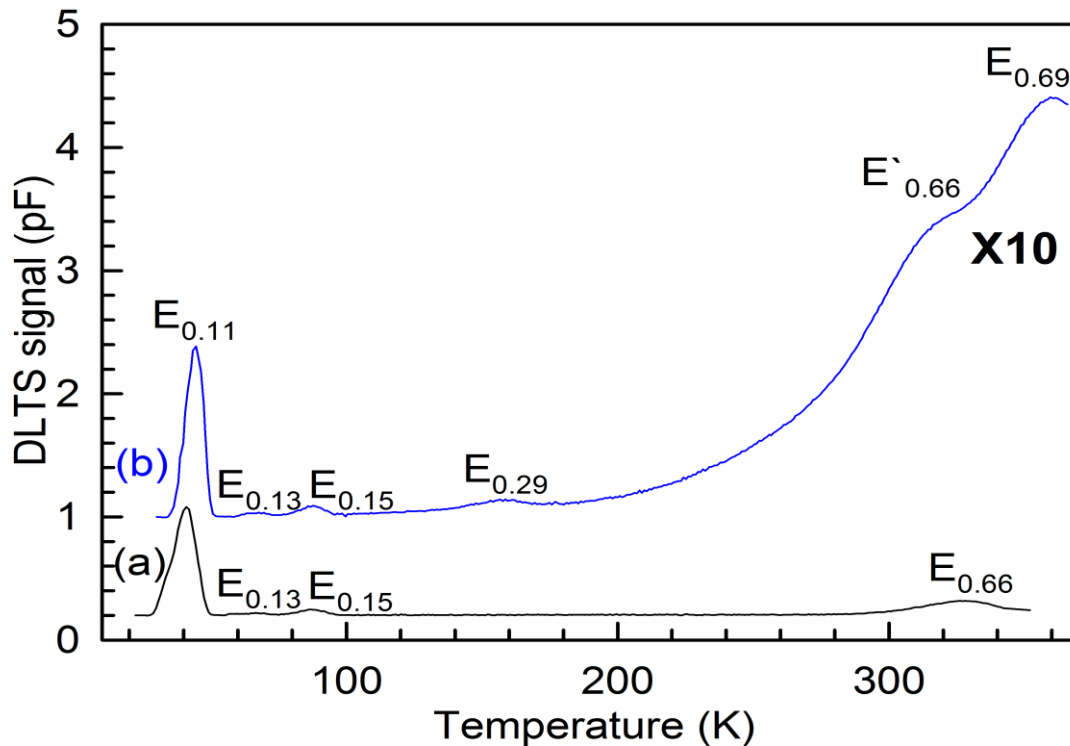


Fig. 5: The DLTS spectra of (a) the control sample obtained from Ni/4H-SiC Schottky barrier diodes fabricated by resistive deposition; (b) W/4H-SiC Schottky barrier diodes fabricated by sputter deposition..

Defects in wide gap silicon carbide for quantum applications

Vladimir Dyakonov¹

¹ *Experimental Physics 6, University of Würzburg, 97074 Würzburg, Germany*
Corresponding author e-mail address: dyakonov@physik.uni-wuerzburg.de

1. Introduction

Atom-scale colour centres in silicon carbide (SiC) are promising candidates for quantum application at room temperature. [1,2] This spin system has many attributes similar to the NV centres in diamond, e.g. it shows high spin polarization and can be initialized and read out by means of magnetic resonance. On the other hand, spin defects in SiC offer many unique advantages: These are intrinsic lattice defects and since there are many different SiC polytypes, a variety of colour centre types such as silicon vacancies, divacancies, carbon antisite carbon vacancy pairs are identified in this technologically mature wide gap semiconductor and can therefore be considered for different application scenarios. The challenge is to achieve a long electron spin coherence with the natural isotope abundance as well as the controlled generation of quantum centres in SiC in the nanostructures.

2. Results

Here I will mainly focus on silicon vacancies (VSi). VSi are intrinsic lattice defects with semi-integer spin ($S = 3/2$) [3], which makes them immune to non-axial strains and enables high-precision vector magnetometry and thermometry. [4] We investigate the coherence properties of VSi in a commercial 4H-SiC wafer with natural isotope abundance using the pulsed-ODMR technique. [5] Applying Rabi-, Ramsey-, spin-echo- and CPMG pulse sequences, the characteristic times of spin-lattice (T_1) and spin spin-spin (T_2) relaxation in the temperature range from 10 to 300 K and at magnetic field strengths of up to 30 mT were determined. It is remarkable that long spin-spin relaxation times in the millisecond range are achieved by dynamic decoupling of the electron spin system from the nuclear spin baths. In addition, the technologically advanced SiC enabled us to realize single p-n junctions and to demonstrate that the ensemble of VSi defects can be electrically driven, leading to efficient electroluminescence. [6]

Finally, we will discuss the generation of optically active VSi in a controlled manner. Using electron and neutron irradiation it is possible to control the defect density over eight orders of magnitude within an accuracy down to a single defect level. [7] However, in order to position the defects more deterministically and in 3D, we have introduced a simple, maskless method for write VSi centres in SiC nanostructures with focused proton beam. [8]

3. References

- [1] W. F. Koehl, B. B. Buckley, F. J. Heremans, G. Calusine, D. D. Awschalom, *Nature* **479** (2011) 84.
- [2] D. Riedel, F. Fuchs, H. Kraus, S. Vöth, A. Sperlich, V. Dyakonov, A. A. Soltamova, P. G. Baranov, V. A. Ilyin, G. V. Astakhov, *Phys. Rev. Lett.* **109** (2012) 226402.
- [3] H. Kraus, V. A. Soltamov, D. Riedel, S. Vöth, F. Fuchs, A. Sperlich, P. G. Baranov, V. Dyakonov, G. V. Astakhov, *Nat. Phys.* **10** (2014) 57.
- [4] H. Kraus, V. A. Soltamov, F. Fuchs, D. Simin, A. Sperlich, P. G. Baranov, G. V. Astakhov, V. Dyakonov, *Sci. Rep.* **4** (2014) 5303.
- [5] D. Simin, H. Kraus, A. Sperlich, T. Ohshima, G. V. Astakhov, V. Dyakonov, *Phys. Rev. B* **95** (2017) 161201R.
- [6] F. Fuchs, V. A. Soltamov, S. Vöth, P. G. Baranov, E. N. Mokhov, G. V. Astakhov, V. Dyakonov, *Sci. Rep.* **3** (2013) 1637.
- [7] F. Fuchs, B. Stender, M. Trupke, D. Simin, J. Pflaum, V. Dyakonov, G. V. Astakhov, *Nat. Commun.* **6** (2015) 7578.
- [8] H. Kraus, D. Simin, C. Kasper, Y. Suda, S. Kawabata, W. Kada, T. Honda, Y. Hijikata, T. Ohshima, V. Dyakonov, G. V. Astakhov, *Nano Lett.* **17** (2017) 2865.

Comments on the refractive index of $\text{InSb}_x\text{As}_{1-x}$

**J.A.A Engelbrecht¹, J.R. Botha², ME Lee¹, J.H. O'Connell, E.G. Minnaar¹, M. van Greunen²
and P. Kühne³**

¹ Centre for HRTEM, Nelson Mandela University, Port Elizabeth, South Africa

² Physics Department, Nelson Mandela University, Port Elizabeth, South Africa

³ Semiconductor Materials, IFM, Linköping University, Linköping, Sweden

Corresponding author e-mail address: Japie.Engelbrecht@nmmu.ac.za

1. Introduction

The binary $\text{InSb}_x\text{As}_{1-x}$ alloy finds application in mid-infrared optoelectronic devices, including lasers [1,2], light emitting diodes [3,4] photodetectors [5,6] and quantum well heterostructures [7]. Consequently, a knowledge of the optical parameters of the alloy, in particular the refractive index n , is a requirement for the design of the optical devices. A literature survey revealed very few references are available for the refractive index of $\text{InSb}_x\text{As}_{1-x}$ [7-9], including a theoretical model based on the Kramers-Kronig dispersion relation for calculating the refractive index [9].

An assessment of the current status of the refractive index of intrinsic $\text{InSb}_x\text{As}_{1-x}$ [9] was made, and compared to refractive indices of InAs and InSb [10] – see example in Fig. 1. This leads to the proposal of an alternative semi-empirical formula to calculate the refractive index of $\text{InSb}_x\text{As}_{1-x}$ as a function of both antimony mole fraction x and the wavelength/wavenumber. The formula was assessed against previously published values of the refractive indices.

2. Results

The results from Seraphin and Bennet [10] for the refractive indices of InSb and InAs were used to extract slopes m and cut-offs c for the assumed linear relations of the refractive index as function of antimony mole fraction x (Fig. 1). Relations were then found for both the slopes and cut-off values as function of wavenumber (or wavelength). These relations were then condensed in the form of a linear relation $y = mx + c$. Refractive index values for InSb and InAs are in good agreement with those from other researchers (Fig. 2). Further proof is that the thickness of an epilayer of $\text{In}_x\text{Sb}_{1-x}\text{As}$ determined using the relevant refractive indices from the proposed model agreed very well with the grown thickness.

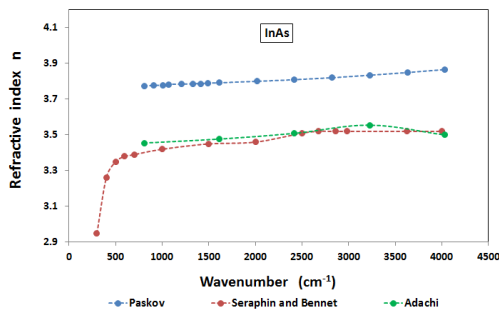


Fig. 6: The refractive index n of InAs from various researchers.

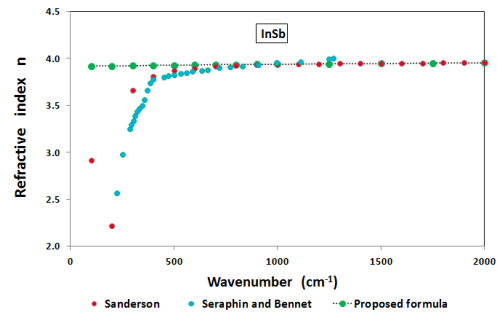


Fig. 2: Comparison of refractive index of InSb from publications and proposed formula

3. References

- [1] H.Q. Le, G.W. Turner, S.J. Eglash, H.K. Choi, and D.A. Coppeta, *Appl. Phys. Lett.* **62** (1984) 152.
- [2] S.R. Kurtz, R.M. Biefield, A.A. Allerman, A.J. Howard, M.H. Crawford and M.W. Pelczynskil, *Appl. Phys. Lett.* **68** (1996) 1332.
- [3] W. Dobbelaere, J. Deboeck, P. Heremans, R. Mertens, G. Borghs, W. Luyten, and J. van Landuyt, *Appl. Phys. Lett.* **60** (1992) 3256.
- [4] SP. J. P. Tang, M. J. Pullin, S. J. Chung, C. C. Phillips, R. A. Stradling, A.G. Norman, Y. B. Li, and L. Hart, *Semicond. Sci. Technol.* **10** (1995) 1177.
- [5] H.H. Wieder and A.R. Clawson, *Thin Solid Films* **15** (1973) 217.
- [6] R. Hasegawa, A. Yoshikawa, T. Morishita, Y. Moriyasu, K. Nagase and N. Kuze, *J. Crystal Growth* **464** (2016) ???
- [7] N.V. Pavlov and G.G. Zegrya, *Journal of Physics: Conference Series* **661** (2015) 012052.
- [8] P.P. Paskov, *Solid State Communications* **82** (1992) 739.
- [9] P.P. Paskov, *J. Appl. Phys.* **81** (1997) 1890.
- [10] B.O. Seraphin and H.E. Bennet in: E.D. Palik (Ed.), *Handbook of Optical Constants of Solids*, vol. 3, Academic Press, NY (1967) p. 499.

Toward near-infrared persistent luminescence of Mn⁴⁺-activated phosphors

Jiaren Du^{1,2}, Olivier Q. De Clercq^{1,2}, Dirk Poelman^{1,2}

¹ LumiLab, Department of Solid State Sciences, Ghent University, Krijgslaan 281-S1, B-9000 Ghent, Belgium;

² Center for Nano- and Biophotonics (NB-Photonics), Ghent University, B-9000 Ghent, Belgium.

Corresponding author e-mail address: Dirk.Poelman@ugent.be;

Several visible-light emitting persistent phosphors have been developed in recent years, and are now widely used as self-sustained night-vision materials ranging from toys, decoration to safety signage and road markings. The growing demand for medical imaging and night-vision surveillance has also led to an interest in exploring deep-red or near-infrared emitting persistent phosphors.[1] Manganese in its 4+ state is considered as a promising alternative for europium or chromium for the design of deep-red or near-infrared emitters.[2,3] To achieve the effective doping of Mn⁴⁺ ions, several classes of hosts (aluminates, germanates, titanates, etc.) with octahedral symmetry are explored (see Figure 1). Strategies such as compositional modification and co-doping are adopted to optimize the optical properties. Temperature dependence of trap filling process and afterglow behavior is discussed in LaAlO₃:Mn⁴⁺ phosphor (Figure 2). Despite the trial-and-error nature of the persistent luminescence research, we are presenting a series of temperature dependent charging, afterglow experiments and thermoluminescence measurements trying to give clear information on the afterglow behavior and shed more light on the nature of the traps.

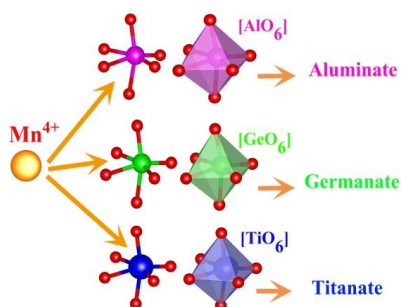


Fig. 7: A schematic of Mn⁴⁺-activated aluminates, germanates and titanates in octahedral symmetry environment.

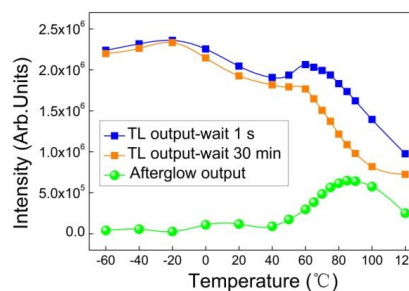


Fig. 2: The temperature dependent integrated afterglow output during 30 minutes of the LaAlO₃:Mn⁴⁺ phosphor, deduced from a series of TL measurements with different fading times.

3. References

- [1] Van den Eeckhout, K., Poelman, D. & Smet, P. F. Persistent luminescence in non-Eu²⁺-doped compounds: a review. *Materials* **6**, 2789-2818 (2013).
- [2] Du, J., De Clercq, O. Q. & Poelman, D. Thermoluminescence and near-infrared persistent luminescence in LaAlO₃:Mn⁴⁺, R (R= Na⁺, Ca²⁺, Sr²⁺, Ba²⁺) ceramics. *Ceram. Int.* **44**, 21613-21620 (2018).
- [3] De Clercq, O. Q., Du, J., Smet, P. F., Joos, J. J. & Poelman, D. Predicting the afterglow duration in persistent phosphors: a validated approach to derive trap depth distributions. *Phys. Chem. Chem. Phys.* **20**, 30455-30465 (2018).

Scientific Programme and Abstracts
Wednesday 8 May 2019

07:00		BREAKFAST	
Oral Session 4 – Session Chair: Walter Meyer			
08:00	Pg 18	Invited Speaker: Chris van de Walle	First-principles studies of loss mechanisms in light emitters
08:40	Pg 19	Abraham Barnard	The effect of Pd vapour deposition on electron-irradiated Si substrates
09:00	Pg 20	Ivan Ivanov	Divacancy in 4H-SiC: Photoluminescence properties and charge-state control
09:20	Pg 21	Shandirai Tunhuma	Visible single defects in electronics grade silicon carbide
09:40	Pg 22	Invited Speaker: Lasse Vines	Electrically active defects in β -Ga ₂ O ₃
10:20		TEA	
Oral Session 5 – Session Chair: Setumo Motloung			
10:40	Pg 23	Invited Speaker: Olga Shenderova	Fluorescent Diamond Particles: Synthesis, Properties, and Applications
11:20	Pg 24	Nyasha Suliali	Control of pore density on TiO ₂ nanostructure films: effect of etchant quantity and anodic voltage
11:40	Pg 25	Philipp Kuehne	Free charge carrier properties in group-III nitride high electron mobility transistor structures determined by optical Hall effect
12:00	Pg 26	Leandré Brandt	Synthesis, Characterizations, and Optical properties of Copper (I) Sulphide Quantum dots
12:20	Pg 27	Martin Ntwaeaborwa	Improved Performance of Quantum Dots Light-emitting Diodes using Modified Energy Structure of Selected Nanoparticles as Electron Transport Layers
12:40	Pg 28	Emad Hasabeldaim	Luminescence properties of Eu ³⁺ doped ZnO spin coating films
13:00		LUNCH	
Oral Session 6 – Session Chair: Japie Engelbrecht			
14:00	Pg 29	Dirk Poelman	Trap levels in persistent phosphors for bio-imaging
14:20	Pg 30	NAM Saeed	Photoluminescence Studies of YOF:Bi Phosphor
14:40	Pg 31	Jorma Hölsä	On the Persistent Luminescence of Ce ³⁺ , Cr ³⁺ , Nd ³⁺ Doped Y ₃ (Al,Ga) ₅ O ₁₂
15:00		TEA	
15:15		POSTER SESSION 2	

First-principles studies of loss mechanisms in light emitters

Chris G. Van de Walle

*Materials Department, University of California, Santa Barbara, CA 93106-5050, USA
vandewalle@mrl.ucsb.edu*

Nitride semiconductors are the key materials for solid-state lighting; however, their efficiency is still limited, caused by loss mechanisms that are experimentally difficult to probe. I will discuss the theoretical advances that are enabling us to quantitatively evaluate the rate of nonradiative processes such as Auger recombination [1] and defect-assisted carrier recombination [2]. Our approach allows us to suggest specific strategies for increasing the efficiency of nitride light emitters, and is also transferable to other materials systems.

In this talk, I will focus on point-defect-assisted recombination, often referred to as Shockley-Read-Hall recombination. The recombination centers could be point defects, but unintentional impurities often play an equally important role. For instance, carbon that is unavoidably incorporated during metal-organic chemical vapor deposition can act as a source of yellow luminescence [3], and we have found iron to be a strong nonradiative recombination center in GaN [4]. Theoretical advances now enable us to calculate the energetics as well as electronic and optical properties of point defects with unprecedented accuracy [5]. We have developed a first-principles methodology to determine nonradiative carrier capture coefficients. Accurate calculations of electron-phonon coupling, combined with results for defect formation energies and charge-state transition levels, enable the calculation of nonradiative capture rates for electrons and holes [6] and the evaluation of Shockley-Read-Hall coefficients [2,7]. This approach allows us to identify specific defects that play a key role in limiting the efficiency of nitride semiconductor devices.

Work performed in collaboration with A. Alkauskas, C. Dreyer, A. Janotti, E. Kioupakis, G. Kresse, J. Lyons, J. Shen, J. Speck, J. Varley, D. Wickramaratne, and Q. Yan, and supported by DOE and NSF.

References

- [1] E. Kioupakis, D. Steiauf, P. Rinke, K. T. Delaney, and C. G. Van de Walle, *Phys. Rev. B*, **92** (2015) 035207.
- [2] C. E. Dreyer, A. Alkauskas, J. L. Lyons, J. S. Speck, and C. G. Van de Walle, *Appl. Phys. Lett.* **108** (2016) 141101.
- [3] J. L. Lyons, A. Janotti, and C. G. Van de Walle, *Phys. Rev. B* **89** (2014) 035204.
- [4] D. Wickramaratne, J.-X. Shen, C. E. Dreyer, M. Engel, M. Marsman, G. Kresse, S. Marcinkevičius, A. Alkauskas, C. G. Van de Walle, *Appl. Phys. Lett.* **109** (2016) 162107.
- [5] C. Freysoldt, B. Grabowski, T. Hickel, J. Neugebauer, G. Kresse, A. Janotti, and C. G. Van de Walle, *Rev. Mod. Phys.* **86** (2014) 253.
- [6] A. Alkauskas, Q. Yan, and C. G. Van de Walle, *Phys. Rev. B* **90** (2014) 075202.
- [7] A. Alkauskas, C. E. Dreyer, J. L. Lyons, and C. G. Van de Walle, *Phys. Rev. B* **93** (2016) 201304(R).

The effect of Pd vapour deposition on electron-irradiated Si substrates

Abraham Barnard¹, Walter Meyer¹, Danie Auret¹, Vladimir Kolkovsky²

¹ Department of physics, University of Pretoria, private bag X20, Hatfield 0028, Pretoria

² Fraunhofer Institute for Photonic Microsystems IPMS, Konrad-Zuse-Str. 1 03046 Cottbus
Abrahamwillembarnard@gmail.com

1. Introduction

Using deep-level transient spectroscopy, it was observed that a different set of unknown deep levels were observed depending on whether a sample was irradiated before or after the fabrication of Schottky contacts. This is counterintuitive to the popular belief that vapour deposition of Schottky diodes would not have an effect on the radiation induced traps within the substrate. This effect was only observed with Pd, while other metals (e.g. gold, platinum) had no observable effect on the irradiation induced complexes in Si. Thermal effects were also ruled out. Through careful experiments, it was possible to correlate the defects observed in the two procedures, giving insight in the physics involved. Since silicon is technologically a very important material, and the manipulation of radiation-induced defects could have many uses, we believe that this, as yet unreported phenomenon, might find significant applications in defect engineering.

2. Method

P-doped Si was irradiated by electron irradiation either before or after deposition of Pd Schottky diodes with a thickness of 400 nm. These procedures will be referred to as pre- and post-irradiation, respectively. In the case of post-irradiation, irradiation was performed through the Schottky diodes, which were thin enough to allow most of the radiation to pass through unimpeded. The experiment was repeated a number of times on samples with different carbon and oxygen concentrations as well as after annealing procedures. By looking for correlations between defects, it was possible to identify which peaks in the pre-irradiated sample corresponded with which in the post-irradiated sample.

2. Results

The first of a series of experiments is shown below in Figure 1. In the post-irradiated samples, DLTS peaks due to the well-known radiation induced complexes (C_i , C_iC_s , $C_iO_i^*$, O_iV , VV^- , $VV^=$ and P_sV) [1-4] were observed (Curves (a - d)), while a different set of DLTS peaks were observed in the pre-irradiated samples (Curves (e - h)). Samples a and e were irradiated at room temperature (297 K) and immediately processed and measured, while samples b and f were left at room temperature for a week after irradiation before processing and measurement, Samples c and g were irradiated at 275 K and Samples d and h were irradiated 303 K. By comparing curves (a) and (b), it is clear that the C_i and $C_iO_i^*$ anneals out when the sample is left at room temperature. When comparing curves (e) and (f), it is clear that the peaks at 55 K and 80 K has this same property. By comparing curves (c) and (g), it is clear that the $C_iO_i^*$ and the peak at 55 K are not present. We therefore conclude that the C_i is transformed to a defect with a peak at 80 K by the deposition of Pd. Similarly, by comparing curves (d) and (h), it follows that the $C_iO_i^*$ is converted to a defect with a DLTS peak at 55 K. By corroborating this evidence with depth profiles and further experiments, we were able to show that the deposition of Pd does in deed transform the well-known radiation-induced defects. We postulate that this could be due to hydrogen passivation of the defects and show that there is some correspondence between the defects observed in this study and those observed in hydrogen passivation studies in other studies.

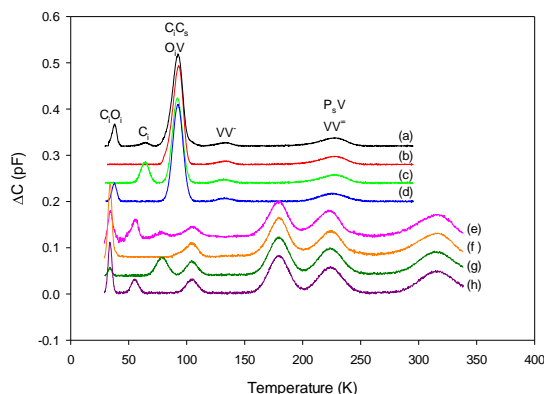


Fig. 8: C-DLTS spectra of the 8 samples (Substrate 1) prepared under different conditions. Samples a, b, c and d, Pd Schottky diodes were fabricated before

3. References

- [1] Makarenko, L., Korshunov, F., Lastovskii, S., Murin, L. and Moll, M. (2009). DLTS Studies of Carbon Related Complexes in Irradiated N- and P-Silicon. *Solid State Phenomena*, 156-158, pp.155-160
- [2] Shinoda, K. and Ohta, E. (1992). Interstitial carbon-oxygen complex in near threshold electron irradiated silicon. *Applied Physics Letters*, 61(22), pp.2691-2693.
- [3] Auret, F., Peaker, A., Markevich, V., Dobaczewski, L. and Gwilliam, R. (2006). High-resolution DLTS of vacancy-donor pairs in P-, As- and Sb-doped silicon. *Physica B: Condensed Matter*, 376-377, pp.73-76.
- [4] Svensson, B., Mohadjeri, B., Hallén, A., Svensson, J. and Corbett, J. (1991). Divacancy acceptor levels in ion-irradiated silicon. *Physical Review B*, 43(3), pp.2292-2298.

Divacancy in 4H-SiC: Photoluminescence properties and charge-state control

Ivan G. Ivanov¹, András Csóré², Björn Magnusson¹, Takeshi Ohshima³, Adam Gali^{2,4}, Nguyen Tien Son¹

¹ Department of Physics, Chemistry & Biology, Linköping University, 581 83 Linköping, Sweden

² Department of Atomic Physics, Budapest University of Technology and Economics, Budafoki út 8, H-1111 Budapest, Hungary

³ National Institutes for Quantum and Radiological Science Technology, 1233 Watanuki, Takasaki, Gunma 370-1292, Japan

⁴ Wigner Research Centre for Physics, Hungarian Academy of Sciences, PO. Box 49, H-1525, Hungary

Corresponding author e-mail address: ivaiv28@liu.se

The divacancy (DV) in 4H-SiC, consisting of nearest-neighbour Si and C vacancies, has been considered recently as one of the prospective defects for quantum bits and/or single-photon sources. Due to the presence of inequivalent sites, the DV possesses four configurations in 4H-SiC giving rise to the PL1 – PL4 no-phonon lines shown in Fig. 1. Recent work [1-3] has studied the quenching of the DV photoluminescence (PL) observable at excitation photon energies below ~ 1.3 eV, and its recovery under higher-energy illumination. The effect of quenching is interpreted in terms of charge-state switching of the defect.

We provide quite exhaustive explanation of the quenching/recovery effect, based on comparison with first-principles theoretical calculations of the energy levels of the DV in different charge states. We show that the quenching is due to conversion of the neutral DV to the negatively-charged one and provide evidence that the charge conversion occurs because of capture of electrons emitted from other defects (traps). A dynamic model built on the idea that the DV captures electrons emitted from other defects (traps) is in excellent agreement with the experimentally observed quenching dynamics. The use of much lower laser power excitation density than in other work enables us to rule out two-photon processes proposed earlier [2,3] as a possible mechanism for charge conversion.

We compare also the results from the PL measurements with results from electron paramagnetic resonance (EPR) conducted on the same samples in illumination conditions similar to those in PL. The comparison allows us to draw some conclusions on the nature of the traps involved in the charge conversion.

We study also the temperature dependence of the quenching/recovery dynamics. In contrast to other work concluding that quenching/recovery is only observed at temperatures below ~ 150 K, we show that the effect can be observed up to room temperature provided that low enough laser energies are used for excitation, as illustrated in Fig. 2. The physics underlying the temperature dependence is discussed in terms of phonon-assisted photoionization of the negatively-charged DV. The notion of phonon-assisted photoionization is confirmed experimentally.

We will discuss briefly also the potential for implementing new concepts in quantum technology based on the observed charge-state conversion. In particular, we shall discuss the realization of an all-optical quantum bit (optical initialization and readout) for information storage, as well as an “on demand” single-photon source which can be prepared in “dark” or “luminescent” state using suitable optical excitation.

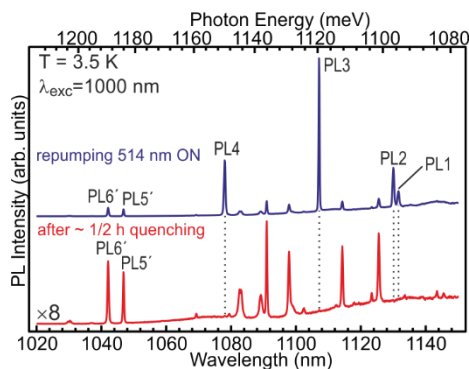


Fig. 9: Illustration of the complete quenching of the divacancy after $\sim 1/2$ hour excitation with laser at 1000 nm (1.24 eV, bottom spectrum). The top spectrum is obtained in non-quenching conditions and shows the zero-phonon PL1 – PL4 lines associated with the DV in the neutral charge state. Note the vertical scale change. The rest of the peaks are due to unknown defects.

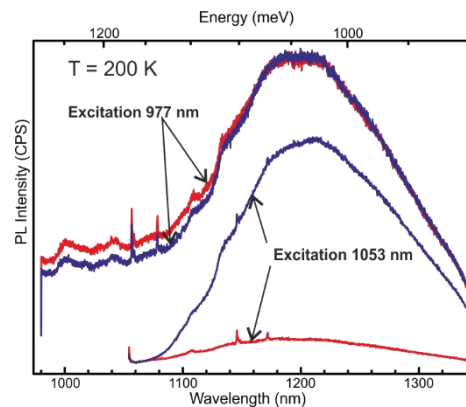


Fig. 2: Illustration of the quenching behavior at 200 K with two different excitations, 977 and 1053 nm (both cause quenching at 2 K). The blue curves are recorded in non-quenching conditions, the red are the “quenched” spectra. No quenching can be seen with 977-nm excitation, whereas it is well pronounced when 1053-nm excitation is used.

References

- [1] B. Magnusson, N.T. Son, A. Csóré, ..., I.G. Ivanov. *Phys. Rev. B* **98** (2018) 195202.
- [2] D. A. Golter and C. W. Lai, *Sci. Rep.* **7** (2017) 13406.
- [3] G. Wolfowicz, C. P. Anderson, et al. *Nat. Commun.* **8** (2017) 1876.

Visible single defects in electronics grade silicon carbide

Shandirai M Tunhuma, Farooq Kyeyune, Tjaart P J Krüger, Mmantsae Diale

¹ Department of Physics, University of Pretoria, Pretoria 0002, South Africa

Corresponding author e-mail address: malven.tunhuma@email.ac.za

The realisation of optically and electrically driven single photon generation in high purity silicon carbide has presented a promising foundation in the fields of quantum metrology, computing and cryptography [1]. Using defect engineering, this technology is set to surpass other similar systems because it is being developed on existing standard industrial fabrication protocols. In addition, SiC has outstanding semiconductor properties which favour device fabrication. In order to implement quantum applications, efficient and high quality single-photon sources are needed. Activation and control of photo-stable and bright sources has already been achieved in SiC through dry oxidation [2]. However, it is still vital to investigate other physical factors contributing to the creation of defects and their properties with the aim of both identifying its atomic origin and using it as a quantum sensor.

The source is composed of an intrinsic defect, known as the carbon antisite–vacancy pair, created by carefully optimized electron irradiation and annealing of ultrapure SiC. Initially the silicon vacancy has been induced but it can be transformed to the carbon antisite–vacancy pair through high temperature annealing [3]. The relative ease with which devices can be formed in SiC using standard industrial fabrication techniques also provides promising avenues for further electrical and optical device development.

In this study, we present the results on inducing the single photon sources in electronics grade wafers which were observed using a confocal microscope connected to a single-photon sensitive avalanche photodiode. Past studies have emphasized that the photon sources can be realised only in high purity semi insulating wafers. We successfully induced clusters and isolated the single defects using standard industrial practices. Our method of inducing these defects does not require expensive equipment like beam writers [4]. On electronic grade wafers, contacts can be deposited in-order to do Laplace-DLTS and identify the “signatures” of the defect. The generation and detection of single photons play a central role in the experimental foundation of quantum mechanics.

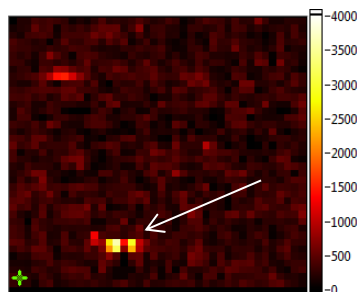


Fig 1. A typical confocal map showing the photoluminescence of single defects in silicon carbide at 3 μ W laser power and 633 nm wavelength excitation.

- [1] S. Castelletto, B.C. Johnson, V. Ivády, N. Stavrias, T. Umeda, A. Gali, T. Ohshima, A silicon carbide room-temperature single-photon source, *Nat Mater*, **13** (2014) 151-156.
- [2] A. Lohrmann, S. Castelletto, J.R. Klein, T. Ohshima, M. Bosi, M. Negri, D.W.M. Lau, B.C. Gibson, S. Praver, J.C. McCallum, B.C. Johnson, Activation and control of visible single defects in 4H-, 6H-, and 3C-SiC by oxidation, *Applied Physics Letters*, **108** (2016) 021107.
- [3] S. Tarasenko, A. Poshakinskiy, D. Simin, V. Soltamov, E. Mokhov, P. Baranov, V. Dyakonov, G. Astakhov, Spin and Optical Properties of Silicon Vacancies in Silicon Carbide– A Review, *physica status solidi (b)*, **255** (2018) 1700258.
- [4] T. Ohshima, T. Satoh, H. Kraus, G.V. Astakhov, V. Dyakonov, P.G. Baranov, Creation of silicon vacancy in silicon carbide by proton beam writing toward quantum sensing applications, *Journal of Physics D: Applied Physics*, **51** (2018) 333002.

Electrically Active Defects in β -Ga₂O₃

Lasse Vines¹, Mads E. Ingebrigtsen¹, Christian Zimmermann¹, Vegard Rønning¹, Andrej Yu. Kuznetsov¹

¹ Department of Physics and Centre for Material science and Nanotechnology,
University of Oslo, Pb 1048 Blindern, 0316 Oslo, Norway
Corresponding author e-mail address: lassevi@fys.uio.no

1. Introduction

The physics of gallium oxide (Ga₂O₃) – an interesting wide bandgap semiconductor – is currently under intensive investigations within a broad research community. This interest is due to the intriguing fundamental properties of Ga₂O₃, with potential use in a range of other applications, e.g. in power electronics, solar blind photodetectors, scintillators for medical diagnostics, transparent and passivating layers in solar cells, detectors tolerating high radiation/temperature, etc. The most stable phase at ambient conditions, β -Ga₂O₃, has wide band gap of $E_g \sim 4.8$ eV, and a high breakdown field, estimated at ~ 8 MV/cm, which is a major advantage in power electronics. Already, a significant progress has been made with depletion mode and enhancement-mode devices attaining off-state breakdown voltages of over 750 V and 600 V, respectively.

One of the issues slowing down the development of Ga₂O₃ is the lack of fundamental understanding and difficulties in controlling electrically active point defects and defect complexes. Indeed, starting from “simplest” point defects, due to the low symmetry of typically used monoclinic β -Ga₂O₃, there are two different configurations of Ga in the unit cell (tetragonal and octagonal, Ga_T and Ga_O, respectively) and three different environments in the O sub-lattice in β -Ga₂O₃. Such complexity results in equally many different vacancy configurations and sites for extrinsic impurities to reside, provoking a number of electronic states in the bandgap. Further, taking into consideration potential extrinsic impurities and corresponding defect complexes, the result is a plethora of potential localized electronic states.

Here, the present status of understanding electrically active defects in β -Ga₂O₃ will be reviewed, and recent results will be discussed related to the formation and thermal behavior of irradiation induced defects centers. Indeed, deep level transient spectroscopy (DLTS) and steady state photocapacitance spectroscopy (SSPC) show that several electrically active defect levels are present in as grown material, or arise after processing. In particular, recent results combining DLTS with secondary ion mass spectrometry (SIMS) and ion irradiation on a range of different samples will be shown. The results reveal both intrinsic and extrinsic defects present in the samples, and give insight into the nature new and previously reported energy levels. For example, iron is shown to be an important impurity in bulk samples with an energy level position around 0.78 eV below the conduction band edge, acting as a deep compensating center, while irradiation demonstrate the appearance of a nearby intrinsic defect level, and the results are further supported by density functional calculations. Further, a reorganization occur after irradiation at temperatures below 300°C, indicating a high diffusivity among some of the prominent defects.

References

- [1] M. H. Wong, K. Sasaki, A. Kuramata, S. Yamakoshi, and M. Higashiwaki, *IEEE Electron Device Lett.* **37**, 212 (2016)
- [2] K. D. Chabak, N. Moser, A. J. Green, D. E. Walker, Jr., S. E. Tetlak, E. Heller, A. Crespo, R. Fitch, J. P. McCandless, K. Leedy, M. Baldini, G. Wagner, Z. Galazka, X. Li, and G. Jessen, *Appl. Phys. Lett.* **109**, 213501 (2016)
- [3] M. E. Ingebrigtsen, J. B. Varley, A. Yu. Kuznetsov, B. G. Svensson, G. Alfieri, A. Mihaila, U. Badstübner, and L. Vines, *Appl. Phys. Lett.*, **112**, 042104 (2018).
- [4] A. Bauknecht, S. Siebentritt, J. Albert and M. C. Lux-Steiner. *J. Appl. Phys.* **89** (2001) 4391.

Fluorescent Diamond Particles: Synthesis, Properties, and Applications

Olga Shenderova

Adamas Nanotechnologies, 8100 Brownleigh Dr., Raleigh, NC 27617

Diamond particles containing color centers, the crystallographic defects embedded within the diamond lattice, outperform other classes of fluorophores by providing a combination of outstanding photostability, magneto-optical properties and intrinsic biocompatibility. Within the N-related family of optical defects, the nitrogen-vacancy defect (NV) has received the greatest consideration due to numerous applications in both emerging and mature technologies: background-free and long-term cell imaging in the red/near infrared spectral region, super-resolution imaging, correlative and multiphoton microscopy. The spin properties of NV centers in nanodiamonds promise exciting applications in ultrasensitive metrology at the nanoscale detecting changes in magnetic and electric fields, temperature and pressure. An exciting recent discovery that ^{13}C polarization can be strongly enhanced in diamond at room temperature based on optical pumping of NV centers advocates nanodiamonds as a new paradigm for optical hyperpolarization in magnetic resonance (MRI) clinical imaging. Recently, our group succeeded in large-scale production of fluorescent diamond particles (FDP) containing NV centers in hundred-gram per batch scales using irradiation with 2-3 MeV electrons. Major factors influencing the efficiency of color centers production in diamond particles as well as compromises between brightness and particles size will be discussed. One limitation in FND production has been the narrow fluorescent color palette while one of the important requirements for fluorescent bioprobes is multicolor emission for multiplexed imaging of few markers in a single study. Our recent achievements in production of multicolor diamonds (from blue to NIR emission) will be reported as well as our efforts toward their adaptation for use in the biological science community will be reviewed.

Acknowledgment: NIH NHLBI SBIR Phase I and Phase II Contract HHSN268201500010C; NIH NCI Phase I SBIR grant R43CA232901.

Control of pore density on TiO₂ nanostructure films: effect of etchant quantity and anodic voltage

Nyasha J. Suliali¹, William E. Goosen² and Johannes R. Botha¹

¹ Department of Physics, Nelson Mandela University, P.O. Box 77000, Port Elizabeth 6031

² Centre for HRTEM, Nelson Mandela University, P.O. Box 77000, Port Elizabeth 6031

Corresponding author e-mail address: S214197786@mandela.ac.za

1. Introduction

The density and diameter of pores in a TiO₂ nanotube array film determine its specific surface area, which is a critical factor in applications such as photo electrochemical water splitting. In this work, we show that while both anodization voltage and etchant quantity determine the TiO₂ nanostructure pore distribution [1], it is the quantity of the etchant that has a greater effect on pore density. Two sets of experiments were carried out, each involving four samples. In one set, titanium foils were anodized for an hour at different anodic voltages in ethylene glycol containing 0.5 wt% of NH₄F. In the next set, the anodic voltage was fixed at 50 V for an hour, while the quantity of NH₄F was varied. The results showed an increase in pore diameter in both experiments. With an increase in anodic voltage, the higher pore diameters resulted in a decrease in nanotube density. However, with an increase in etchant quantity, the development of inter-pore voids that create tubular structures, was much faster, resulting in a remarkable increase in pore density. The study shows that at lower quantities of NH₄F, the pore density can be significantly reduced. Based on these findings a mechanism of preparing Ti foil templates that are suitable for the development of spatially distributed nanotubes by multiple-step-anodization techniques [2] is proposed.

2. Results

Figures 1 and 2 show nano-pores obtained in 0.1 and 0.3 wt% of NH₄F respectively. The nano-pore density increased significantly from 45 pores/μm² in figure 1 to 75 pores/μm² in figure 2. In this work, we show that the nano-pore density is affected more strongly by the etchant quantity than by the anodization voltage.

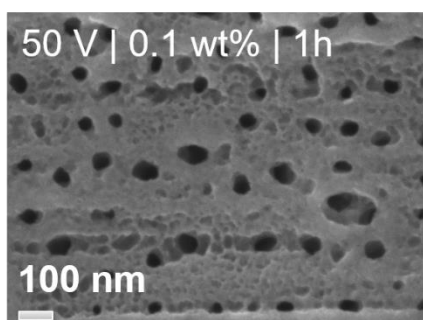


Fig. 1: FESEM micrograph of the sample anodized in 0.1 wt% of NH₄F.

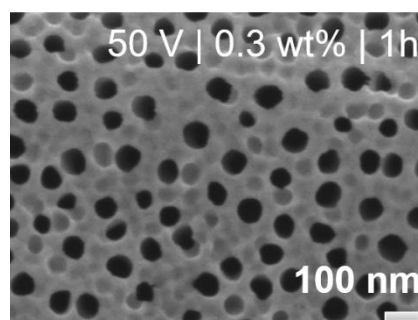


Fig. 2: FESEM micrograph of the sample anodized in 0.3 wt% of NH₄F.

3. References

- [1] D. Regonini, A. Satka, A. Jaroenworarluck, D.W.E. Allsopp, C.R. Bowen and R. Stevens. *Electrochimica Acta* **74** (2012) 244 - 253.
- [2] S. Li, G. Zhang, D. Guo, L. Yu and W. Zhang. *J. Phys. Chem.* **113** (2009) 12759 - 12765.

Free charge carrier properties in group-III nitride high electron mobility transistor structures determined by optical Hall effect

Philipp Kühne^{1,2,3,*}, Nerijus Armakavicius^{1,2,3}, Vallery Stanishev^{1,2,3}, Jr-Tai Chen^{2,3}, Olle Kordina^{2,3}, Mathias Schubert^{1,3,4} and Vanya Darakchieva^{1,2,3}

¹ Terahertz Materials Analysis Center (THeMAC), Department of Physics, Chemistry and Biology (IFM), Linköping University, SE-58183 Linköping, Sweden

² Center for III-Nitride Technology, C3NiT-Janzen, Linköping University, SE-58183 Linköping, Sweden

³ Semiconductor Materials Department of Physics, Chemistry and Biology (IFM), Linköping University, SE-58183 Linköping, Sweden

⁴ Department of Electrical and Computer Engineering, University of Nebraska-Lincoln, Lincoln, Nebraska, 68588-0511, USA

Corresponding author e-mail address: philipp.kuhne@liu.se

The optical Hall effect (OHE) is a physical phenomenon which manifests itself as optical birefringence caused by a static external magnetic field acting on free charge carriers. An excellent tool to quantify the OHE is generalized spectroscopic ellipsometry. Depending on the free charge carrier parameter i.e. carrier concentration, mobility and effective mass, the optimal spectral range to detect the OHE may lay between the mid-infrared to the terahertz (THz). For free charge carriers in 2-D materials or in 2-dimensional electron gases, the OHE is best studied at THz frequencies. Furthermore, for the effective masses in common semiconductors, such as silicon, germanium or group-III nitrides, the cyclotron frequency falls into the THz spectral range for magnetic fields of several tesla.

Here we employed the THz Frequency-Domain Ellipsometer of the Terahertz Materials Analysis Center at Linköping University [1] to determine temperature and magnetic field dependent free charge carrier properties in GaN based high electron mobility structures (HEMTs). The results reveal strong changes in the effective mass and mobility parameters that are assigned to the penetration of the electron wave function into the barrier [2,3]. We study the influence of the barrier material (AlGaIn vs. AlInN) on the electron confinement and analyze the temperature-dependence of the carrier scattering, employing models that include the temperature dependence of the effective mass. In addition, in order to disentangle effects from the magnetic field and the temperature on the effective mass parameter the magnetic field dependence of the OHE is measured and analyzed.

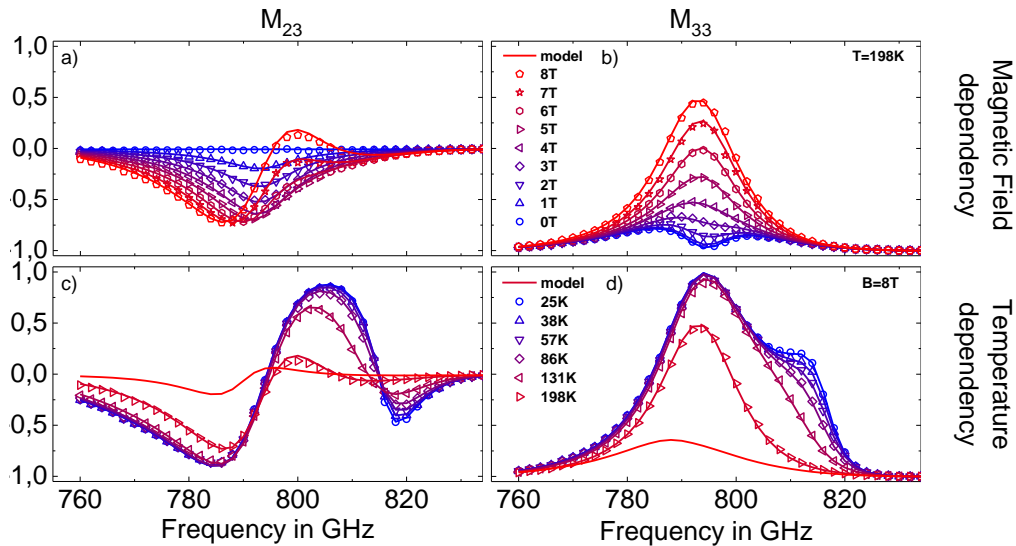


Figure 10: Experimental OHE data (symbols) and best model calculations (lines) from a GaN based HEMT structure. While panels a) and b) depict the magnetic field dependency, show panels c) and d) the temperature dependency of the OHE, each for a representative on-block-diagonal (panel a and c) and off-block-diagonal element (panel b and d) of the Mueller matrix. Best model parameter for the mobility range from 1350Vs/cm² to 30200Vs/cm and a strong temperature dependence of the effective mass is observed and used to analyze the temperature-dependence of the carrier scattering.

References

1. P. Kühne, *et al.*, IEEE Transactions on Terahertz Science and Technology **8**, 257 (2018)
2. N. Armakavicius, *et al.*, phys. stat. sol. C **13**, 369 (2016)
3. T. Hofmann, *et al.*, Appl. Phys. Lett. **101**, 192102 (2012)

Synthesis, Characterizations, and Optical properties of Copper (I) Sulfide Quantum dots

Leandre B. Brandt¹, Martin O. Onani¹, Francis Dejene², Paul Mushonga³,

¹ Department of Chemistry, University of the Western Cape, Private Bag X17, Bellville, 7535, South Africa, Email: monani@uwc.ac.za

² Department of Physics, University of the Free State (QwaQwa Campus), Private Bag X13, Phuthaditjhaba, 9866, South Africa, Email: dejenebf@qwa.ufs.ac.za

³ Department of Chemistry, University of the Zimbabwe, Harare, 00263, Zimbabwe, Email: mushonga777@gmail.com

1. Introduction

Semiconductor nanostructures have been extensively applied in the development of photovoltaic devices, for example in dye sensitized solar cells, [1], and hybrid nanocrystal-polymer composite solar cells [2], and all-inorganic nanoparticle solar cells [3]. The challenge arise Challenges of such developments arise in the aptitude to find a semiconductor nanocrystal with a suitable bandgap, near 1 eV for a conventional, single-gap device having unique characteristics such as being an earth-abundant element and of environmentally benign composition. Due to their high stability, low toxicity and unique properties, copper(I) sulfide(Cu₂S) supersedes these challenging requirements making it a suitable candidate for applications in such devices. Wu and co-workers [4] successfully synthesized hexagonal Cu₂S nanocrystals exhibiting near-infrared emission in a mixed anhydrous solvent of dodecanethiol and oleic acid. These Cu₂S nanocrystals in combination with CdS nanorods demonstrated their application as an active light absorbing component in solution -processed solar cells. Cu₂S is a p-type semiconducting materials with a both an indirect and direct band gap materials, with E_gbulk ≈ 1.2 eV and 1.8 eV, respectively [4]. Although significant promises in thin film studies of Cu₂S/CdS have been reported on, however, to the best of our knowledge, a little detailed information is available on a solvent-less synthesis for stable near-infrared (NIR) emitting Cu₂S QDs with dodecanethiol as capping ligand.

Motivated to improve the structural and optical properties of Cu₂S nanocrystals, we present on the synthesis and characterization of copper sulphide quantum dots and demonstrates their significant potential in photovoltaic devices.

2. Results

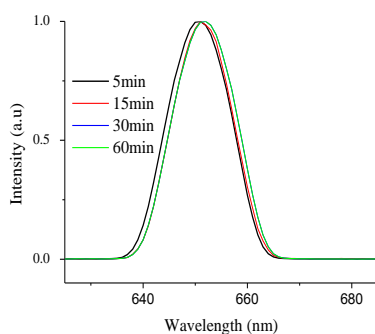


Fig. 11: Population dynamics of the various vibrational levels. (in 8 pt)

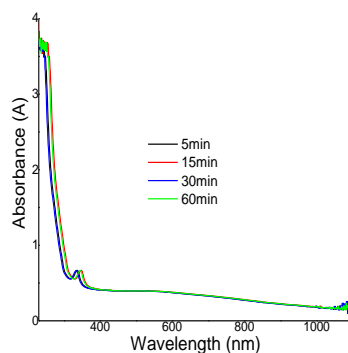


Fig. 2: The best fitness as a function of generation.

3. References

- [1] M. Law, L. E. Greene, J. C. Johnson, R. Saykally, P. D. Yang; *Nat. Mater.*, **4**, (2005), 455.
- [2] I. Gur, N. A. Fromer, C. Chen, A. G. Kanaras, A. P. Alivisatos, *Nano Lett.*, **7** (2007), 409.
- [3] B. Tian, X. Zheng, T. J. Kempa, Y. Fang, N. Yu, G. Yu, J. Huang, C. M. Lieber, *Nature*, **449**, (2007), 885.
- [4] L. Sen, H. Wang, W. Xu, H. Si, X. Tao, S. Lou, Z. Du, L.S. Li, *J. Colloid Interface Sci.*, **330**, (2009), 483.

Improved Performance of Quantum Dots Light-emitting Diodes using Modified Energy Structure of Selected Nanoparticles as Electron Transport Layers

Martin Ntwaeaborwa¹, David Kumi¹, Sohye Cho²

¹ School of Physics, University of the Witwatersrand, Private Bag 3, Wits, Johannesburg, 2050

² Materials Architecturing Research Centre, Korea Institute of Science and Technology, 217 Gajeong-ro Yuseong-gu, Daejeon, 04763, Republic of Korea

Corresponding author e-mail address: ntwaeab@gmail.com

1. Introduction

Zinc oxide (ZnO) nanoparticles have been recognized as a good electron transport layer material in solution-processed quantum dots (QDs) light-emitting diodes (Q-LEDs). The layer has been found to improve stability and efficiency of the Q-LED devices. However, due to the high work function of ZnO, charge transfer occurs at the QD/ZnO interface resulting in reduced performance of such LED devices [1]. To weaken charge transfer at the interface, we prepared magnesium(Mg)/gallium (Ga) doped ZnO nanoparticles with low work function and tailored the band structures. We fabricated LED devices on ITO coated glass consisting of poly(3,4-ethylenedioxythiophene)polystyrene sulfonate or PEDOT PSS hole injection layer (HIL), poly[(9,9-dioctylfluorenyl-2,7-diyl)-co-(4,4-(4-sec-butylphenyl)diphenylamine)] or TFB hole transport layer (HTL), CdSe quantum dots emission layer (QD EML) MgZnO/GaZnO electron transport layer (ETL) and aluminium (Al) top electrode acting as cathode. We observed remarkable improved in luminances and efficiencies of our layered Q-LED devices with Mg/Ga doped ZnO nanoparticles. This improvement is ascribed to reduced electron injection barrier between the ETL and the QD EML that is enabled by the upshift of their conduction band minimum levels [2].

2. Results

Fig. 1 shows the layered structure of Q-LED with MgZnO ETL, while Fig 2 shows the electroluminescence (EL) spectra measured from the Q-LED device with MgZnO ETL inserted between the QD EML and the top Al electrode. The spectra were measured at different voltages and the highest EL intensity and luminance of 334.7 Cd/m² were obtained at a voltage of 4.0 V. The inset of Fig 2 is the EL spectrum of the Q-LED device with ZnO ETL measured at 4.0 V with luminance of 241.1 Cd/m². The difference in the luminance of ZnO versus MgZnO ETLs and the improvement in efficiency of the Q-LED devices will be discussed.

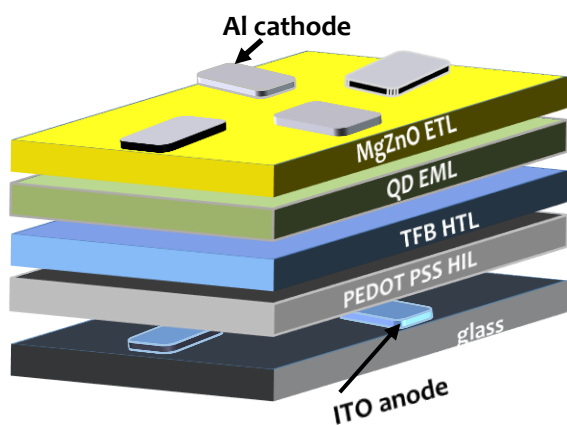


Fig. 12: Layered structure of Q-LED with MgZnO electron transport layer

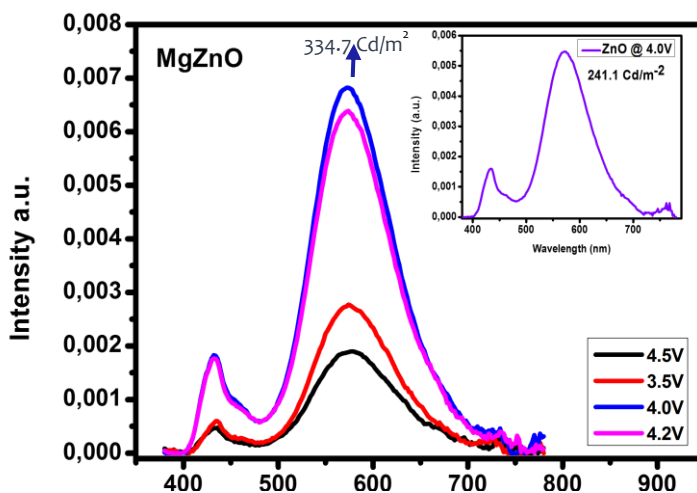


Fig. 2: EL spectra of Q-LED with MgZnO electron transport layer. The inset shows the EL spectrum of Q-LED with ZnO.

3. References

- [1] S. Cao, J. Zheng, J. Zhao, Z Yang, C. Li, X. Guan, W. Yang, M. Shang, T. Wu, *ACS Appl. Mater. Interfaces*, **9**(2017) 15605.
- [2] J-H Kim, C-Y Han, K-H Lee, K-S An, W Song, J. Kim, M.S. Oh, Y.R. Do, H. Yang, *Chem Mater.* **27**(2015) 197

Luminescence properties of Eu³⁺ doped ZnO spin coating films

Emad Hasabeldaim^{a,b,*}, O.M. Ntwaeaborwa^c, R.E. Kroon^a, E. Coetsee^a, H.C. Swart^{a,*}

^a Department of Physics, University of the Free State, Bloemfontein, ZA-9300, South Africa

^b Department of Physics, University of Al-Fashir, Al-Fashir, Sudan

^c School of Physics, University of the Witwatersrand, Private Bag 3, Wits, Johannesburg, 2050, South Africa

Corresponding author email address: omda180@gmail.com, SwartHC@ufs.ac.za

1. Introduction

ZnO having a wide bandgap (3.37 eV at room temperature) and exciton binding energy of 60 meV has been studied extensively in the past 50 years because of its useful properties, which resulted in many applications [1]. Eu³⁺ doped ZnO thin films were successfully prepared by a sol-gel method using the spin coating technique. The Eu³⁺ concentration was varied from 0 to 4 mol%. After the coating process, the films were annealed in air for two hours at 500 °C. The structure, morphology and luminescence properties of the films were studied.

2. Results

The crystallite size, particle size, root mean square roughness and the optical band gap were found to systematically decrease with increasing the Eu³⁺ concentration from 0, 1, 2, 3 and 4 mol%. The films were excited using different excitation sources; a 325 nm He-Cd laser, resonant excitation for the Eu³⁺ ions using a 464 nm xenon lamp, and impact ionization using a high-energy electron beam (2000 eV). The 325 nm laser excitation revealed that the films exhibited ZnO exciton emission around 376 nm, broad defects related emission and the Eu³⁺ characteristic emission at ~ 590 nm, 614 nm, 654 nm and 704 nm protruding from the broad defect's emission of ZnO. For the resonant excitation, the doped samples exhibited only the characteristic emission of the 4f-4f transitions of Eu³⁺ ions due to the ⁵D₀-⁷F_J (J=0, 1, 2, 3, 4) transitions, respectively. The Eu³⁺ emission intensity has increased with increasing the Eu³⁺ concentration up to 3 mol% and was then quenched. Multipole-multipole interaction was the major mechanism behind the quenching. When the samples were excited with a high-energy electron beam, a bright red emission was observed even with the naked eye for the doped samples. Cathodoluminescence (CL) spectra showed only Eu³⁺ emission originated from the ⁵D₀-⁷F_J (J=0, 1, 2, 3, 4) transitions. The undoped sample did not exhibit any emission from the electron beam excitation. Judd-Ofelt intensity parameters (Ω_2 and Ω_4) were performed based on the PL spectra excited at 464 nm. The value of Ω_2 was found to be higher than Ω_4 and increased with increasing the Eu³⁺ concentration until 3 mol% and then decreased, whereas the Ω_4 value decreased with increasing the Eu³⁺ concentration. This indicates strong covalency between Eu=O and higher asymmetry near the Eu³⁺ ions. The sample with the highest Eu³⁺ emission intensity (3 mol%) was degraded in vacuum under electron beam for 160 C/cm² (about 22 hours). The CL intensity showed a slight decrease at the initial electron dose at ~ 30 C/cm² and then stabilized at further electron dosages. These films can be useful as red emissive material for lighting applications that utilizes blue light/electron beam as excitation sources.

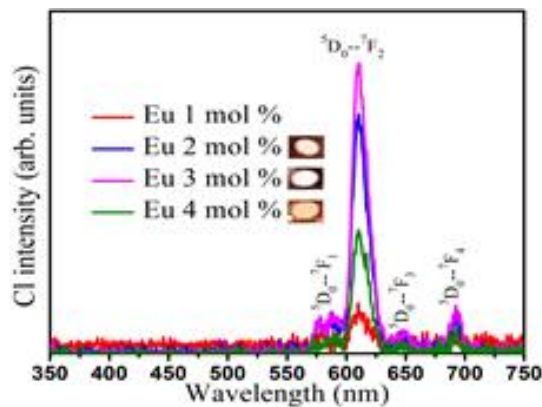


Fig. 13: CL spectra of the ZnO spin coating films with different Eu³⁺ concentration.

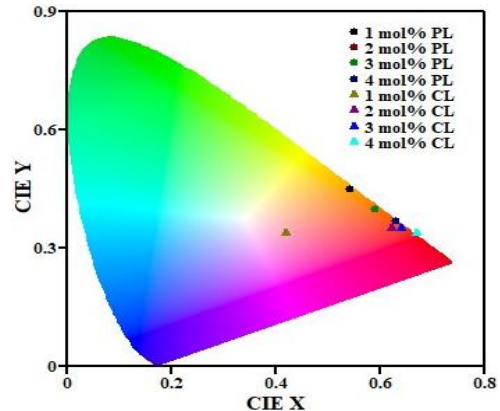


Fig. 2: CIE diagram of the ZnO spin coating films with different Eu³⁺ concentration.

3. References

- [1] V. Kumar, H. C. Swart, O. M. Ntwaeaborwa, R. E. Kroon, J. J. Terblans, S. K. K. Shaat, A. Yousif, M. M. Duvenhage, *Mat. Lett.* 101 (2013) 57.

Trap levels in persistent phosphors for bio-imaging

Dirk Poelman^{1,2}, **Olivier Q De Clercq**^{1,2}, **Jiaren Du**^{1,2},
Aranit Harizaj^{2,3}, **Ine Lentacker**^{2,3}, **Kevin Braeckmans**^{2,3}

¹ LumiLab, Department of Solid State Sciences, Ghent University, Krijgslaan 281-S1, B-9000 Ghent, Belgium;

² Center for Nano- and Biophotonics (NB-Photonics), Ghent University, B-9000 Ghent, Belgium;

³ Laboratory for General Biochemistry and Physical Pharmacy, Ghent University, B-9000 Ghent, Belgium.

Corresponding author e-mail address: Dirk.Poelman@ugent.be;

1. Introduction

Since more than two decades, efficient and long afterglow persistent luminescent materials are available for emergency signalization, road markings and toys. Available emission colors range from violet to red, but longer wavelengths are hard to achieve with rare earth dopants. While near-infrared emitting phosphors could be useful in night vision or security applications, they are especially promising for medical imaging. Next to Mn^{4+} [1], Cr^{3+} is an excellent dopant for emission in the so-called first optical window for bio-imaging, from 650 to 950 nm [2]. In this work, the spinel LiGa_5O_8 is used as the host for Cr^{3+} ions, leading to a combination of broadband and narrowband emission around 720 nm [3,4]. Even without any co-dopants, afterglow can be measured for several hours.

2. Results

A combination of the initial rise and $T_{\text{stop}}-T_{\text{max}}$ methods was shown to be an efficient way to retrieve the distribution of trap depths in the persistent phosphor $\text{LiGa}_5\text{O}_8:\text{Cr}^{3+}$. A large data set was produced by making a series of TL (thermoluminescence) measurements at different excitation temperatures. All these data were fitted simultaneously using a single set of trapping parameters. The traps were found to consist of three broad Gaussian trap distributions, see figure 1 [5]. This single set of model parameters allowed to accurately describe the experimental afterglow characteristics of the phosphor, as shown in figure 2. In addition, the parameters can be used to predict other effects of fading and the temperature dependence of the afterglow, which was measured independently.

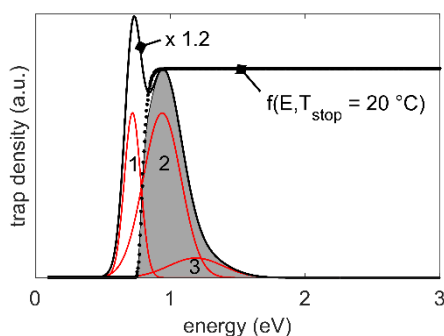


Fig. 14: Trap distribution calculated from the TL data. The expected trap filling factor at 20°C is also indicated.

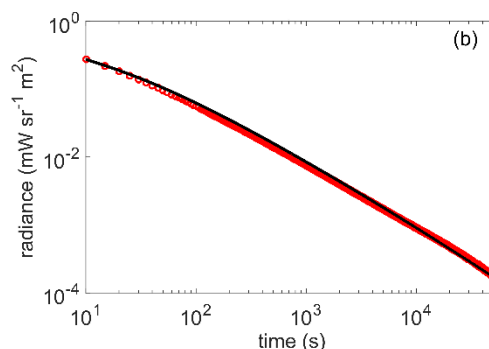


Fig. 2: Experimental (markers) and predicted afterglow (full line), based on the calculated trap distributions.

3. References

- [1] J. Du, O.Q. De Clercq, D. Poelman, Toward near-infrared persistent luminescence of Mn^{4+} activated phosphors; *this conference*.
- [2] J. Xu, S. Tanabe, Persistent luminescence instead of phosphorescence: History, mechanism, and perspective; *J. Lumin.* **205** (2019) 581.
- [3] O.Q. de Clercq, L. Martin, K. Korthout, J. Kusakovskii, H. Vrielinck, D. Poelman, Probing the Local Structure of the Near-infrared Emitting Persistent Phosphor $\text{LiGa}_5\text{O}_8:\text{Cr}^{3+}$; *Journal of Materials Chemistry C* **5** (2017) 10861.
- [4] F. Liu, W. Yan, Y-J Chuang, Z. Zhen, J. Xie, Z. Pan, Photostimulated near-infrared persistent luminescence as a new optical read-out from Cr^{3+} -doped LiGa_5O_8 ; *Scientific Reports* **3** (2013) 1554.
- [5] O.Q. de Clercq, J. Du, P.F. Smet, J.J. Joos, D. Poelman, Predicting the afterglow duration in persistent phosphors: a validated approach to derive trap depth distributions; *Physical Chemistry Chemical Physics* **20** (2018) 30455.

Photoluminescence Studies of YOF:Bi Phosphor

N.A.M. Saeed, E. Coetsee* and H.C. Swart

Department of Physics, University of the Free State, Bloemfontein, South Africa

CoetseeE@ufs.ac.za

1. Introduction

Yttrium oxyfluoride (YOF) is a promising host for many applications such as biosensing, optical nanodevices, field-emission-driven phosphors, X-ray detectors, and efficient solar cells. It has unique properties, which are similar to yttrium fluoride (YF₃) and yttrium oxide (Y₂O₃), because of the low phonon energy $\sim 400\text{cm}^{-1}$. They are thermally and chemically more stable than YF₃ [1]. YOF can be considered a good candidate for studying of the photoluminescence (PL) properties of trivalent bismuth (Bi³⁺). The room temperature PL emission of YOF:Bi³⁺ has been investigated and reported with different doping concentration (0%, 0.2%, 0.3%, 0.4%, 0.5%, 0.6% and 0.8%) of Bi³⁺. The prepared samples were synthesized using the reported pyrolysis of the trifluoroacetate precursor [2] and showed a rhombohedral structure at 900 °C (space group: R $\bar{3}m$ (166)) [3]. The PL revealed a broad UV emission at 314 nm originated from the A band $^3P_1 \rightarrow ^1S_0$ with an excitation of 267 nm corresponding to the $^1S_0 \rightarrow ^3P_1$ level of Bi³⁺ with an optimum concentration of 0.4% of Bi³⁺. Also the theoretical investigation on the position of the high energy C band ($^1S_0 \rightarrow ^1P_1$) confirmed the occurrence of the C band at 183 nm (6.79 eV) in the VUV region. The investigation of the existence of the MMCT band resulted in a value at 262 nm, which matched well with our experimental value. The deconvolution of the broad excitation and the emission bands of YOF:Bi³⁺ yielded three excitation peaks, corresponding to the transitions ($^1S_0 \rightarrow \text{MMCT}$) at 258 nm, ($^1S_0 \rightarrow ^3P_1$) at 270 nm and to the oxygen vacancies at 282 nm and three peaks for the emission ($^3P_1 \rightarrow ^1S_0$) at 306 nm, (MMCT $\rightarrow ^1S_0$) at 318 nm and ($^3P_0 \rightarrow ^1S_0$) at 336 nm. The previous report by G. Blasse and A. Brill [4] on YOF:Bi³⁺ revealed the emission centered at 330 nm, which was ascribed to the transition $^3P_1 \rightarrow ^1S_0$ with no investigations of the occurrence of the C band in the excitation spectrum. The prepared samples were investigated during the excitation at 267 nm, with an optimum concentration of 0.4 %. Whereas, the variation of the excitation band to the reported value is due to the nature of the surrounding ligands [4]. The decay time of the prepared samples was also investigated in the range of ns. The quantum yield of the optimum concentration 0.4% was also recorded upon excitation of 267 nm with a high quantum yield of about 60 %.

2. Results

The PL excitation and emission were done for the prepared samples YOF:xBi³⁺ (x=0%, 0.2%, 0.3%, 0.4%, 0.5%, 0.6% and 0.8%). The excitation and emission spectra consist of two broad bands centered at 267 nm ($^1S_0 \rightarrow ^3P_1$) for excitation and 314 nm ($^3P_1 \rightarrow ^1S_0$) for emission in fig. 1. The PL shows a broad UV emission, which can be used as a sensitizer for lanthanide ions through the energy transfer mechanism.

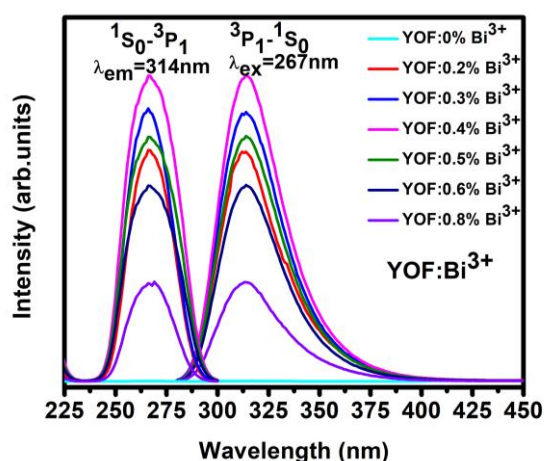


Fig. 4: PL excitation and emission of YOF:xBi³⁺ (x = 0 %, 0.07 %, 0.1 %, 0.2 %, 0.3 %, 0.4 % and 0.5 %), $\lambda_{ex} = 267$ nm and $\lambda_{em} = 314$ nm.

References

- [1] R. Anjana, K. M. Kurias, M. K. Jayaraj, Opt. Mater. 72 (2017) 730 - 736.
- [2] Z. Li, L. Zheng, L. Zhang and L. Xiong, J. Lumin. 126 (2007) 481 - 486.
- [3] Y. Zhang, D. Geng, X. Kang, M. Shang, Y. Wu, X. Li, H. Lian, Z. Cheng, and J. Lin, Inorg. Chem., 52 (2013) 12986 - 12994.
- [4] G. Blasse and A. Brill, J. Chem. Phys., 47 1920 (1967) 217 - 222.

On the Persistent Luminescence of $\text{Ce}^{3+}, \text{Cr}^{3+}, \text{Nd}^{3+}$ Doped $\text{Y}_3(\text{Al}, \text{Ga})_5\text{O}_{12}$

Zhengfa Dai¹, Vitalii Boiko¹, Karina Grzeszkiewicz¹, Maria Luisa Saladino²,
Hendrik C. Swart³, Dariusz Hreniak, Jorma Hölsä^{1,3,*}

¹ Polish Academy of Sciences, Institute of Low Temperature and Structure Research, PL-50-422 Wrocław, Poland

² University of Palermo, STEBICEF Department, Viale delle Scienze, I-90128 Palermo Italy

³ University of the Free State, Department of Physics, Bloemfontein ZA-9300, South Africa

*Corresponding Author E-mail address: jholsa@ufu.fi

1. Introduction

The $\text{Y}_3\text{Al}_5\text{O}_{12}$ (YAG) as well as the gallium offshoots $\text{Y}_3(\text{Al}_{5-x}\text{Ga}_x)\text{O}_{12}$ (YAGG) are among the most known optical materials yielding strong luminescence rated high in *e.g.* laser applications. Since the design of persistent (nano)phosphors is still based on the trial and error (most frequently) methods [1], the idea of combining a strong luminescence center/host (YAG) modified with defects to produce strong persistent luminescence sounds seducing. The main problem of YAG is the low solid solubility of the dopants such as Nd^{3+} (too big to replace the Y^{3+} host cation) which could be used as red/NIR emitting dopant for bioimaging applications. Though replacing Y^{3+} with Ga^{3+} may remove this solubility problem, the use of gallium seems to enhance, in a presently unknown manner, the persistent luminescence, as well. The Nd^{3+} dopant may also be replaced with Cr^{3+} which allows the persistent emission of these nanocrystalline materials to shift even further into the IR region. The present work focuses on the study of the energy transfer to Nd^{3+} and/or Cr^{3+} from Ce^{3+} the latter thus acting as a sensitizer; the entire process may be called as *persistent energy transfer*. The effect of gallium in $\text{Y}_3\text{Al}_2\text{Ga}_3\text{O}_{12}$, is investigated, too. The methods of research included, but were not restricted to X-ray powder diffraction, emission and excitation spectroscopies and thermoluminescence (TL). The final aim, in order to facilitate a systematic development of persistent luminescence materials, was to generate a model/mechanism of persistent luminescence (of Ce^{3+} and $\text{Nd}^{3+}/\text{Cr}^{3+}$) and energy transfer (from Ce^{3+} to Cr^{3+}).

2. Results

To start with Nd^{3+} , the persistent luminescence most probably originates from Ce^{3+} absorbing and storing the energy followed by $\text{Ce}^{3+} \rightarrow \text{Nd}^{3+}$ energy transfer. The process is not efficient, at least at present. The TL glow curves (Fig. 1) reveal only one trap for each dopant; the Ce^{3+} trap being rather shallow (@ 61 °C) explaining the weak persistent luminescence of Ce^{3+} (and subsequently that of Nd^{3+}). The TL band @ 98 °C associated with Cr^{3+} is the strongest one and situates close to the optimum position for room temperature persistent luminescence. An interesting detail found was the principle of one trap feeding only one dopant. This is probably due to low concentrations of the dopants and indicates local trapping. The symmetric band shapes indicate retrapping and local processes, as well.

As to the mechanism of persistent luminescence, the electron trapping model is the most probable for Ce^{3+} and Cr^{3+} since there are deep electron traps created by the antisite occupation of Al^{3+} and Ga^{3+} . Though originally not considered feasible, several Rietveld refinement studies have shown that the large Ga^{3+} occupies not only the larger octahedral site but also the smaller tetrahedral site usually accepting the smaller Al^{3+} . The two sites formed constitute the essence of the model providing both the electron and hole trap, *i.e.* Al^{3+} in octahedral and Ga^{3+} in the tetrahedral site (Fig. 2). No cumbersome and much energy requiring redox processes [2] are thus needed.

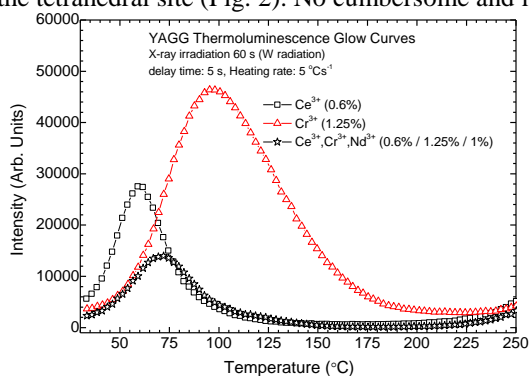


Fig. 15: The TL glow curves of $\text{Y}_3(\text{Al}, \text{Ga})_5\text{O}_{12}:\text{Ce}^{3+}, \text{Nd}^{3+}, \text{Cr}^{3+}$ after X-ray (W source) irradiation.

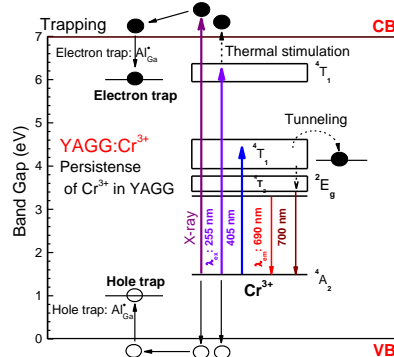


Fig. 2: Persistent Luminescence mechanism for Cr^{3+} doped $\text{Y}_3(\text{Al}, \text{Ga})_5\text{O}_{12}$.

3. References

[1] Y. Li, M. Gecevicius, and J.R. Qiu. *Chem Soc Rev.* **45** (2016) 2090.

[2] A. Bessière, S. Jacquart, K. Priolkar, A. Lecointre, B. Viana, and D. Gourier. *Opt. Express.* **19** (2011) 10131.

Scientific Programme and Abstracts
Thursday 9 May 2019

07:00		BREAKFAST	
Oral Session 7 – Session Chair: Ernest van Dyk			
08:00	Pg 33	Invited Speaker: Otwin Breitenstein	The Role of Inhomogeneities for Understanding Current-Voltage Characteristics of Solar Cells
08:40	Pg 34	Isaac Kwembur	Detection of Potential Induced Degradation in Mono and Multi-Crystalline Silicon Photovoltaic Modules
09:00	Pg 36	Solomon Werta	Influence of deposition voltage on the structural and optical properties of Cd _{1-x} Zn _x S thin films grown by electrodeposition method
09:20	Pg 37	David Kumi	Ultraviolet to visible down conversion of SiO ₂ -Ce ³⁺ , Tb ³⁺ nanospheres-poly-EVA films for solar cell application
09:40	Pg 38	Rebecca Mhlongo	Analysis of Mn ²⁺ concentration on the structure, morphology and photoluminescence of sol-gel SrAl ₂ O ₄ /Sr ₃ Al ₂ O ₆ /ZnAl ₂ O ₄ /ZnO mixed phase nanophosphor
10:00	Pg 39	Donald Hile	Structural, morphological and optical studies of zinc selenide (ZnSe) thin films deposited at different time intervals using photo-assisted chemical bath deposition technique
10:20		TEA	
Oral Session 8 – Session Chair: Martin Ntwaeaborwa			
10:40	Pg 39	Invited Speaker: Wieslaw Strék	Laser induced lighting of graphene porous materials
11:20	Pg 40	Zamaswazi Tshabalala	The influence of morphology on surface to volume ration and CO gas sensing properties of TiO ₂ nanostructure
11:40	Pg 41	Dina Naude Oosthuizen	Gas Sensors Based on CeO ₂ Nanoparticles Prepared by Chemical Precipitation Method and their Temperature-Dependent Selectivity towards NO ₂ Gas
12:00	Pg 42	Babiker Jaffar	Cathodoluminescence degradation of bismuth doped La ₂ O ₃ and La ₂ O ₂ S phosphor powders
12:20		Conference Photo	
13:00		LUNCH	
Oral Session 9 – Session Chair: Ted Kroon			
14:00	Pg 43	Invited Speaker: Oscar L. Malta	Modelling the luminescence due to 4f – 4f transitions in rare earth based materials: Recent advance
14:40	Pg 44	Reinert Verstraete	Surface Treatment of Fluoride Phosphors using Atomic Layer Deposition
15:00	Pg 45	Edward Lee	Luminescence properties of Y ₂ O ₃ :Bi ³⁺ , Yb ³⁺ thin films synthesised by pulsed laser deposition and spin coating
15:20		TEA	

The Role of Inhomogeneities for Understanding Current-Voltage Characteristics of Solar Cells

O. Breitenstein, Max Planck Institute of Microstructure Physics, Halle, Germany

All solar cells show inhomogeneous electronic properties. These inhomogeneities degrade the conversion efficiency of the cells. This holds in particular for multicrystalline (mc) silicon cells, where local differences of the lifetime of more than an order of magnitude exist. This contribution summarizes our research in this field in the last two decades. It explains how these inhomogeneities can be imaged and quantified, and the physical origins and the efficiency degradation potential of J_{01} , J_{02} , and ohmic current inhomogeneities are reviewed. Recent STEM investigations have revealed that the dominant defect-induced recombination in mc material is due to so-called Lomer dislocations, dominating the recombination in small-angle grain boundaries. J_{02} currents are flowing in positions where extended defects like scratches or the cell edge are crossing the pn-junction. Therefore J_{02} currents are always highly localized, in contrast to J_{01} currents. Also the nature of ohmic currents, which are also always localized, is reviewed. Hence, for describing most of the area of silicon solar cells, a one-diode model is sufficient, but J_{02} and ohmic currents reduce the efficiency in particular at low illumination intensity. Examples for quantitatively estimating the degradation potential of local J_{01} , J_{02} , and ohmic currents are given for two typical solar cells under two illumination intensities. Finally, different pre-breakdown mechanisms are reviewed. Except of the three previously known mechanisms, one new mechanism is described, which is dominant for monocrystalline cells.

Detection of Potential Induced Degradation in Mono and Multi-Crystalline Silicon Photovoltaic Modules

I.M Kwembur¹, J.L. Crozier¹, E.E. van Dyk¹, F.J. Vorster¹

¹ Nelson Mandela University; P.O Box 77000, Port Elizabeth, 6031
Corresponding author e-mail address: s215379446@mandela.ac.za

1. Introduction

Potential induced degradation (PID) is a performance limiting defect that profoundly impacts the output of Photovoltaic (PV) modules. PID occurs as a result of small leakage current between the solar cells and the aluminium frame. The leakage current develops due to high potential difference between the string voltage and the ground (aluminium frame). In this study, two PV modules, one Mono (module A) and one Multi-Crystalline Silicon (module B) were subjected to PID stressing by placing them in a conditioned environment ($35\pm 2^\circ\text{C}$ and $70\pm 5\% \text{RH}$), was confirmed by Dark Current-Voltage measurements (I-V), light I-V measurements and Electroluminescence (EL) imaging.

I-V characteristic curves show a decrease in shunt resistance (Rsh) and power output after PID induction. EL imaging is a powerful tool in giving information on the state of a module. EL relies on the same principle as a light emitting diode, when current is injected into the cell radiative recombination takes place and the CCD camera detects a luminescence. Non uniform luminescence may occur due to impurities in the cells, cell regions that are inactive or cells affected by PID [1][2]. EL images of cells recorded at a current equal to I_{sc} may often not detect PID. EL imaging at 10% of short circuit (I_{sc}) effectively maps out individual cells affected by PID, which manifest itself as a checker-board like distribution of intensity and may be confirmed by two distinct peaks in the image histogram. At I_{sc} EL imaging, sufficient number of (electron-holes) e-h recombination is responsible for uniform luminescence, while at 10% I_{sc} e-h recombination's are either lacking or insufficient.

Keywords: Potential Induced Degradation (PID), Electroluminescence, Degradation, Shunt Resistance, Series Resistance,

2. Results

Figures 1 shows light and dark I-V characteristic curves for the Multi-Crystalline module before and after the induction of PID. The performance parameters were extracted by PSO (Particle Swarm Optimization) and in both modules it is noticed that there is a decrease in Shunt Resistance from large ($> G \Omega$) for both modules to 1119Ω and 489Ω for modules Multi-Crystalline and Mono-Crystalline, respectively, while the power also dropped by 14.0% for module A and 18.7% for modules B.

Figure 2 shows EL images, the Multi-Crystalline module taken before and after PID was induced. The images were recorded at I_{sc} and in the case of after PID induction, at 10% (I_{sc}) as well.

The images taken at I_{sc} Fig 2 (i and ii) indicates that PID may be present and is confirmed by the checker-board pattern observed in the 10 % I_{sc} post-PID image (iii). From the images it is also observed that there is a very high possibility of not detecting PID in an EL image taken I_{sc} .

The reduced power output (14%) shows that the degradation caused by PID has the potential to have a large effect on the performance of a PV power plant if the modules in the plant suffer PID as the performance of the modules directly impacts on the power output of a PV power plant.

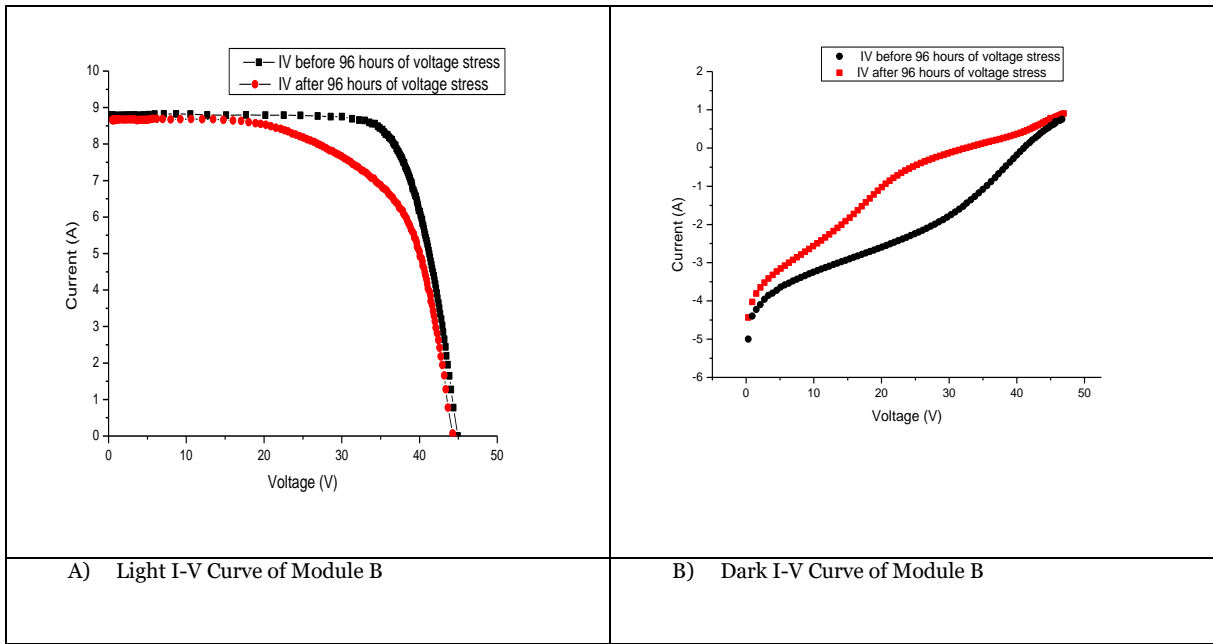


Fig 1: light and dark I-V Curve measurements

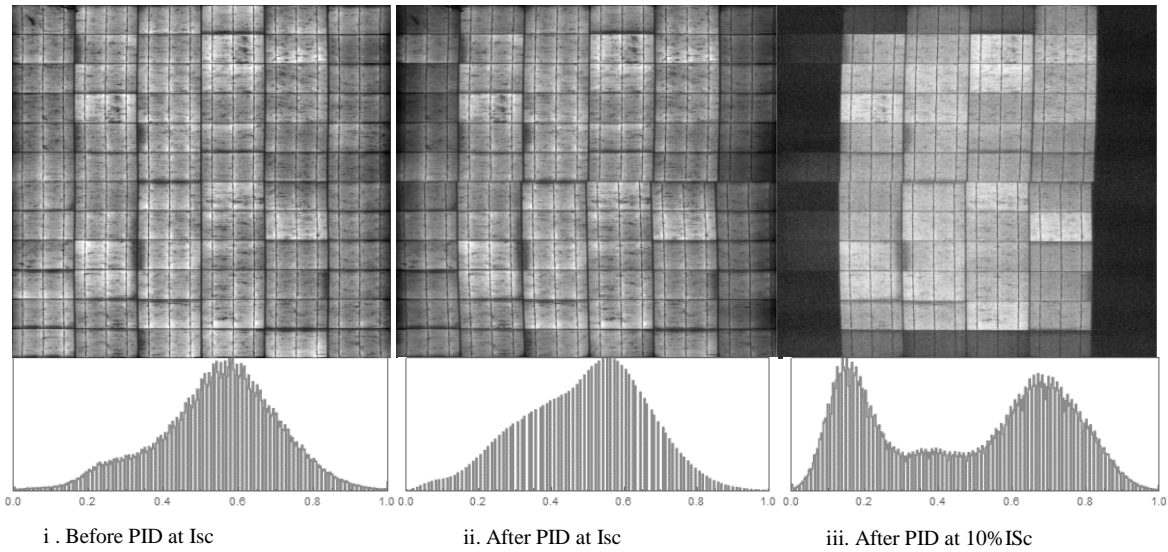


Fig: 2 EL images of module B

3. References

- [1] J. Hylský, D. Strachala, P. Vyroubal, P. Čudek, J. Vaněk, and P. Vanýsek, "Effect of negative potential on the extent of PID degradation in photovoltaic power plant in a real operation mode," *Microelectron. Reliab.*, vol. 85, no. April, pp. 12–18, 2018.
- [2] M. Barbato, A. Barbato, M. Meneghini, G. Tavernaro, M. Rossetto, and G. Meneghesso, "Potential induced degradation of N-type bifacial silicon solar cells: An investigation based on electrical and optical measurements," *Sol. Energy Mater. Sol. Cells*, vol. 168, no. November 2016, pp. 51–61, 2017.

Influence of deposition voltage on the structural and optical properties of $\text{Cd}_{1-x}\text{Zn}_x\text{S}$ thin films grown by electrodeposition method

S.Z Werta, O.K. Echendu, F.B. Dejene

University of the Free State, Qwa Qwa campus

Corresponding author e-mail address: solomonwerta@gmail.com

1. Introduction

Recently, group II-VI semiconductor compounds have received substantial attention from researchers due to their potential applications especially in the fabrication of n-type in solar cells and other optoelectronic devices [1]. Cadmium sulphide (CdS) is one of the compounds that belong to this group with band gap energy of 2.42 eV which has been found as the best n-type window material for the fabrication of CdTe, $\text{CuIn}(\text{Se},\text{S})_2$ and $\text{Cu}(\text{In},\text{Ga})\text{Se}_2$ solar cell films [2]. Although CdS is a promising window material, it has high absorption coefficient which results in window absorption loss when used as solar cell window material. To avoid such loss, CdS can be replaced with materials with wider energy band gap as well as lower absorption coefficient, such as the ternary compound $\text{Cd}_{1-x}\text{Zn}_x\text{S}$ can lead to decrease in window absorption loss. Various techniques such as electrodeposition [3], chemical bath deposition [4], and close space sublimation (CSS) [5] have been employed for the synthesis of $\text{Cd}_{1-x}\text{Zn}_x\text{S}$ thin films. Among these techniques electrodeposition has been used due to its numerous advantages such as use in large area deposition, easy process control, minimum waste generation and self-purification of electrolytes. It is reported that, in the deposition of thin films using electrodeposition method for application in macroelectronic and nanotechnology based devices, parameters such as concentration of ions in the electrolytic bath, deposition time, electrolytic bath temperature, stirring, pH, electrodes used and applied voltage play a vital role in the quality of the film produced. If these parameters are optimized, efficient $\text{Cd}_{1-x}\text{Zn}_x\text{S}$ thin films which can be applied for different applications will be produced. Among these deposition parameters, influence of electrolytic solution pH on physic-chemical properties of thin film has not been investigated adequately. Hence, in this paper, the effect of deposition voltage on structural, optical and morphological properties of electroplated $\text{Cd}_{1-x}\text{Zn}_x\text{S}$ thin films is investigated using cadmium chloride (CdCl_2), zinc chloride (ZnCl_2) and sodium thiosulphate ($\text{Na}_2\text{S}_2\text{O}_3$) as Cd, Zn and S source respectively.

2. Results

The structural, optical and morphological properties of $\text{Cd}_{1-x}\text{Zn}_x\text{S}$ thin films grown at three different electrolytic solution pH (1.8, 2.7 and 3.5) were investigated using glancing incidence X-ray diffraction (GIXRD), Raman spectroscopy, UV-Vis spectrophotometry, scanning electron microscopy (SEM) and energy-dispersive X-ray (EDX) spectroscopy. The films are deposited at 85 °C electrolytic bath temperature for 60 min deposition time, and annealed at 400 °C for 20 min. From the structural measurement it is observed that the films have only hexagonal phases. With increase in pH the intensity of peaks decrease because of more Zn ions incorporated into the film. According to optical band gap measurement the band gap increases from 2.43 to 2.55 eV. SEM image show uniform and densely packed surface morphology while EDX results reveal that increase in pH increases zinc ions incorporation into $\text{Cd}_{1-x}\text{Zn}_x\text{S}$ thin film.

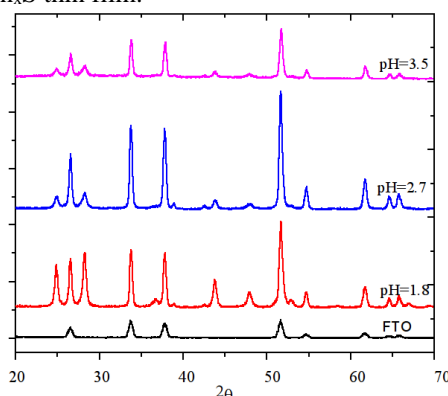


Fig. 16: GIXRD patterns of $\text{Cd}_{1-x}\text{Zn}_x\text{S}$ thin films grown at 1.8, 2.7 and 3.5 pH

3. References

- [1] Ju Wu, Chu, Chao, Chen, Lai, Kang, Yen Chen, and Chou, *Nano Lett.*, **7** (2007) 1908-1913
- [2] O. K Echendu and I.M Dharmadasa, *Materials chemistry and physics* **157** (2015) 39-44
- [3] A.Sh. Abidinov, H.M. Mamedov, H.A. Hasanov, S.I. Amirova, *Thin Solid Films* **480-481** (2005) 388 – 391
- [4] Hanyu Yao, Honglie Shen, Xiangrong Zhu, Jing Jiao, *Ceramics International* **42** (2016) 2466-2471
- [5] Waqar Mahmood, Nazar Abbas Shah, *Optical Materials* **36** (2014) 1449-1453

Ultraviolet to visible down conversion of $\text{SiO}_2\text{-Ce}^{3+}$, Tb^{3+} nanospheres-poly-EVA films for solar cell application

David Kumi¹, Martin Ntwaeaborwa¹, Sohye Cho²

¹ School of Physics, University of the Witwatersrand, Private Bag 3, Wits, Johannesburg, 2050

² Materials Architecting Research Centre, Korea Institute of Science and Technology, 217 Gajeong-ro Yuseong-gu, Daejeon, 04763, Republic of Korea

Corresponding author e-mail address: ntwaeab@gmail.com

1. Introduction

Despite the many advantages solar cells have over other forms of renewable energy sources, solar energy efficiency still has major drawbacks such as energy loss that limit their operation and commercialization. One of the main reasons for the energy loss is the ineffective utilization of short wavelength photons, especially within the ultraviolet (UV) region [1, 2] of the sunlight spectrum. Therefore, we have prepared and investigated down-converting nanophosphors composed of SiO_2 co-doped with Ce and Tb. These nanophosphors act to harvest high energy UV photons from the sunlight spectrum and down-convert them to low energy visible photons where they could be conveniently absorbed by solar cell devices and improve their power conversion efficiency. The phosphors synthesised were incorporated into poly-ethylene-vinyl acetate film (poly-EVA) by dissolving the powder phosphors in chloroform with 1 g of the poly-EVA added. The films prepared were dried and later overlaid on a commercial crystalline silicon (c-Si) solar cell and the photocurrent efficiency of the device was measured.

2. Results

The scheme in Fig. 1(a) represent the device setup with a layer of EVA film with the nanophosphor, while Fig. 1(b) shows the current-voltage curve measurements for both the plain EVA and the EVA with the silica phosphors films overlaid on a c-Si solar cell. The phosphor films recorded a significantly good transmittance ($\geq 76\%$) and also displayed a UV absorption capacity compared to that of the plain poly-EVA film. The film that was prepared from 15 mg of SiO_2 : 1% Ce, 0.8% Tb recorded an increase in the photocurrent efficiency when overlaid on the solar cell, while the film with SiO_2 : 1% Ce, 1% Tb phosphor recorded marginal decrease in the power conversion efficiency compared to that of the plain EVA film. The effect of a down-converting SiO_2 : 1% Ce, 0.8% Tb layer on the power conversion efficiency of the commercial c-Si solar cell device will be discussed.

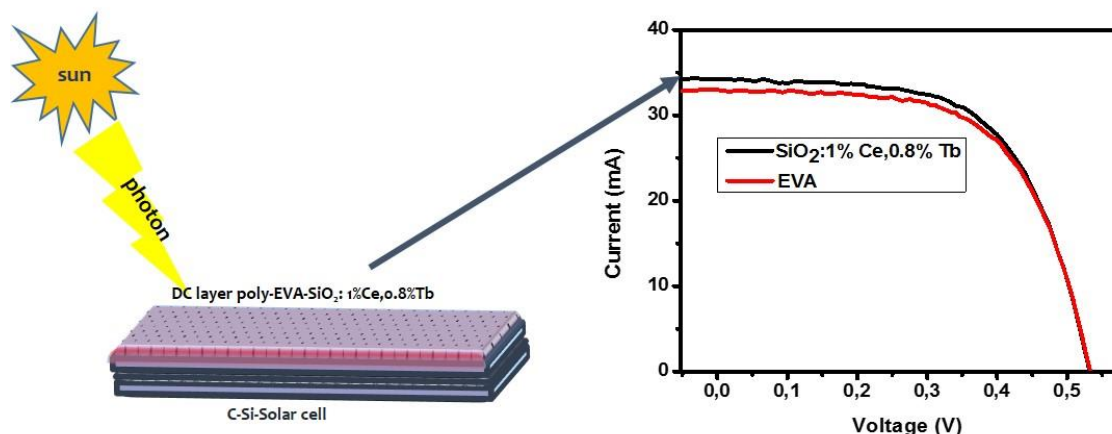


Fig 1: (a) c-Si solar cell with EVA-SiO₂:Ce,Tb DC layer (b) IV curves of EVA and EVA- SiO₂:Ce³⁺,Tb³⁺DC layers on c-Si solar cell

3. References

- [1] N.S. Lewis, *Science* 315 (2007) 798.
- [2] G.D. Scholes, G.R. Fleming, A. Olaya-Castro, R. van Grondelle, *Nature Chemistry* 3 (2011) 763.

Analysis of Mn²⁺ concentration on the structure, morphology and photoluminescence of sol-gel SrAl₂O₄/Sr₃Al₂O₆/ZnAl₂O₄/ZnO mixed phase nanophosphor

M.R. Mhlongo¹, L.F. Koao², R.E. Kroon³, T.E. Motaung⁴, S.V. Motloung^{1,5}

¹Department of Physics, Sefako Makgatho Health Sciences University, P.O. Box 94, Medunsa, 0204, South Africa

²Department of Physics, University of the Free State (Qwaqwa Campus), Private Bag X 13, Phuthaditjhaba, 9866, South Africa

³Department of Physics, University of the Free State, P. O. Box 339, Bloemfontein, 9300, South Africa

⁴Department of Chemistry, University of Zululand, KwaDlangezwa, 3886, South Africa

⁵Department of Physics, Nelson Mandela University, P. O. Box 77000, Port Elizabeth 6031, South Africa
Corresponding authors: rebsmhlongo@gmail.com

1. Introduction

Recently, many researchers are focusing on the synthesis of different nanocrystals with sizes ranging from 1 to 100 nm. This type of nanocrystals presents interest due to the interesting size-dependent physical, chemical, electrical, magnetic and optical properties in comparison with those of their bulk crystals [1]. Previous studies have shown that the mixed oxide ZnO/ZnAl₂O₄ has excellent stability and much higher photocatalytic activity than their bulk oxide counterparts [2]. The primary aim of this study is to synthesize a phosphor material based on mixed oxides for practical applications such as in light emitting diodes (LEDs). This study investigates the effect of Mn²⁺ on the structure and photoluminescence (PL) of the mixed phases SrAl₂O₄/Sr₃Al₂O₆/ZnAl₂O₄/ZnO:x% Mn²⁺ (0 ≤ x ≤ 2) (SSZZ:x% Mn²⁺) nanophosphor. The emission channels associated with the observed PL emissions are also proposed.

2. Results

SSZZ:x% Mn²⁺ nanophosphors were successfully prepared using sol-gel technique. The X-ray diffraction (XRD) patterns showed that the prepared material is composed of the mixed phases of cubic SrAl₂O₄, Sr₃Al₂O₆, ZnAl₂O₄ and hexagonal ZnO as shown in Fig. 1. The scanning electron microscope (SEM) showed that the prepared nanophosphor consists of some nanorods. Energy dispersive X-ray spectroscopy (EDS) confirmed the presence of all expected elements (Sr, Zn, Al, O and Mn). The ultraviolet visible spectrophotometer (UV-vis) results showed that the band gap of the prepared nanophosphor can be tuned. The PL results reveal that when SSZZ:x%Mn²⁺ samples were excited with 374 nm wavelength, two emission peaks at 580 and 600 nm (with some shoulders at 414 and 435 nm) were observed. The emission at 580 nm is due to the presence of oxygen interstitials (O_i) within the ZnO whereas the 600 nm emission is due to the ⁴T_{1g}(G) → ⁶A_{1g}(S) transitions of Mn²⁺ [3].

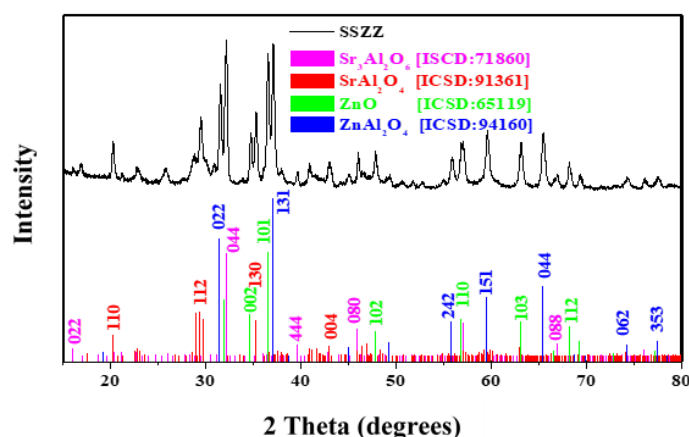


Fig. 1: XRD patterns of SrAl₂O₄/Sr₃Al₂O₆/ZnAl₂O₄/ZnO nanophosphor

References

- [1] I. Miron, C. Enache, I. Grozescu, J. Nanomat. Biostructures. **7** (3) (2012) 967 – 972.
- [2] X. Yuan, X. Cheng, Q. Jing, J. Niu, D. Peng, Z. Feng, X. Wu, Materials, **11** (2018) 1624.
- [3] G. Lakshminarayana, L. Wondraczek, J. Solid State Chem. **184** (2011) 1931–1938.

Structural, morphological and optical studies of zinc selenide (ZnSe) thin films deposited at different time intervals using photo-assisted chemical bath deposition technique

Donald Dehiin Hile¹, Lehlohonolo Fortune Koao¹, Hendrik C. Swart¹, Setumo Victor Motloung², Tshwafo E. Motaung³

¹Department of Physics, University of the Free State, 9866, Phuthaditjhaba, South Africa

²Department of Physics, SefakoMakgatho Health Science University, Medunsa, South Africa

³Department of Chemistry, University of Zululand, KwaDlangezwa 3886, South Africa

Corresponding author email: donald.hile@gmail.com; and koaolehlohonolo@gmail.com

1. Introduction

ZnSe is a direct and wide band gap (2.7 eV) chalcogenide material with a large exciton binding energy (21 meV) [1]. It has wide transmittance range and its excellent transparency to infrared, low dispersion and absorption coefficient, high luminescence efficiency and highly resistant to thermal shock, make ZnSe an excellent candidate for lenses, lasers, light emitting diodes, window materials for solar cells and infrared cameras [1]. These properties could however be influenced by many factors such as deposition method, deposition time, annealing temperature, annealing time, complexing agent, deposition pH and substrates. Photo-assisted Chemical bath deposition (PACBD) was adopted in this work based on its numerous advantages found in the literature [2].

2. Results

ZnSe thin films were deposited using photo-assisted chemical bath deposition technique at different time intervals. Zinc acetate ($Zn(CH_3OOC)_2$) and sodium selenosulphate (Na_2SeSO_3) were used as the source of Zn^{2+} and Se^{2+} ions respectively while hydrazine hydrate ($N_2H_4 \cdot H_2O$) was used as the complexing agent. The deposited films were annealed at 300 °C for 2 hours and the structure, morphology and optical properties of the films were investigated. The X-ray diffraction (XRD) measurement revealed nanocrystalline with peaks indexed to the face-centered cubic phase of ZnSe according to the JCPDS file no.800021. Fig.1 shows the XRD patterns of (a) as-deposited and (b) annealed ZnSe thin films. Average crystallite sizes D (nm) were observed to increase with increase in deposition time and decreases in size after annealing. The cell parameters were estimated and found to be in agreement with the standard values according to the JCPDS file no. 80-0021. The scanning electron microscopy (SEM) revealed uniform grain nanoparticles which gradually turned to nanoflakes as the deposition time increase. The presence of Zn and Se was detected by energy dispersive X-ray and the elemental mappings showed uniform distribution of the elements in the films. UV-Vis spectra showed red shift when the deposition time was increase while the energy band gap and transmittance decrease as the deposition time increased. The annealed samples showed higher transmittance when compared with the as-deposited. The samples showed two emission bands in the green and red region of the spectrum. The XRD showed that the crystallinity of the films increased with increase in deposition time and the materials became more nano-particulates after annealing as indicated by broader peaks in Fig.1 (b).

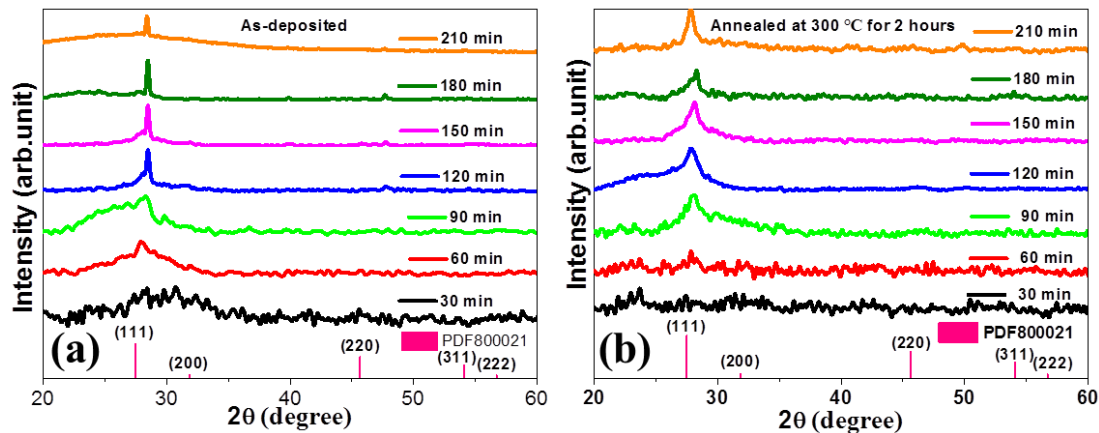


Fig. 17: XRD of (a) as-deposited and (b) annealed samples of the ZnSe thin films deposited at different time intervals

3. References

- [1] N. Benmehdi, A. Chelouche, T. Touam, D Djouadi, A Doghmane. *J. Mater. sci: Mater. electron.* **27** (2016) 5526.
- [2] T.L. Remadevi, A.C. Dhanya, K.Deepa. *J. electron. mater.* **43** (2014) 3984

Laser induced lighting of graphene porous materials

W. Strek

*Institute of Low Temperature and Structure Research Polish Academy of Sciences
Okolna 2 street, 50-422 Wrocław, Poland*

Corresponding author e-mail address: w.strek@intibs.pl

1. Introduction

In the matter of white light (WL) generation, considerable scientific interest has been recently devoted to the studies of carbon materials where laser light or electrical current are used for incandescence or light emission. Experiments have been performed on a number of structures, including carbon nanotubes, fullerenes, graphene, and graphene QDs, which are being considered as materials for next-generation light sources. The broadband anti-Stokes white emission was observed for the first time by Tanner in 2010 from fully concentrated lanthanide oxides [1]. To obtain such emission special conditions such as high power excitation source operating under near infrared region and reduced pressure are required.

2. Results

The investigations considering WL emission observed from graphene-based materials such as foam [2] or ceramic [3] are reported. The intense broadband white luminescence was obtained in vacuum atmosphere upon a focused beam of CW laser diodes operating at various excitation lines, from the visible to the near infrared range (Fig. 1). It was found that the WL emission from graphene materials was a threshold process exhibiting supralinear behavior. The intensity was strongly dependent on the surroundings pressure. Relatively low temperature of the sample was estimated to be around 600 °C. The WL emission was accompanied by efficient photoconductivity that increased with increasing excitation power density of the laser beam. The possible mechanism of white light generation will be discussed as a photoinduced, transient, domain-like $sp^2 \rightarrow sp^3$ phase transitions.



Figure 1. Broadband anti-Stokes white emission observed from graphene upon 975 excitation line in vacuum.

3. References

- [1] J. Wang, P.A. Tanner, *J. Am. Chem. Soc.*, **132** (2010) 947.
- [2] W. Strek, R. Tomala, M. Lukaszewicz, D. Cichy P. Gluchowski, Y. Gerasymchuk, L. Marciniak, A. Bednarkiewicz, D. Hreniak, *Scientific Reports* **7** (2017) 41281.
- [3] W. Strek B. Cichy, L. Radosinski, P. Gluchowski, L. Marciniak, M. Lukaszewicz, D. Hreniak, *Light: Science and Applications* **4** (2015) e237.

The influence of morphology on surface to volume ration and CO gas sensing properties of TiO₂ nanostructures.

Zamaswazi Tshabalala^{1,2}, David Motaung^{1,2}, Hendrik swart²

¹ DST/CSIR, National Centre for Nano-structured Materials, Council for Scientific Industrial Research, Pretoria, 0001, South Africa

² Department of Physics, University of the Free State, P. O. Box 339, Bloemfontein ZA9300, South Africa

Corresponding author e-mail address: tshabalala@csir.co.za

1. Introduction

Strict regulations are being implemented by the government for environmental monitoring such as air quality in offices and working spaces, carbon emission and other pollutant emitted into the air by vehicle and industries. Chemiresistive gas sensors based on nanostructured semiconducting oxides such as TiO₂ are mostly used due to ease in synthesis and low cost. TiO₂ nanostructure are known for large surface to volume ratio, high porosity and electroptical properties that are highly influential to gas sensing [1]. In this work we explore the effect of morphology, surface area and defect state of hydrothermally synthesized TiO₂ nanostructure for CO gas sensing.

2. Results

The scanning electron microscope (SEM) images shown in the insert of figure 1 (a) depict the different morphologies of the hydrothermally synthesized TiO₂ nanoparticles and nanoflowers. The nanoflowers have a significantly higher specific surface area and broad distribution in pore diameter of about 95.38 m²g⁻¹ and 31.44 nm respectively where else the nanoparticles have 71.33 m²g⁻¹ and 21.52 nm respectively. Increase in intensity of the emission peak is observed from figure 1 (b). Due to use of hydrothermal method for synthesis, oxygen vacancies and surface hydroxyl groups are dominant sites for trapped charges. An intense emission peak at 423 nm was observed which signals that the TiO₂ nanostructures are dominated by surface states compared to excitonic emissions.

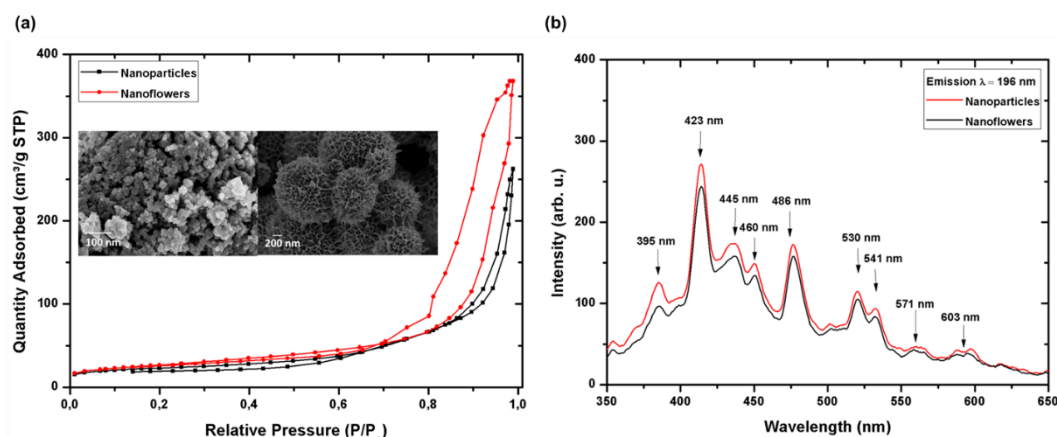


Figure 1: (a) N₂ adsorption-desorption isotherms. insert: SEM images of the TiO₂ nanostructures. (b) Emission spectra of the TiO₂ nanostructures.

3. References

[1] B. Wang, L. Deng, L. Sun, Y. Lei, N. Wu, Y. Wang, Sensors and Actuators: B, 276 (2018) 57-64.

Gas Sensors Based on CeO₂ Nanoparticles Prepared by Chemical Precipitation Method and their Temperature-Dependent Selectivity towards NO₂ Gas

D.N. Oosthuizen^{1,2}, D.E. Motaung^{1,2} and H.C. Swart²

¹DST/CSIR National Centre for Nano-structured Materials, Council for Scientific Industrial Research, Pretoria, 0001, South Africa

²Department of Physics, University of the Free State, P. O. Box 339, Bloemfontein ZA9300, South Africa

Corresponding author e-mail address: doosthuizen1@csir.co.za

1. Introduction

Cerium oxide (CeO₂) is a rare earth compound with various properties including abundant oxygen vacancy defects, remarkable redox properties and ability to uptake and release oxygen via the transformation between Ce³⁺ and Ce⁴⁺. It has been extensively studied and employed in many applications, including solid oxide fuel cells, catalysts for CO oxidation and high temperature gas sensors.[1-4] Limited gas sensing studies have focussed on low operating conditions (ranging from room temperature to 200 °C).[1, 5] In the presence of 10 and 50 ppm NO₂ gas responses of 1.7 and 5.5 % were observed for CeO₂ nanofibers and nanoparticles at room temperature and 200 °C, respectively.[3, 5] Previous studies have reported that the gas sensing properties, of the metal oxide based sensing layer, are dependent on the point defects (i.e. oxygen and metal vacancies) and crystallite sizes.[6-9] In this work, we report on the low temperature gas sensing of as-prepared CeO₂ nanoparticles that were characterized using various analytical techniques, including X-ray diffraction, X-ray photoelectron and photoluminescence spectroscopy (PL) etc., to probe the structure, chemical state, optical band gap and point defects properties. To give further insight into what governs the gas sensing mechanism of the CeO₂ nanostructure-based sensors, the calculated structural and defect properties was then correlated with the sensing performance of each sensor.

2. Results

A series of CeO₂ nanoparticles with crystallite sizes in the range of 6 to 8 nm and defect levels below 10 % was synthesized at room temperature in the presence of various concentrations of ethanol (A-0 mL, B 10 mL, C 20 mL up to F 50 mL).. The band-gap narrowing of around 0.4 eV was observed for the products compared to reported bulk CeO₂, attributed to the concentration defects (Ce³⁺ and oxygen vacancies) present in the products. Upon exposure to various gases at room temperature, the sensors were found to be sensitive to H₂S and NO₂, compared to previously reported cases. This was attributed to the synergistic effect of the small crystallite size and concentration of surface oxygen vacancies (V_O), as seen in Figs. 1 and 2. At higher operating temperatures of 100 and 200 °C, improved selectivity was witnessed for the C-CeO₂ and F-CeO₂ based sensors, respectively. The observed variation on the optimal operating temperatures among the sensors with the crystallite sizes variation implied that the gas selectivity is morphology and crystallite size dependent. The D-CeO₂ based sensor's response towards H₂S was dependent on relative concentration of Ce³⁺ and V_O, while the NO₂ response of the F-CeO₂ based sensor was dependent on the surface area and relative concentration of V_O.

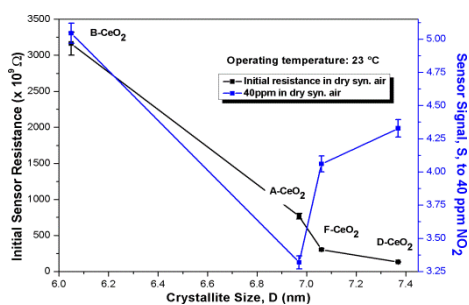


Fig. 18: The relationship between the initial sensor resistance, crystallite size and the NO₂ gas sensing response of A-CeO₂, B-CeO₂, D-CeO₂ and F-CeO₂ at room

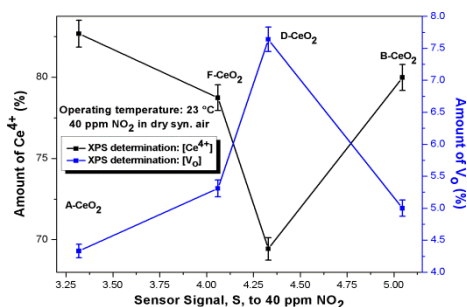


Fig. 2: The relationship between XPS determined Ce⁴⁺ and V_O concentrations and the NO₂ gas sensing response of A-CeO₂, B-CeO₂, D-CeO₂ and F-CeO₂ at room temperature

3. References

- [1] Li, Z., et al., *Journal of Alloys and Compounds*, **682** (2016) 647-653.
- [2] Alammar, T., et al., *ACS Sustainable Chemistry & Engineering*, **3** (2015) 42-54.
- [3] Gardner, J.W., *Sensors and Actuators B: Chemical*, **27** (1995) 261-266.
- [4] Motaung, D.E., et al., *Sensors and Actuators B: Chemical*, **254** (2018) 984-995.
- [5] Zhang, L., et al., *Journal of Materials Chemistry C*, **5** (2017) 6973-6981.
- [6] Zhang, J., et al., *The Journal of Physical Chemistry C*, **120** (2016) 3936-3945.
- [7] Motaung, D.E., et al., *Rsc Advances*, **6** (2016) 26227-26238.
- [8] Katoch, A., et al., *Sensors and Actuators B: Chemical*, **185** (2013) 411-416.
- [9] Sypien, B.L., et al., *Procedia Engineering*, **47** (2012) 1057-1060.

Cathodoluminescence degradation of bismuth doped La_2O_3 and $\text{La}_2\text{O}_2\text{S}$ phosphor powders

B. M. Jaffar¹, H. C. Swart¹, H. A. A. Seed Ahmed², A. Yousif², R. E. Kroon^{1*}

¹Department of Physics, Box 339, University of the Free State, Bloemfontein 9300, South Africa

²Department of Physics, Box 321, University of Khartoum, Omdurman 11115, Sudan

Corresponding author e-mail address: KroonRE@ufs.ac.za

1. Introduction

Lanthanum oxide (La_2O_3) and lanthanum oxysulphide ($\text{La}_2\text{O}_2\text{S}$) have attracted significant research interest due to their use as phosphor hosts [1,2]. However, it has been difficult to compare their potential because most studies consider only one or the other. The luminescence from Bi ions in various hosts has recently been surveyed [3] and Bi ions offer the possibility of replacing expensive lanthanide ions as phosphor activators for certain applications. Freshly prepared $\text{La}_2\text{O}_3\text{:Bi}$ emitted slightly stronger blue photoluminescence (PL) emission than $\text{La}_2\text{O}_2\text{S}\text{:Bi}$ samples, but this host quickly underwent hydroxylation and loss of luminescence when exposed to that atmosphere, suggesting that $\text{La}_2\text{O}_2\text{S}\text{:Bi}$ is more useful for general PL applications. In the present work, cathodoluminescence (CL) of the two phosphors was compared and they were assessed for possible application in field emission displays (FEDs). Since the phosphor is not exposed to the atmosphere during this application, bulk hydroxylation of the $\text{La}_2\text{O}_3\text{:Bi}$ cannot occur. However, electron-stimulated surface chemical reactions caused by the electron beam are known to induce changes on the surface of phosphors that can lead to CL degradation [4]. Simultaneous CL and Auger electron spectroscopy (AES) measurements were performed during long term exposure of the samples to an electron beam to assess the CL degradation and chemical changes on the surface. X-ray photoelectron spectroscopy (XPS) measurements were also made on the samples before and after CL degradation.

2. Results

$\text{La}_2\text{O}_3\text{:Bi}$ and $\text{La}_2\text{O}_2\text{S}\text{:Bi}$ phosphor powders, both having the same Bi doping concentration which was optimized for blue PL emission, were prepared using citric acid sol-gel combustion and ethanol-assisted solution combustion, respectively. They were excited by a 2.5 keV electron beam of current 4 μA in a chamber pumped to a vacuum pressure of 1.3×10^{-8} Torr. It was found that after a small amount of initial CL degradation, associated with removal of contamination from the surface, the $\text{La}_2\text{O}_3\text{:Bi}$ sample (Fig. 1) remained stable under the electron beam and it may be suitable for use in FEDs. However, the $\text{La}_2\text{O}_2\text{S}\text{:Bi}$ (Fig. 2) showed continuous and severe CL degradation and is not suitable for CL applications. During electron beam exposure the AES measurements showed that there was a decrease in the surface concentration of S, suggesting the formation of a non-luminescent La_2O_3 surface layer which was responsible for degradation. However, some S remained on the surface and XPS spectra revealed that a sulphate, possibly $\text{La}_2\text{O}_2\text{SO}_4$, was present on the surface, which may have contributed to the degradation.

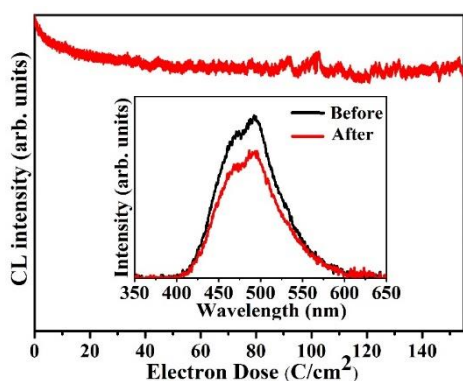


Fig. 1: CL intensity as a function of electron dose for $\text{La}_2\text{O}_3\text{:Bi}$ phosphor powder. The inset show the CL spectra before and after degradation.

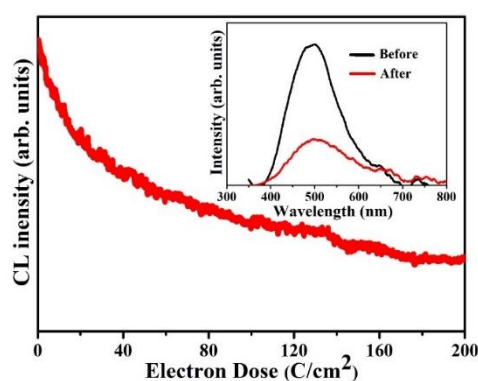


Fig. 2: CL intensity as a function of electron dose for $\text{La}_2\text{O}_2\text{S}\text{:Bi}$ phosphor powder. The inset show the CL spectra before and after degradation.

3. References

- [1] Z. Xu, S. Bian, J. Wang, T. Liu, L. Wang and Y. Gao. *RSC Adv.* **3** (2013) 1410.
- [2] H. Luo, A. J. J. Bos and P. Dorenbos. *J. Phys. Chem. C* **121** (2017) 8760.
- [3] R. H. P. Awater and P. Dorenbos. *J. Lumin.* **184** (2017) 221.
- [4] J. S. Sebastian, H. C. Swart, T. A. Trotter, S. L. Jones and P. H. Holloway. *J. Vac. Sci. Technol. A* **15** (1997) 2349.

MODELLING THE LUMINESCENCE DUE TO $4f-4f$ TRANSITIONS IN RARE EARTH BASED MATERIALS: RECENT ADVANCES

Oscar Malta

An overview of our recent work on the nature and behavior of the intraconfigurational $4f-4f$ transitions in chemical environments of controllable characteristics, as well as on non-radiative energy transfer processes involving trivalent rare earth ions (both ion-to-ion and intramolecular) and their emission quantum yields, is presented. Perspectives and challenges on this fascinating subject is discussed.

Surface Treatment of Fluoride Phosphors using Atomic Layer Deposition

Reinert Verstraete^{1,2}, Hannes Rijckaert³, Geert Rampelberg^{2,4}, Elizabeth Coetsee-Hugo⁵, Mart-Mari Duvenhage⁵, Christophe Detavernier^{2,4}, Hendrik Swart⁵, Philippe F. Smet^{1,2} and Dirk Poelman^{1,2}

¹ LumiLab, Department of Solid State Sciences, Ghent University, 9000 Ghent, Belgium.

² Center for Nano- and Biophotonics (NB-Photonics), Ghent University, 9000 Ghent, Belgium

³ Sol-Gel Centre for Research on Inorganic Powders and Thin Film Synthesis (SCRiPTS), Department of Chemistry, Ghent University, Krijgslaan 281-S3, 9000 Ghent, Belgium

⁴ Conformal Coating of Nanomaterials (CoCooN), Department of Solid State Sciences, Ghent University, 9000 Ghent, Belgium

⁵ Department of Physics, University of the Free State, P.O. Box 339, Bloemfontein, ZA 9300, South Africa

Corresponding author e-mail address: Reinert.Verstraete@UGent.be

Red fluoride phosphors such as $\text{K}_2\text{SiF}_6:\text{Mn}^{4+}$ has recently gained a lot of attention as the red component of white light-emitting diodes (wLEDs). They incorporate $[\text{MnF}_6]^{2-}$ complexes which show a narrow luminescence band centred at around 630 nm upon blue excitation at 450 nm. Therefore, fluoride phosphors have distinct advantages over the frequently used Eu^{2+} -based nitride phosphors. The latter suffer from reabsorption issues due to a rather small Stokes shift combined with broad excitation and emission bands. Moreover, a considerable fraction of the Eu^{2+} emission in nitrides extends above 650 nm, a spectral region in which the human eye sensitivity is negligible. The attainable luminous efficacy of a red nitride based wLED is therefore limited.

Despite the excellent optical properties and the high attainable internal quantum efficiency of many fluoride phosphors, their sensitivity to moisture is hindering their wide-spread commercial use. Several methods have been investigated in the past to passivate the surface of fluoride phosphors³⁻⁸. However, common wet chemical methods lower the efficiency of the moisture-sensitive phosphor after treatment. Moreover, for heterogeneous core-shell structures, the fluorine terminated surface of the core shows a lack of functional sites (e.g. hydroxyl groups) inhibiting efficient bonding with typical shell materials.

In this work we investigate the use of atomic layer deposition (ALD) for growth of Al_2O_3 and TiO_2 seed layers that can functionalize the fluoride phosphor surface. The coated phosphors have hydroxyl-saturated surfaces that are compatible for further bonding with hydrophobic shells. It was found that an Al_2O_3 seed layer cannot straightforwardly be grown on $\text{K}_2\text{SiF}_6:\text{Mn}^{4+}$. Pore-formation and blistering led to delamination of the film. In contrast, conformal layers of TiO_2 can be grown without delamination. Unlike the uncoated phosphor, the TiO_2 coated phosphor could easily be further treated with a hydrophobic adhesive.

References

- (1) Sijbom, H. F.; Verstraete, R.; Joos, J. J.; Poelman, D.; Smet, P. F. $\text{K}_2\text{SiF}_6:\text{Mn}^{4+}$ as a Red Phosphor for Displays and Warm-white LEDs: a Review of Properties and Perspectives. *Opt. Mater. Express* 2017, 7, 3332-3365.
- (2) Verstraete, R.; Sijbom, H. F.; Joos, J. J.; Korthout, K.; Poelman, D.; Detavernier, C.; Smet, P. F. Red Mn^{4+} -Doped Fluoride Phosphors: Why Purity Matters. *ACS Applied Materials & Interfaces* 2018, 10, 18845-18856.
- (3) Nguyen, H. D.; Lin, C. C.; Liu, R. S. Waterproof Alkyl Phosphate Coated Fluoride Phosphors for Optoelectronic Materials. *Angewandte Chemie* 2015, 54, 10862-10866.
- (4) Murphy, J. E.; Garcia-Santamaria, F.; Setlur, A. A.; Sista, S. PFS, $\text{K}_2\text{SiF}_6:\text{Mn}^{4+}$: the Red-line Emitting LED Phosphor behind GE's TriGain Technology™ Platform. *SID Symposium Digest of Technical Papers* 2015, 46, 927-930.
- (5) Huang, L.; Liu, Y.; Yu, J.; Zhu, Y.; Pan, F.; Xuan, T.; Brik, M. G.; Wang, C.; Wang, J. Highly stable $\text{K}_2\text{SiF}_6:\text{Mn}^{4+}/\text{K}_2\text{SiF}_6$ Composite Phosphor with Narrow Red Emission for White LEDs. *ACS Applied Materials & Interfaces* 2018.
- (6) Zhou, Y. Y.; Song, E. H.; Deng, T. T.; Zhang, Q. Y. Waterproof Narrow-Band Fluoride Red Phosphor $\text{K}_2\text{TiF}_6:\text{Mn}^{4+}$ via Facile Superhydrophobic Surface Modification. *ACS Applied Materials & Interfaces* 2018, 10, 880-889.
- (7) Arunkumar, P.; Kim, Y. H.; Kim, H. J.; Unithrattil, S.; Im, W. B. Hydrophobic Organic Skin as a Protective Shield for Moisture-Sensitive Phosphor-Based Optoelectronic Devices. *ACS Applied Materials & Interfaces* 2017, 9, 7232-7240.
- (8) Jiang, C.; Brik, M.; Srivastava, R. I.; Li, L.; Peng, M. Significantly Conquering Moisture-induced Luminescence Quenching of Red Line-Emitting Phosphor $\text{Rb}_2\text{SnF}_6:\text{Mn}^{4+}$ through $\text{H}_2\text{C}_2\text{O}_4$ Triggered Particle Surface Reduction for Blue Converted Warm White Light-Emitting Diodes. *Journal of Materials Chemistry C* 2018.

Luminescence properties of $\text{Y}_2\text{O}_3:\text{Bi}^{3+}, \text{Yb}^{3+}$ thin films synthesised by pulsed laser deposition and spin coating

E. Lee¹, V. Craciun², J.J. Terblans¹, H.C. Swart¹

¹Department of Physics, University of the Free State, South Africa

²Laser Department, National Institute for Laser, Plasma and Radiation Physics, Bucharest-Magurele, Romania

Corresponding author email address: LeeE@ufs.ac.za, SwartHC@ufs.ac.za

1. Introduction

One of the main factors influencing the low solar to electrical energy conversion efficiency of silicon based solar cells is due to the loss of energy due to thermalisation [1]. For many years researchers have been looking at using phosphor materials to alter the solar spectrum in order to enhance the efficiency of solar cells [2]. Although phosphor are generally available in the form of powders, they serve their greatest potential as thin films. $\text{Y}_2\text{O}_3:\text{Bi}^{3+}, \text{Yb}^{3+}$ thin films were synthesised using the pulsed laser deposition (PLD) and spin coating techniques to study their effects on the morphology and luminescence properties of the thin films. The PLD prepared thin films were deposited using two different lasers, a Nd:YAG laser (266 nm, 10 Hz and 40 mJ) and a KrF laser (248 nm, 10 Hz and 200 mJ) to investigate how the increased laser powder would affect the surface morphology of the thin films. The background gas pressure within the PLD chamber and substrate temperature were also varied to test their effects on the surface morphology and luminescence properties. The spin coating prepared thin films were synthesised with the aid of the sol-gel technique. The sol-gel preparation method was used to convert the $\text{Y}_2\text{O}_3:\text{Bi}^{3+}, \text{Yb}^{3+}$ powder into a solution, making it possible to control the viscosity of the gel solution. The thin films were characterised using X-ray diffraction (XRD), scanning electron microscopy (SEM) and photoluminescence (PL) spectroscopy.

2. Results

The XRD patterns revealed that the $\text{Y}_2\text{O}_3:\text{Bi}^{3+}, \text{Yb}^{3+}$ thin films were successfully deposited using both the PLD and spin coating methods. The patterns showed that thin films prepared using the spin coating technique crystallised as a single phase cubic structure similar to that of the initial powder sample, while films prepared using the PLD technique contained a mixture of different phases namely the single phase cubic structure and the monoclinic phase. The SEM images (Fig 1) showed that films prepared using the Nd:YAG laser were rough and consisted of round particle of varying sizes. The particles were present due to the laser ablation process, which has an explosive-like nature that causes particles to eject from the target. However, under the same parameters (background gas and substrate temperature) the KrF laser was capable of producing significantly smoother films with only a few particles present on the surface. Films prepared using the spin coating technique produced the smoothest films but suffered from poor adhesion between the film and substrate. The PL spectra indicated that the smoother films had low emission intensities as compared to the rougher films. This was due to the effect of total internal reflection, which is more prominent in smoother surfaces.

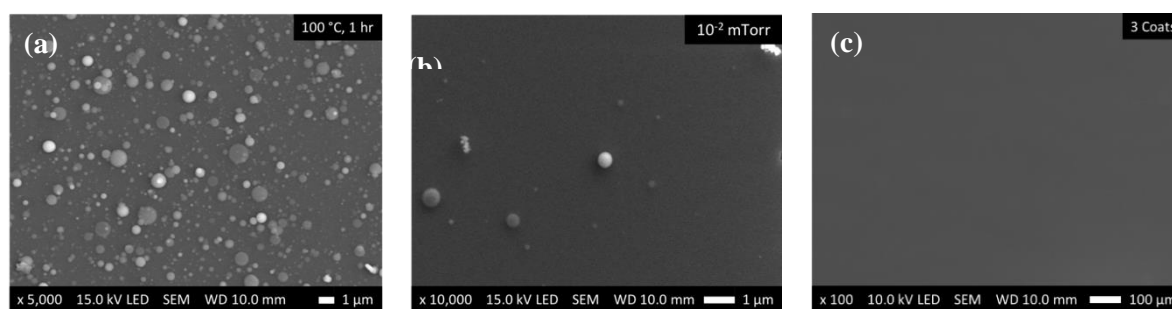


Fig 1: Surface morphology of thin films prepared using, (a) a Nd:YAG laser, (b) a KrF laser for PLD and (c) the spin coating technique.

3. References

- [1] E. Nakazawa, "Fundamentals of luminescence", in Fundamentals of Phosphors (eds. Yen, W., Shionoya, S. & Yamamoto, H.), Chapt. 1 Sec. 7, CRC Press, Taylor and Francis Group, New York, (2007)
- [2] Y. Zhydachevskii, L. Lipi, Mater. Chem. Phys., 143 (2014) 622.

Poster Abstracts - Session 1: Tuesday 18:00

Abstract	Poster	Pg	Presenting author	Title of Poster
1	1	51	Prof. ENGELBRECHT, Japie	An evaluation of theoretical and experimentally obtained values for the refractive index of $\text{In}_x\text{Ga}_{1-x}\text{As}$
2	2	52	Mr. AKINKUADE, Shadrach	Effect of thermal treatment on structural and electrical properties of NiO thin films
10	3	53	Mr. SEID, Endris Taju	Refluxed sol-gel synthesized ZnO: The effect of solvent volume ratio (Ethano:Water) on the properties of nanopowders
13	4	54	Mr. HABTE, Abebe G	Influence of annealing temperature on structural, morphological and optical properties of SnO_2 nanoparticles
15	5	55	Mr. HABTE, Abebe G	Effect of solution PH on structural, optical and morphological properties of SnO_2 prepared by Sol-gel method
16	6	56	Ms. LE ROUX, Samantha	A re-evaluation of neutron-irradiated 3C-SiC using FTIR reflectance infrared spectroscopy
17	7	57	Mrs. MALIMABE, Moipone Alice	Structural morphology, optical properties and photoluminescence of Ce^{3+} doped ZnO nano-powders co-doped with different mole % of Eu^{3+}
20	8	58	Mr. ABDURRAZAQ, Abdulgaffar	Ab initio study of hydrogen passivation in carbon and oxygen related defect complexes in silicon.
25	9	59	Mr. ALI, Abdulraoof	Synthesis and characterization of gallium nitride thin films using electrochemical deposition
26	10	60	Mr. MUNGUTI, Lawrence Kioko	Effects of Zn:Ti molar ratios on the Morphological, Optical and Photocatalytic properties of ZnO/TiO_2 Nanostructured composites for water purification
27	11	61	Mr. MUNGUTI, Lawrence Kioko	Effects of annealing Temperature on Structural and Optical properties of ZnO/TiO_2 Nanocomposites for Water Purification
28	12	62	Dr. MALEVU, Thembinkosi	The influence of post heat treatment on the morphological behavior and particle sizes of nano-crystalline TiO_2 for solar cell applications
29	13	63	Ms. TAGHIZADEH, Fatemeh	Electrical characterization of sputter deposition induced defects of Au Schottky contacts in GaAs
30	14	64	Dr. KUMAR, Vinod	Effect of oxygen partial pressure during pulsed laser deposition on defect related emission of Eu doped ZnO thin films

31	15	65	Ms. BRANDT, Leandre'	Synthesis and Characterisation of Cadmium-free CuInS/ZnS nanocrystals in combination with a [FeFe]-H ₂ ase mimic for visible light-driven H ₂ production in water
34	16	66	Dr. KUMAR, Vinod	Upconversion emission study of SrWO ₄ :Er ³⁺ -Yb ³⁺ thin films prepared by radio frequency magnetron sputtering
42	17	67	Mr. MBONGO, Mduduzi	Photoluminescence and thermoluminescence properties of ZnGa ₂ O ₄ prepared by solid-state chemical reaction
46	18	68	Dr. LEPHOTO, Mantwa Annah	Photoluminescent and Thermoluminescent properties of LiBaBO ₃ :Dy ³⁺ phosphors prepared by solid state reaction method
47	19	69	Dr. LEPHOTO, Mantwa Annah	Synthesis and photoluminescent properties of dysprosium doped BaB ₈ O ₁₃ phosphor
55	20	70	Ms. MRWETYANA, Nosicelo	Investigation of Ion Migration in Methylammonium Lead Bromide (MAPbBr ₃) Perovskite Crystals using Current Deep Level Transient Spectroscopy (I-DLTS)
		71	Prof. HOLSA, Jorma	Persistent Luminescence Excitation of BaAl ₂ O ₄ :Eu ²⁺ ,Dy ³⁺

Poster Abstracts - Session 2: Wednesday 15:15

Abstract	Poster	Pg	Presenting author	Title of Poster
57	22	72	Mr. NYARIGE, Justine	Effect of L-arginine concentration on hematite nanostructures synthesized by spray pyrolysis
58	23	73	Mr. ABDELREHMAN, Mogahid	Effect of background atmosphere and substrate temperature on SrO:Bi thin films produced using pulsed laser deposition with different lasers
59	24	74	Mr. MOFOKENG, Sefako John	Stimulated luminescence study of MgO:Al ³⁺ ,Li ⁺ prepared by solution combustion method
60	25	75	Mr. FRU, Juvet Nche	Synthesis of Methyl Ammonium Lead Tribromide Perovskite by Sequential Physical Vapour Deposition for Solar Cell Applications
64	26	76	Mr. AHMED, Mohammed	Effect of Er and Yb doping on morphology, optical and Schottky diode properties of ZnO thin films prepared by sol-gel spin coating
65	27	77	Ms. DANGA, Helga	An investigation of defects introduced in Si during sputter-deposition using deep-level transient spectroscopy
66	28	78	Mr. SELEPE, Theophilus	Green Synthesis of Metal Nanoparticles using Phycocyanin
68	29	79	Mr. TRAN, Dat	Thermal Conductivity of Ultra-Wide Bandgap Thin Layers: High-Al Content AlGaN and β -Ga ₂ O ₃
70	30	80	Ms. MATHEVULA, Langutani	Effect of Er ³⁺ on Structural and optical properties of microwave synthesized α -Fe ₂ O ₃ nanoparticles
71	31	81	Mrs. QOTSO, Angelina Seithati	Luminescence properties of P3HT-ZnO: RE ions nanoparticles: A photon up-conversion materials for organic solar cell application
72	32	82	Mr. MOJI, Rantooa	Morphology, structural and luminescent properties of sol-gel synthesized SiO ₂ :Sr:xTb nanopowders.
73	33	83	Mr. DIX-PEEK, Ross	Temperature dependence of opto-electric response of Si PV cells
76	34	84	Ms. SHINGANGE, Katekani	LaBO ₃ (B= Fe, CO) nanofibers and their structural, optical and gas sensing characteristics
82	35	85	Prof. TERBLANS, Koos	Investigations of Pd diffusion through ZrC thin films
85	36	86	Ms. PAULSEN, Zuraan	CdX (X=S, Se, Te) Quantum Dots and a Bi-Iron Chalcogenide for Hydrogen Generation

87	37	87	Dr. MAPASHA, Edwin	Electronic properties of vacancies in hydrogenated bilayer graphene
90	38	88	Mr. MOKOENA, Teboho Patrick	Transformation of 1D to 0D nickel oxide nanostructures induced by ramping rate during heat treatment: Gas sensing and luminescence properties
103	39	89	Mr. NGOEPE, PNM	Electrical characterization of swift heavy ion irradiated GaN by DLTS
		90	Prof. HOLSA, Jorma	$4f^N$ Energy Level Schemes for the Di-, Tri-, and Tetravalent Lanthanides

An evaluation of theoretical and experimentally obtained values for the refractive index of $\text{In}_x\text{Ga}_{1-x}\text{As}$

J.A.A Engelbrecht¹ and E.G. Minnaar¹, W.E. Goosen¹ and P. Kühne²

¹ HRTEM Facility, NMU, Port Elizabeth, South Africa

²Semiconductor Materials, IFM, Linköping University, Linköping, Sweden

Corresponding author e-mail address: Japie.Engelbrecht@nmmu.ac.za

1. Introduction

The binary $\text{In}_x\text{Ga}_{1-x}\text{As}$ alloy, with a bandgap that can be varied from 0.36 to 1.425 eV, finds many applications in semiconductor optical devices such as lasers, photodiodes and detectors with important applications in optical fibre communication systems [1,2]. Knowledge of the refractive index n is hence essential for the design of such optical devices. A recent literature survey yielded only limited information about the refractive index of $\text{In}_x\text{Ga}_{1-x}\text{As}$ in the infrared region, and an assessment of theoretical models to calculate the refractive index was performed [3]. Results of the theoretical models were extrapolated to the infrared range, and a preliminary indication of the value of possible theoretical models when compared to available experimental results was obtained.

The current investigation reports on a further evaluation of the refractive index of $\text{In}_x\text{Ga}_{1-x}\text{As}$ as obtained from simulations of the reflectance spectra obtained from a range of samples with varying indium content. $\text{In}_x\text{Ga}_{1-x}\text{As}$ epilayers of various compositions were grown by metalorganic chemical vapour phase epitaxial deposition (MOCVD) on n^+ and semi-insulating GaAs substrates orientated 2° off (001) towards $\langle 110 \rangle$ at deposition temperatures of 610 - 690°C. The compositions were determined using photoluminescence (PL), while layer thicknesses were determined from capacitance-voltage (CV) measurements and Nomarski interference spectroscopy [4]. Infrared reflectance spectra of the $\text{In}_x\text{Ga}_{1-x}\text{As}$ epilayers were measured using a Magma 550 FTIR spectrometer with horizontal stage reflection attachment, which allowed for near-normal angle of incidence, taking 200 scans at a resolution of 8 cm^{-1} . A front surface Al mirror was used as reference. Theoretical reflectance spectra were simulated using the multi-oscillator [5], one and two epilayers models [6]. BMPD[®], a nonlinear regression statistical software package, was employed for curve fitting to obtain the best fit between theory and experiment. These simulations allowed for an evaluation of the refractive indices obtained, while a final assessment was found from determining the epilayer thicknesses from interference fringe analysis [7].

2. Results

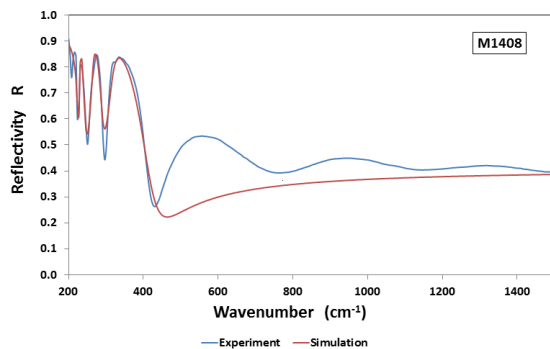


Fig. 19: Experimental reflectance spectrum of $\text{In}_{0.046}\text{Ga}_{0.954}\text{As}$ and simulated spectrum obtained from the multi-oscillator model.

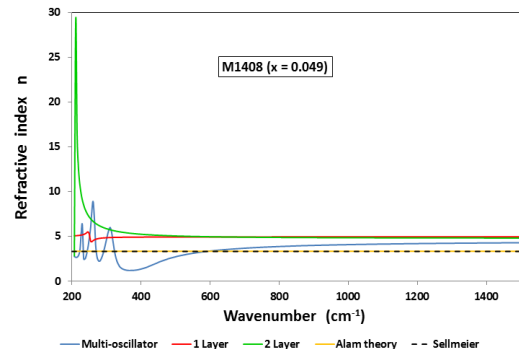


Fig. 2: Refractive index of $\text{In}_{0.046}\text{Ga}_{0.954}\text{As}$ obtained from various curve fitting models and two theoretical models.

3. References

- [1] S.L. Geelhaar, R.A. Bartynski, F. Ren, M. Schnoes and D.N. Buckley. *J. Appl. Phys.* **80** (1996) 3075.
- [2] J.C. Woolley, M. B. Thomas and A.G. Thompson. *Can. J. Phys.* **46** (1968) 157.
- [3] J.A.A. Engelbrecht. *Physica B* **535** (2018) 8.
- [4] E.E. van Dyk, PhD Thesis, University of Port Elizabeth (1992).
- [5] J. Misiewicz, A. Lemiec, K. Jezierski, J.W. Wróbel and B.P. Claymans. *Infrared Phys. & Technol.* **35** (1994) 775.
- [6] T. R. Baisitse, A. Forbes, G. Katumba, J. R. Botha, and J. A. A. Engelbrecht. *phys. stat. sol. (c)* **5** (2008) 573.
- [7] F. Reizman, *J. Appl. Phys.* **36** (1965) 3804.

Effect of thermal treatment on structural and electrical properties of NiO thin films

Shadrach Akinkuade^{1,2}, Walter Meyer¹, Jacqueline Nel¹

¹ Physics Department, University of Pretoria, Pretoria, 0002, South Africa

² Physics Unit, Science Technology Department, Federal Polytechnic, Ado-Ekiti, Nigeria

Corresponding author e-mail address: akinkuadeshadrach@gmail.com

1. Introduction

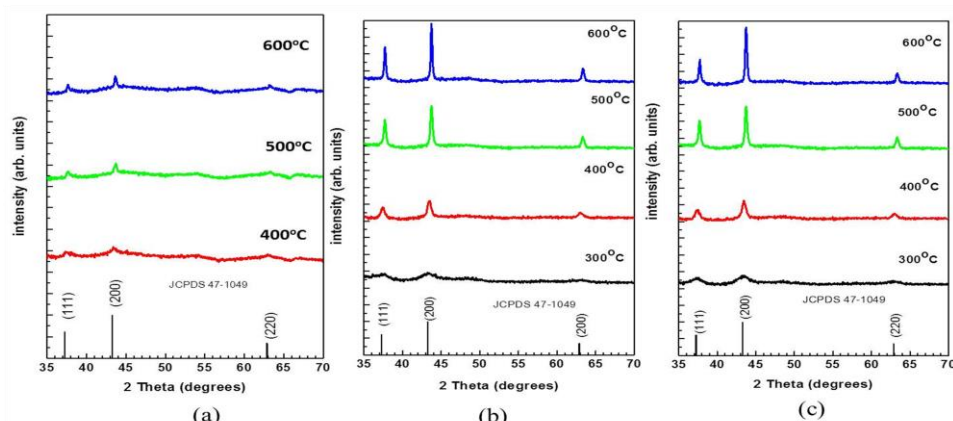
Nickel oxide (NiO) is one of the transition metal oxides, it has a wide optical band gap between 3.6 and 4.0 eV [1] and it crystallizes in the cubic rock-salt structure. Stoichiometric NiO is an insulator, it has a resistivity of about 10^{13} Ω .cm therefore has not been used extensively as a semiconductor. P-type conductivity in NiO has been attributed to nickel vacancies or oxygen interstitials. Due to interesting properties of nickel oxide such as chemical stability, wide and tunable optical band gap, transparency and p-type conductivity, it has been found suitable for use in many applications such as electrochromic display, p-type conducting oxide, active layer in chemical sensor, hole transporting layer in solar cells, ultra violet detectors, light emitting diode and photoelectrolysis.

Several methods have been used to produce thin films of nickel oxide; such methods include sputtering, thermal evaporation, electron beam evaporation, pulsed laser deposition, chemical bath deposition, sol-gel spin-coating and dip-coating and spray pyrolysis. Properties of these films that make them suitable for specific applications depend on conditions and techniques of deposition [2]. Some of the advantages of sol-gel over other methods include simplicity, low cost, low temperature of deposition and ease of control of the microstructure of the deposited film.

NiO thin films have been produced through sol-gel spin coating method by many research groups. Hydrated nickel acetate being a common precursor, 2-methoxy ethanol and monoethanolamine (MEA) are often used as solvent and stabilizer respectively. The films are usually subjected to two thermal processes during fabrication: drying to evaporate organic solvents and annealing for the transformation of precursor or any intermediate products formed during drying into NiO. Three temperature regions have been identified in the thermal decomposition of hydrated metal acetates: (a) temperature of dehydration (80 – 130°C), temperature at which intermediates are formed (105 – 230°C) and the decomposition temperature at which intermediates are converted to final products (100 – 440°C) [3]. To the best of our knowledge, there is no report on the effects of thermal processing on the properties of NiO thin films. In this study, effects of different temperature of drying and annealing on structural optical and electrical properties of nickel oxide thin films deposited on glass substrates were investigated.

2. Results

The XRD patterns of the films (a) dried at 160°C (b) dried at 200°C and (c) dried at 250°C are shown in Figure 1.



XRD patterns of the films (a) dried at 160 °C (b) dried at 200 °C and (c) dried at 250 °C.

3. References

[1] H Sato, T Minami, S Takata, and T Yamada. Transparent conducting p-type NiO thin films prepared by magnetron sputtering. *Thin solid films*, 236(1-2):27(31), 1993.

[2] Prabakaran Shankar and John Bosco Balaguru Rayappan. Gas sensing mechanism of metal oxides: The role of ambient atmosphere, type of semiconductor and gases-a review. *Sci. Lett. J*, 4:126, 2015.

[3] Theodor Schneller, Rainer Waser, Marija Kosec, and David Payne. *Chemical solution deposition of functional oxide thin films*, Springer, 2013.

Refluxed sol-gel synthesized ZnO: The effect of solvent volume ratio (Ethano:Water) on the properties of nanopowders

Endris Taju Seid¹, Francis B Dejene¹

¹ University of the free state, Physics Department, Private Bag X13, Phuthaditjhaba, 9866, South Africa
Corresponding author e-mail address: tend3000@gmail.com

1. Introduction

ZnO is a promising tunable wide band gap semiconductor for ultraviolet (UV) and visible light optoelectronics applications. Because of the simple and low production costs, ZnO nanoparticles have a lot of potentials applications for light emitting diodes (LEDs), solar cells and luminescence materials. Herein, a simple, high yield with superior quality, refluxed sol-gel method is used to prepare ZnO for solar cell application by varying the percentage of solvent volume ratio of ethanol to water from 0:1 to 1:0. It is known that solvent type and volume ratio significantly affect the morphology, structural and photo-luminescence properties of ZnO[1]. For this study XRD, SEM with EDX, UV-Vis spectroscopy and photoluminescence measurements were taken to investigate the properties of the produced material.

The size of nanocrystallite ZnO is calculated from XRD measurement results using Scherrer equation[2]

$$D = \frac{K\lambda}{\beta \cos(\theta_{\beta})} \quad (1)$$

where λ is the wavelength of the incident x-ray (1.5406 Å), K is Scherrer constant (0.9) and β is the full width at half maximum of the given plane with the corresponding angle θ_{β}

2. Results

All the prepared ZnO samples have spherical and nanorod like structures in their morphology (Fig. 1) and pure single phase hexagonal wurtzite in structure. The crystallite size varies from 23.20 to 18.68 nm by changing the amount of ethanol in solvent from 0:1 to 1:0 and the average lattice parameters are calculated as $a=0.3246$ nm and $c=0.5202$ nm. The room temperature PL spectra in Fig. 2 showed that both near bandgap emission(NBE) at around 380nm and Deep Level Emission(DLE) between 432 and 628 nm are displayed with the excitation wavelength of 248.6nm from NeCu laser source. The ratio of the intensities I_{NBE} to I_{DLE} decreases as the amount of ethanol increases in the solvent. Both NBE and DLE of the prepared ZnO samples were blue shifted and the emitted photon energy also increases from 3.23 to 3.27 eV as ethanol amount increases in the solvent. The Free and donor-bound excitonic emissions also studied using low temperature PL measurements and quantum quenching effects are observed from the results. The result from UV-Vis measurement also showed that the energy band gap increases with increase the volume of ethanol in the solvent solvent. This result also consistent with XRD results.

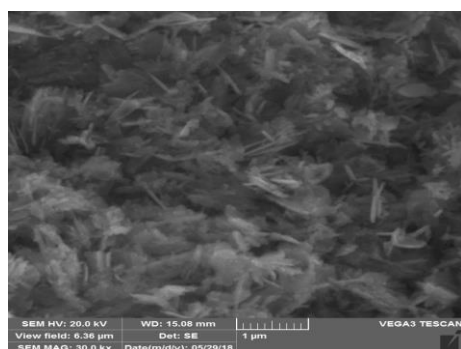


Fig. 1: SEM image of sol-gel synthesized ZnO with 0:1 ethanol to water solvent volume ratio.

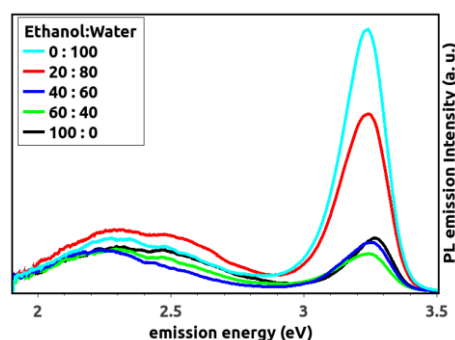


Fig. 2: PL spectra of refluxed sol-gel synthesized ZnO at varying ethanol to water solvent volume ratio.

3. References

- [1] M.Rezapour, N. Talebian, *Materials Chemistry and Physics* **129** (2011) 249
- [2] B.D. Cullity, S.R. Stock, *Elements of X-ray diffraction*, 3rd edn. (Prentice Hall, Upper Saddle River, 2001), Chap. 5.

Influence of annealing temperature on structural, morphological and optical properties of SnO₂ nanoparticles

Abebe G. Habte¹, Fekadu Gashaw Hone¹, F.B. Dejene¹

¹University of the Free State, Department of Physics (Qwa Qwa Campus), South Africa
habteabebe@gmail.com

1. Introduction

Tin oxide(SnO₂) is a wide band gap n-type semiconductor. Its unique optical and electrical properties makes it very useful in many fields such as gas sensor, lithium ion storage batteries, optoelectronic devices, etc. The practical performance of SnO₂ is dependent on its crystallinity, morphology, crystallite size, crystal defects and surface properties[1]. These properties can be tuned by varying synthesis methods and conditions. A number of factors such as solution PH, reaction time, dopant material and type of solvent affect the properties of synthesized SnO₂ nanostructures. In addition, the structure , morphology and optical properties of the tin oxide nanoparticles can be effectively modified by the process of annealing [2]. In the present work, a rutile tetragonal phase SnO₂ nanoparticles were synthesized by the reaction of SnCl₂.2H₂O in DI water via sol–gel method and the Tin oxide nanopowder was annealed at various temperatures(400⁰c-800⁰c) to investigate the modification in their properties.

$$D = \frac{k\lambda}{\beta \cos\theta} \quad (1)$$

where D is average Scherrer crystallite size; λ is X-ray wavelength ($\lambda=1.5406\text{\AA}$); k is shape factor (0.9) ; β is full width at half maximum of the diffraction peak in radians and θ is Bragg diffraction angle.

2. Results

The microstructural changes, surface morphology, compositional and optical properties of SnO₂ due to thermal annealing were studied by using different characterization techniques. The XRD result showed well crystallized single phase tetragonal rutile structure of all SnO₂ samples. The average crystalline size was calculated from the Debye-Scherrer's equation (eqn.1) and it was found to increase with increasing annealing temperature. The Williamson–Hall plot confirms the strain value decreases whereas the particle size increases with increasing annealing temperature. The obtained values for the lattice parameters a and c are in good agreement with the reported values (JCPDS card no. 72-1147). The SEM image(Fig.3) showed nearly spherical and some agglomerated nanostructures that increase in size with annealing temperature. The EDX analysis showed that our samples are purely Tin and Oxygen. Optical properties of the nanoparticle were studied by means of UV-vis spectroscopy. The band gap energies were calculated using Tauc's method and it was found to decrease from 3.68eV to 3.43eV(Fig.2) with the increase of annealing temperature. The photoluminescence measurement result revealed that both UV and visible emissions were displayed at excitation wavelength of 280nm. The PL spectra revealed five different emission bands including strong ultraviolet emission peaks at 363.7 nm and 383.7nm along with a weak band edge emission peak at 345.4nm, a violet emission peak at 410.2nm and a shoulder peak at 393.3nm.

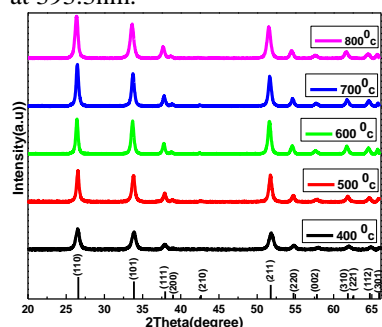


Fig. 20: The XRD pattern of SnO₂ nanoparticles annealed at different temperatures

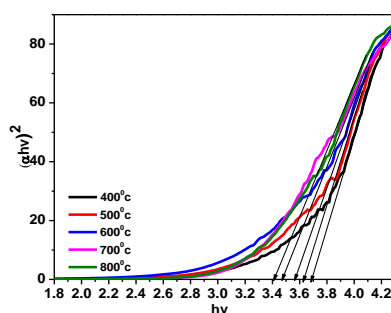


Fig. 2: variations of optical band gap with annealing temperature

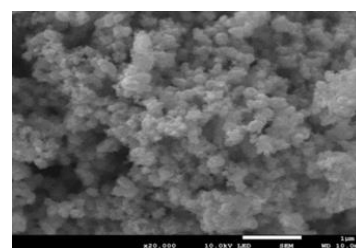


Fig. 3:SEM Image of SnO₂ nano particle annealed at 600⁰c

3. References

- [1] Y. Shirahata, T. Oku, Y. Kanamori et al. *Journal of the Ceramic Society of Japan*, **125**(2017) 145-149..
- [2] M. P. Subramaniam, G. Arunachalam, R. Kandasamy et al. *Journal of Materials Science: Materials in Electronics*, **29**(2017)658-666..

Effect of solution PH on structural, optical and morphological properties of SnO₂ prepared by Sol-gel method

Abebe G. Habte¹ Fekadu Gashaw Hone¹, F.B. Dejene¹

¹University of the Free State, Department of Physics (Qwa Qwa Campus), South Africa
habteabebe@gmail.com

1. Introduction

Tin Oxide (SnO₂) is n-type wide band gap semiconductor which possesses good electrical, optical and electrochemical properties. Due to these properties SnO₂ nanoparticles have been used for numerous practical applications such as solar cells, field-effect transistors, lithium batteries, transparent conductive electrodes, photo conductors, gas sensor etc [1]. The crystallite, morphology, crystallite size, crystal defects and surface properties influence practical performance of SnO₂. These properties can be tuned by a number of factors such as solution PH, reaction time, reaction temperature, solute concentration, dopant material type of solvent, etc. In this work, tetragonal phase polycrystalline SnO₂ nanoparticles of nearly spherical morphologies were synthesized using simple sol-gel method. The PH value of the solution was varied from 6-11 and its influence on structural, morphological and optical properties of SnO₂ nanoparticles was studied.

$$\frac{1}{d_{hkl}^2} = \frac{h^2 + k^2}{a^2} + \frac{l^2}{c^2} \quad (1)$$

Where d_{hkl} is the inter planer spacing given by the Bragg's law ($n\lambda = 2d_{hkl} \sin(\theta_{hkl})$). n is the order of diffraction (usually n = 1 for first order and h, k and l are Miller indices).

2. Results

The XRD result indicated that all samples were well crystallized tetragonal rutile structure with strong peaks of (110), (101) and (211) plane. The lattice parameters (a=b, and c) for the tetragonal phase structure was calculated from the XRD peaks using equation (1). These values are in good agreement with the reported values (JCPDS card no. 72-1147). The SEM image (Fig.2) showed nearly spherical and some agglomerated nanostructures which changes with the PH of the solution. The average crystalline size was calculated from the Debye-Scherrer's formula and it was found to increase with increasing PH of the solution. When the solution PH increases further to 11.6 the crystal size was found to decrease. The optical properties of the nanoparticle were characterized by means of UV-vis spectroscopy. The band gap energies were calculated using Tauc's method and it was found to decrease when the PH increases. The observed variation of the band gap is attributed to the structural defects arisen during synthesis of SnO₂ nanoparticles, giving rise to the allowed energy states near the conduction band. The EDX analysis showed that our samples are purely Tin and Oxygen. Room temperature photoluminescence measurements are made at an excitation wavelength of 280 nm. The PL spectra showed strong and weak emission peaks in the UV and Visible regions. These peaks are attributed to a recombination of free excitons and defect energy levels originated due to oxygen vacancies and Tin interstitials present in the band gap [2].

3.

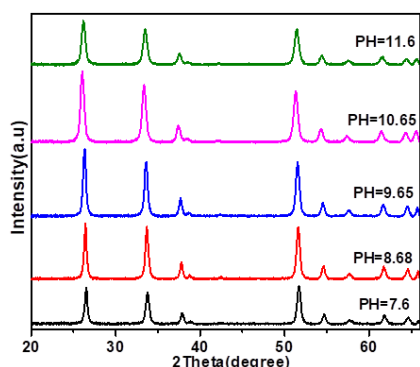


Fig. 21: The XRD patterns of SnO₂ nanoparticles synthesized at different solution PH

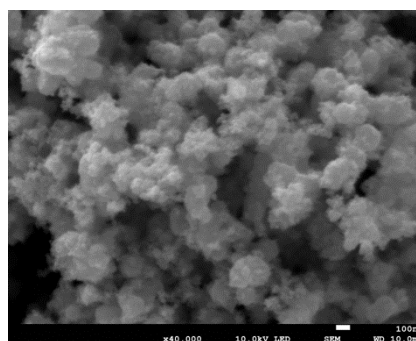


Fig 2. SEM image of nanocrystalline SnO₂ samples at solution PH of 9.65

References

- [1] D. Singh, V. S. Kundu, and A. S. Maan, *Journal of Molecular Structure*, **1115**(2016) 250-257..
- [2] L. C. Nehru, V. Swaminathan, and C. Sanjeeviraja, *American Journal of Materials Science*, **2**(2012) 6-10.

A re-evaluation of neutron-irradiated 3C-SiC using FTIR reflectance infrared spectroscopy

S. Le Roux¹, J.A.A Engelbrecht², E.G. Minnaar² and WE Goosen²

¹Physics Department, NMU, ²CHRTEM, NMU, Port Elizabeth, South Africa
Corresponding author e-mail address: Japie.Engelbrecht@mandela.ac.za

1. Introduction

3C-SiC is used as containment layer in the TRISO particles used in the new generation nuclear reactors [1]. It is a potential material for wall protection of fusion reactors due to its chemical and environmental inertness as well as its impeccable irradiation stability [2]. The knowledge of the contributing factors to the reflectivity of such SiC wafers is imperative for the understanding of the operating tendencies of these wafers in nuclear reactors. IR reflectivity data was obtained to observe any existing trends when 3C-SiC is irradiated at various fluences and irradiation temperatures.

The ongoing investigation reports on the assessment of the reflectivity spectra obtained for 3C-SiC samples of various neutron fluence and irradiation temperatures and their reflectivity of electromagnetic radiation and if there exists any correspondence to the grain size of the sample irradiated. Sample reflectivity, surface roughness and grain size were all measured both prior and post-polishing of the samples. Analysis of data preliminary suggests that for the initial samples tested, that a trend persists between average grain size and maximum reflectivity of the sample. While no coherent trend exists between reflectivity and irradiation temperature, nor between reflectivity and fluence. Measurements of maximum reflectivity were performed using Bruker 80V FTIR/Raman spectrometer taking 32 scans at 8cm⁻¹ resolution. Grain size determination was performed using a Scanning Electron Microscope and surface roughness determination was performed using CSM Instruments Nano-indenter fitted with an atomic force microscope (AFM). Testing for similar trends is underway for additional samples.

2. Results

Reflectivity as a function of irradiation temperature and surface roughness (post-polishing), alongside the relationship between average grain size and reflectivity is shown in Figure 1.

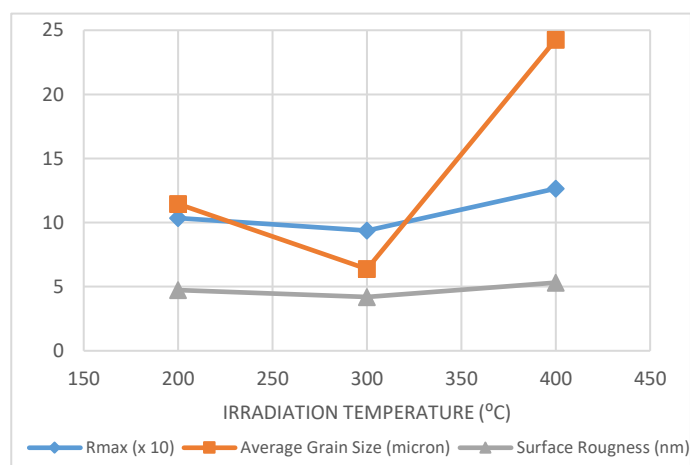


Figure 22 - Correlations between maximum reflectivity and surface roughness, grain size as a function of irradiation temperature. V-shaped curves for both maximum reflectivity and average grain sizes indicated a coherency between the two.

3. References

- [1] W. Wacholz, *International Working Group on Gas-Cooled Reactors (IWGGCAR)*, Vol. 19 (1998) p.61.
- [2] T. Hinoki, Y. Katoh, L.L. Snead et al, *Silicon Carbide and Silicon Carbide Composites for Fusion Reactor Application*. Material Transactions, Vol. 54, No.4 (2013) pp.472-276.

Structural morphology, optical properties and photoluminescence of Ce³⁺ doped ZnO nano-powders co-doped with different mole % of Eu³⁺

Moipone A. Malimabe¹, Lehlohonolo F. Koao¹, Setumo V. Motlounge², Tshwafo E. Motaung³

¹Department of Physics, University of the Free State (Qwaqwa campus), Private Bag X13, Phuthaditjhaba, 9866, South Africa

²Department of Physics, Nelson Mandela University (NMU), P. O. Box 77000, Port Elizabeth 6031, South Africa

³Department of Chemistry, University of Zululand, Private Bag X1001, KwaDlangezwa 3886, South Africa

Corresponding author e-mail address: mokoename@ufs.ac.za

1. Introduction

Rare earth elements like europium (III) are important in this study of doping zinc oxide (ZnO) nanoparticles because they can efficiently adjust their electrical, optical and luminescence properties, and result in various applications of ZnO based nano particles [1]. ZnO semiconductors are of much interest because of its attractive optical properties based on its direct wide band gap of 3.37 eV. Undoped ZnO, Eu³⁺ or Ce³⁺ doped and co-doped were synthesized by chemical bath deposition method (CBD) at synthesis temperature of 80 °C and the entire sample were annealed at 800 °C for two (2) hrs using furnace.

2. Results

The co-doped ZnO powders have the aggregated flower-like particles making it to have irregular particle structures. UV-Vis reflectance spectroscopy displays a slight red shift in singly doped ZnO with reference to undoped ZnO. The photoluminescence results showed that undoped ZnO exhibit luminescence band around 620 nm. The emissions decreased with Ce³⁺ doping while increased with Eu³⁺ doping. The peaks observed at around 580, 533 and 465 nm might be due to the respective electronic transitions of ⁵D₀ → ⁷F₀, ⁵D₀ → ⁷F₁, ⁵D₀ → ⁷F₂ and ⁵D₀ → ⁷F₄ that correspond to the Eu³⁺ intra-4f transitions presence. The luminescence of the co-doped nanoparticles were more efficient at lower excitation wavelengths of 217 and 386 nm.

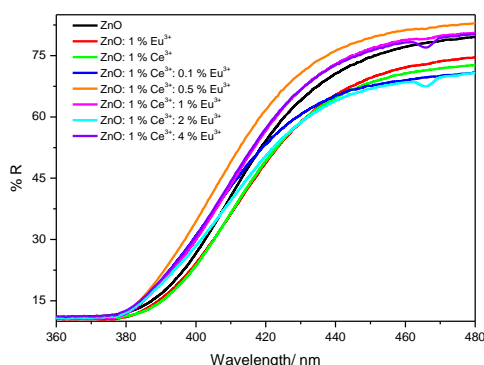


Figure 23. UV-Vis reflectance spectra of ZnO, ZnO:1 % Ce³⁺ and Eu³⁺ doped ZnO co-doped with various concentrations of Eu³⁺

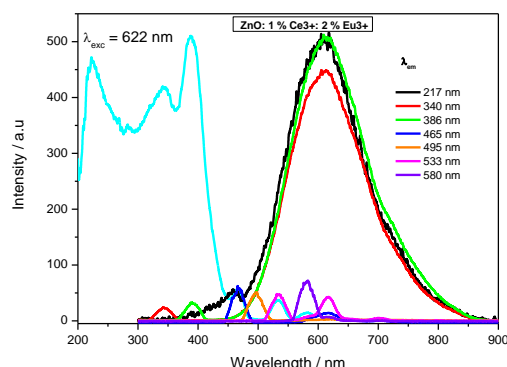


Figure 24. PL spectra excitation ($\lambda_{exc} = 622$ nm) and emissions of ZnO: 1 % Ce³⁺: 2 % Eu³⁺ at various excitation

3. References

[1] B. Mercier, C. Dujardin, G. Ledoux, et al, J. Appl. Phys, **96** (1) (2004) 650.

[2] L. F. Koao, F. B. Dejene, S.V. Motlounge, H. C. Swart and T. E. Motaung, Opt. Mater, **60** (2016) 294-304

Ab initio study of hydrogen passivation in carbon and oxygen related defect complexes in silicon.

Abdulgaffar Abdurrazaq¹ and Walter E. Meyer

*Department of Physics University of Pretoria, Pretoria 0002, South Africa.
Corresponding author e-mail address: abdulfulbe@gmail.com*

1. Introduction

Carbon and oxygen complexes are common defects in silicon and are well investigated by DLTS as well as studied theoretically by means of density functional theory (DFT) using the generalized gradient approximation. However, some of these defects were not yet investigated by means of hybrid functional. In this work we used DFT with the Heyd, Scuseria and Ernzerhof hybrid functional to investigate the formation energy, binding energy, and the thermodynamic transition energy levels of the O_iH_i , $C_iO_iH_i$, $C_sC_iH_i$, C_sO_i , and $C_sO_iH_i$ defect complexes.

2. Results

All the complexes had positive binding energy for the neutral charge states, indicating that the defects are stable. We found that the oxygen interstitial was more stable at the bond center, while the hydrogen interstitial had a lower energy in the tetrahedral site and was found to shift the defect levels to the conduction band, thereby passivating the defects. The results were compared with the available experimental data and a reasonable agreement was found.

For O_iH_i (1/0) and (0/-1) as found at $E_C - 0.08$ eV and at $E_C - 0.36$ eV which was compared to the measured value of (1/0) and (0/-1) at $E_C - 0.17$ eV and at $E_C - 0.68$ eV [1]. For $C_iO_iH_i$ (0/-1) defect level was at $E_V + 0.28$ eV which is very close to the same level measured at $E_V + 0.38$ eV [1]. For $C_sC_iH_i$ defect (1/2) defect level was calculated at $E_V + 0.19$ eV, and for C_sC_i (0/-1) is measured at $E_V + 0.79$ eV [2], for C_sC_i there is no any donor level reported but when hydrogen is passivated the acceptor levels disappears and a donor level appears as above. For C_sO_i with the oxygen at the bond center (1/2) and (0/-1) defect levels are calculated at $E_V + 0.06$ eV and $E_V + 0.89$ eV, but when hydrogen is introduced the (1/2) and (0/-1) defect levels shift to $E_V + 0.26$ eV and $E_V + 0.95$ eV. Finally for C_sO_i with the oxygen at the tetrahedral site (1/0) defect level was calculated at $E_V + 0.67$ eV and when hydrogen is introduced the (1/0) defect level shifts to $E_V + 0.9$ eV.

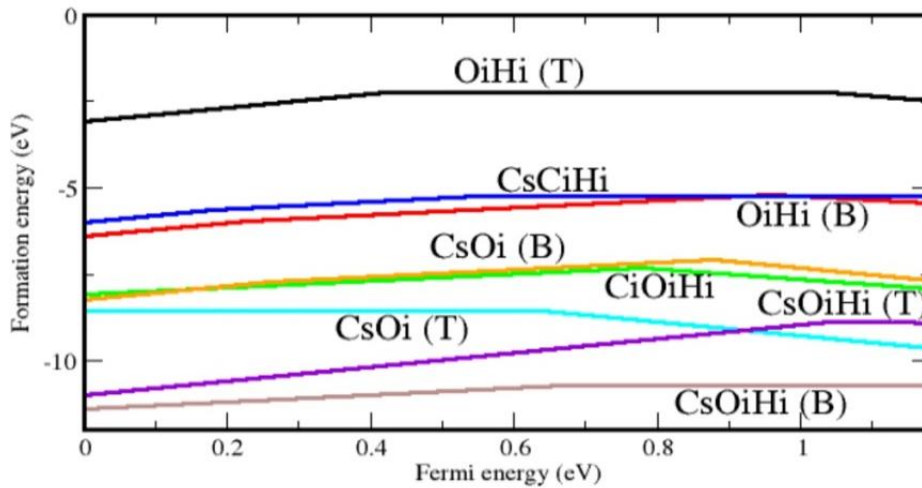


Fig. 25: The thermodynamic stable region of the defect complexes as a function of Fermi energy is presented above (The formation energies are calculated at zero Fermi energy).

3. References

- [1] Santos P, Coutinho J, Oberg S, Vaqueiro M, Markevich P, Halsall P, Peaker R. *Physica Status Solidi (a)*, 2017 **214** (7) 1700309.
- [2] C. N. Ouma, W. E. Meyer. *Computational Material Science*, **118** (2016) 338-341

Synthesis and characterization of gallium nitride thin films using electrochemical deposition

Abdulraoof Ali^{1,2}, Helga T. Danga¹, Jacqueline M. Nel¹, Walter E. Meyer¹

¹University of Pretoria, Private Bag X20, Hatfield 0028, South Africa

²Univesity of Elimam Elmahdi, Kosti White Nile, Sudan

Corresponding author e-mail address: abdulraoof34@gmail.com, u18374710@up.ac.za

1. Introduction

Group III-nitride semiconductor materials such as GaN, AlN and InN are promising materials since their properties are ideal for use in optoelectronic devices, high power and high temperature electronic devices. These materials have wide energy band gaps between 1.9 to 6.3 eV and, for electronic applications, these materials are usually synthesised by means of chemical vapour deposition or molecular beam epitaxy, however, recently K. al-Heuseen and M.R. Hashim (J. Cryst. Growth **324** 274 (2011)) investigated room-temperature electrochemical growth. In this study, room temperature electrochemical deposition has been used to synthesis GaN on Si (100) as well as ITO glass with the aim to determine its electrical properties. Different voltages and deposition times were used with a mixture of gallium nitrate and ammonium nitrate as electrolyte.

2. Results

The XRD results of GaN thin films grown under the different conditions are shown in Figure 1. Sample *a* and *b* were prepared at room temperature at an electrodeposition current of 3 mA for 3 and 12 hours respectively. Sample *c* was prepared at room temperature at 2 mA for 3 hours. The XRD analysis showed the presence of hexagonal and cubic structure with crystallite sizes ranging from 130 to 600 nm. Figure 2 and 3 depict the AFM and SEM images, however, the results varied with growth conditions and substrate.

The band gap of the thin films as determined by UV-vis spectroscopy varied from 3.30 eV to 3.48 eV. Resistivity, as determined by four point probe measurements varied from 1.2×10^{-3} to 9×10^{-4} ohm.cm. Good quality Schottky diodes could be fabricated on the material and DLTS measurements were performed. Figure 4 shows the DLTS spectrum of a sample grown on Si before and after irradiation by α -particles.

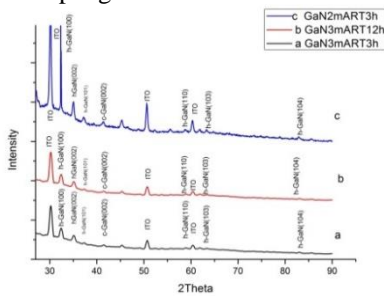


Figure 1: XRD spectrum for samples *a*, *b* and *c*.

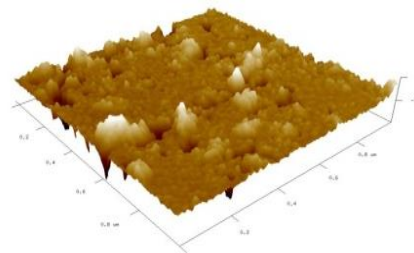


Figure 2: The AFM image of Sample *a* deposited at 3mA for 3 hours and the roughness is 80.4 nm

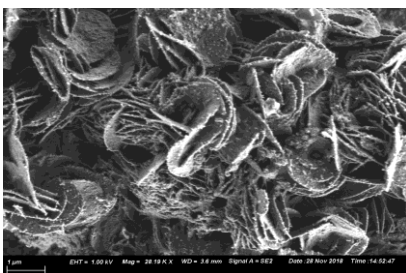


Figure 3: SEM image of the GaN thin film deposited on a Si substrate at 3mA for 30 minutes.

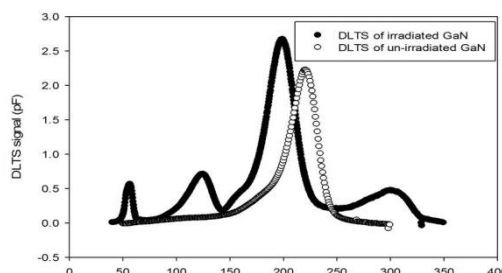


Figure 4: DLTS spectra of un-irradiated GaN and irradiated GaN on Si deposited by electrochemical deposition.

Effects of Zn:Ti molar ratios on the Morphological, Optical and Photocatalytic properties of ZnO/TiO₂ Nanostructured composites for water purification

Lawrence Munguti^{1,2}, Francis Dejene²

¹ University of the Free State QwaQwa Campus Department of Physics private Bagx13
Phuthaditjhaba 9866

² University of the Free State QwaQwa Campus Department of Physics private Bagx13
Phuthaditjhaba 9866

Corresponding author e-mail address: mungutimunlak@yahoo.com

1. Abstract

ZnO/TiO₂ nanostructured composites were synthesized via the facile sol-gel route in varying molar-based sol ratios of ZnO/TiO₂ ranging 1:3, 1:2, 1:1, 2:1 and 3:1 (v/v) leading to gel formation and subsequent drying at 100°C for 2 hours. A similar synthesis procedure was applied for pure TiO₂ as well as bare ZnO nanoparticles for comparison purposes. The nano-structural crystallinity measurements for the powder were determined by the XRD diffraction technique for $20^\circ \leq 2\theta \leq 70^\circ$ whereas the Scanning Electron Microscopy (SEM) was used for the analyses of the nanomorphological images for grain size and shape. Further characterization on the samples was done by various techniques such as the Diffuse Reflectance UV-vis Spectroscopy (DRS) for the reflectance data in $200\text{nm} \leq \lambda \leq 600\text{nm}$ range, the Photoluminescent (PL) emission spectroscopy and the Fourier Transform Infra-Red (FT-IR) for the molecular vibrational bending modes the range $400\text{--}4000\text{ cm}^{-1}$. The obtained Physicochemical characterization results indicated a direct influence of Zn:Ti ratio on the Microstructural, Morphological, Optical properties as well as the Photodegradation performance of the composites. The XRD revealed a strong peak at $2\theta = 24.96^\circ$ indicating crystallization of the TiO₂ anatase phase with more peaks at 31.77, 34.42 and 36.25 corresponding to the ZnO wurtzite structure thus a confirmation of the mobilization of ZnO nanoparticles on TiO₂. The crystallite size estimated by FWHM ranged between 40 to 50 nm which agreed with the values in literature. The SEM images for the lone ZnO revealed aggregates of ZnO granules while those of TiO₂ had smaller particles with enlarged conglomerates. Obvious, ZnO/TiO₂ composite was an express combination of both ZnO and TiO₂ morphologies. Further study carried on the particle distribution of TiO₂ particles in the mixture of aggregated ZnO granules noted that as the ratio approached ZnO:TiO₂ = 1:3, the TiO₂ particles gained fairly uniform distribution with uniform spherical shapes. The elemental composition per atomic percentages was further confirmed via the Energy Dispersive X-ray Spectroscopy (EDX). This was supported by the FT-IR analyses as evidence of strong hybridization of the composites. Compared to either the pure ZnO or TiO₂ samples, the composites revealed a stronger absorption in UV combined by a slight shift towards the visible range and a variation of band gap depended on the ratio of Zn to Ti attaining $E_g = 3.24\text{eV}$ for Zn:Ti = (1:3). The composites showed enhanced photocatalytic degradation compared to either bare TiO₂ or pure ZnO with the highest activity being ZnO:TiO₂ = 1:4. This is as a result of the band gaps for ZnO and TiO₂ being nearly similar at 3.37eV and 3.2 eV respectively, meaning a possible electrons transfer from the ZnO conduction band to that of TiO₂ with concurrent hole transfer from TiO₂ valence to that of ZnO hence efficient charge separation and reduced recombination thus increased charge carrier life time.

2. Results

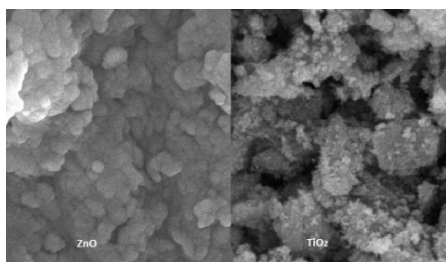


Fig. 26: SEM image for bare ZnO (left) and TiO₂ (right)

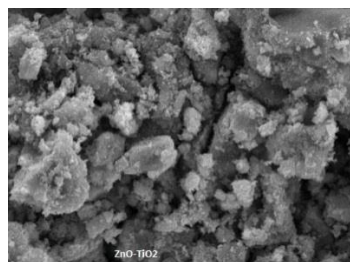


Fig. 2: SEM image for ZnO/TiO₂ nanocomposite

3. References

- [1] C. Ashok and K. V. Rao. *Superlattices and Microstructures*. **76** (2014) 46–54.
- [2] I. Fatimah and Novitasari. *IOP Conf. Ser.: Mater. Sci. Eng.* **107** (2016) 012003

Effects of annealing Temperature on Structural and Optical properties of ZnO/TiO₂ Nanocomposites for Water Purification

Lawrence Munguti^{1,2}, Francis Dejene²

¹ University of the Free State QwaQwa Campus Department of Physics private Bagx13
Phuthaditjhaba 9866

² University of the Free State QwaQwa Campus Department of Physics private Bagx13
Phuthaditjhaba 9866

Corresponding author e-mail address: mungutimunlak@yahoo.com

1. Introduction

Optimized ratios Zn:Ti (1:3) of ZnO/TiO₂ nanocomposites were synthesised via the sol-gel technique by direct mixing of ZnO and TiO₂ sols at room temperature, followed by gelation, ageing and subsequent drying. Heat treatment was done by annealing the samples at temperatures; 500°C, 600°C, 700°C and 800°C. The structural changes provoked by thermal treatment at different temperatures were characterized by the X-ray Diffraction (XRD) Spectroscopy for phase detection, Scanning Electron Microscopy (SEM) for grain size and surface morphology as well as the Energy Dispersive X-ray Spectroscopy (EDX) for the percentage elemental composition. Optical properties were determined by Diffuse Reflectance UV-vis Spectroscopy (DRS) while the Photoluminescence Emission spectroscopy (PL) used detect defects hence quality of the samples. The photodegradation mechanisms were carried out by determination of the decomposition rate of Methyl Orange (MO) dye through decrease in absorbance peak intensity with time. XRD revealed the crystalline phases for both ZnO and TiO₂ indicating hybridization for the two composites. Further, annealed samples observed more intense peaks due to temperature induced crystallization compared to as-deposited. SEM results for annealed powders at different temperatures differed from as-synthesised in their surface morphology namely grain size and shape. Different ZnO/TiO₂ heat treated systems at various temperatures reveal agglomerates with spherical primary particles of less than 100 nm with less distinct edges compared to those annealed at $\geq 600^\circ\text{C}$. The nature of the composites as depicted by EDX portrayed the expected elemental percentages at a lower temperature with alteration that may be attributed to carbon decomposition of solvent remnants for post annealed at 600°C, 700°C and 800°C. The reflectance spectra for ZnO-TiO₂ resembled that of ZnO and TiO₂ with sharp decrease in spectra at about 367nm and 380nm owing to the individual fundamental absorption band edges with a slight shift in optical absorption edge at about 380nm redshifted for the ZnO and blue shifted with respect to TiO₂ absorption edges. Compared to as-synthesised, annealed composites revealed a slight decrease in band gap with lowest as 3.18eV most probably attributed to Zn tuned E_g of highly concentrated TiO₂ in the composite. Photodegradation of MO conducted by the application of the composite powder under UV irradiation indicated enhanced performance with increase in calcination temperatures. This could be attributed to increased surface area with annealing temperatures associated with spheroid shape of the grain in line with SEM results.

2. Results

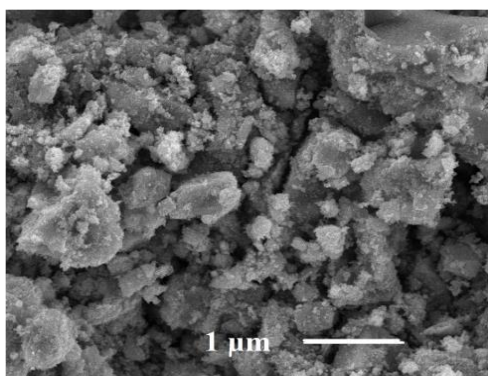


Fig. 27: SEM image for ZnO/TiO₂ nanocomposite annealed at 500°C

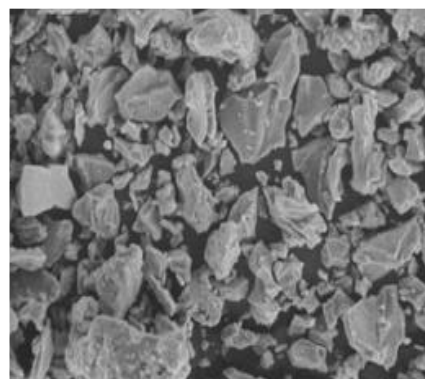


Fig. 2: SEM image for ZnO/TiO₂ nanocomposite annealed at 600°C

3. References

- [1] C. Ashok and K. V. Rao. *Superlattices and Microstructures*. **76** (2014) 46–54.
- [2] J. Wang, W. Mi, J. Tian, J. Dai, X. Wang, and X. Liu. *Composites: Part B*. **45** (2013) 758–767
- [3] T. Ivanova, A. Harizanova, T. Koutzarova, and B. Vertruyen. *Journal of Non-Crystalline Solids*. **357** (2011) 2840–2845

The influence of post heat treatment on the morphological behavior and particle sizes of nano-crystalline TiO₂ for solar cell applications

Malevu TD

School of Chemistry and Physics, Westville Campus, University of KwaZulu-Natal, Private Bag X54001, Durban 4000, South Africa

Corresponding Author: MalevuT@ukzn.ac.za

1. Introduction

The current, high interest in the nanostructures of titanium dioxide (TiO₂) is being driven in part by the abundance of low cost processing methods, which have been shown to impact the resultant morphology, and in part by the fact that a given technology device may perform better when built using a given morphology. The importance of morphology-differentiated behavior is only now being understood. For these reasons, TiO₂ nanostructures are finding applications in photocatalytic processes, photovoltaic and photonic and other sensors [1–3]. In the present work, we have successfully synthesized TiO₂ nanocrystals that have exposed {001} and {101} facets using a hydrothermal method. The influence of post heat treatment on the morphological behavior, particle sizes and thermal stability was investigated.

2. Results

In this study, four samples having different morphologies were used. It was found that the micrographs suggest that synthesized nanostructures are good candidates for solar cell applications because large crystalline islands and the associated large, spatial gaps are thought to improve film uniformity and quality over wider expanses of the surface. Fig. 1 shows SEM images of TiO₂ structures of annealed at 600 °C with exposed {001} and {101} and Fig. 2 shows the corresponding HR-Tem images. Other physical properties like crystal structure, chemical and optical the properties including XRD, PL, UV-Vis transmittance and absorbance will be discussed.

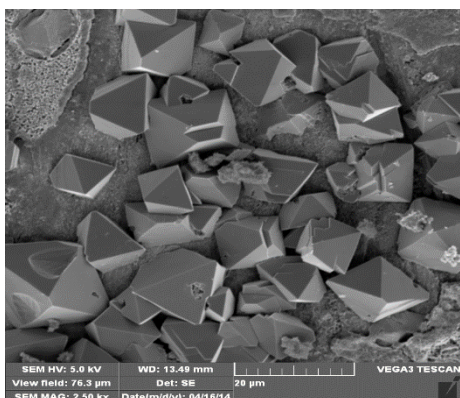


Fig.1: SEM image of TiO₂ structures.

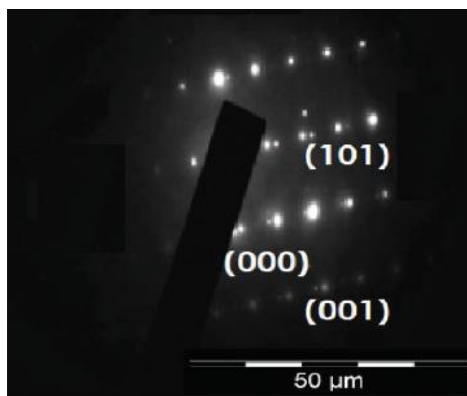


Fig.1: HR TEM image of TiO₂ with exposed {001} and {101} facet

References

- [1] J. Yan, G. Wu, N. Guan, L. Li, Z. Li, X. Cao, Understanding the effect of surface/bulk defects on the photocatalytic activity of TiO₂: anatase versus rutile, *Chem. Phys. Lett.* 15 (26) (2013) 10978–10988.
- [2] J.D. Peng, P.C. Shih, H.H. Lin, C.M. Tseng, R. Vittal, R. Suryanarayanan, K.C. Ho, TiO₂ nanosheets with highly exposed (001)-facets for enhanced photovoltaic performance of dye-sensitized solar cells, *Nanomater. Energy* 10 (26) (2014) 212–221.
- [3] Y. Wang, J. Liu, M. Wang, C. Pei, B. Liu, Y. Yuan, S. Liu, H. Yang, Enhancing the sensing properties of TiO₂ nanosheets with exposed (001) facets by a hydrogenation and sensing mechanism, *Inorg. Chem.* 56 (3) (2017) 1504–1510.

Electrical characterization of sputter deposition induced defects of Au Schottky contacts in GaAs

Fatemeh Taghizadeh, P. J. Janse van Rensburg, W. E. Meyer and F. D Auret

¹ Department of physics, University of Pretoria, Private Bag X20, Hatfield 0028, Pretoria
Corresponding author e-mail address: F.Taghizadeh@tuks.co.za

1. Introduction

The Au Schottky contacts were sputter deposited on Si-doped n-type GaAs at a power of 150 W at Ar pressure of 8×10^{-2} mbar with a DC bias for 5 minutes, for two different carrier density samples ($1.0 \times 10^{15} \text{ cm}^{-3}$ and $1.0 \times 10^{16} \text{ cm}^{-3}$). The diode properties were studied by I - V and C - V measurements. The electrical properties of the sputter induced defects were measured by DLTS and Laplace DLTS.

2. Results

From DLTS spectra we observed five defects (S1, S3, S4, S5 and S6) as shown in Fig. 1, however from Laplace DLTS results we found that there are six defects because one of them have two components, which we labeled S6a and S6b. According to the results there are three defects which are metastable (S1, S3 and S5). From the Arrhenius plots we calculated the energy levels and apparent capture cross sections of all defects, found that these defects do not have same origin as electron irradiation induced defects. Interestingly, two of the metastable defects (S3 and S5) are similar to sputter-etching induced defects reported by Venter *et al.* [1] and nitride encapsulation [2]. The depth profile, electric field (Fig. 2) and real capture cross section measurements were performed to characterize the electrical properties of these defects.

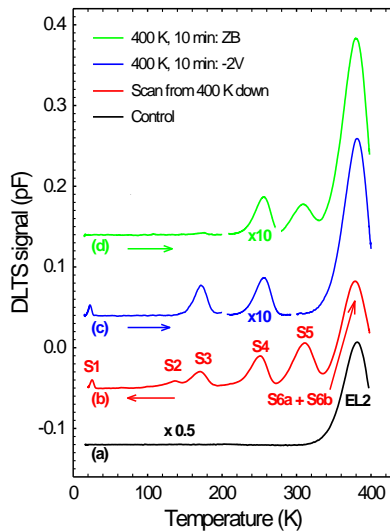


Fig. 28: DLTS spectra of control sample and sputtered sample under different bias condition

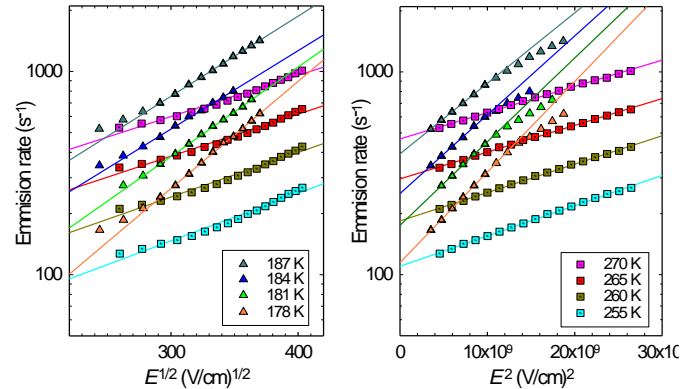


Fig. 2: The electric field of S3 and S4 defects

3. References

- [1] A. Venter *et al.*, "Ar plasma induced deep levels in epitaxial n-GaAs," *J. Appl. Phys.*, vol. 111, no. 1, p. 013703, Jan. 2012.
- [2] W. R. Buchwald, G. J. Gerardi, E. H. Poindexter, N. M. Johnson, H. G. Grimmeiss, and D. J. Keeble, "Electrical and optical characterization of metastable deep-level defects in GaAs," *Phys. Rev. B*, vol. 40, no. 5, pp. 2940–2945, Aug. 1989.

Effect of oxygen partial pressure during pulsed laser deposition on defect related emission of Eu doped ZnO thin films

Vinod Kumar^{1,2*}, O.M. Ntwaeaborwa³ and H.C. Swart²

¹ Centre for Energy Studies, Indian Institute of Technology Delhi, New Delhi 110016, India

² Department of Physics, University of the Free State, P.O. Box 339, Bloemfontein, ZA 9300, South Africa

³ School of Physics, University of the Witwatersrand, Private Bag X3, Wits, 2050, South Africa

Corresponding Author Email:- vinod.phy@gmail.com

1. Introduction

Zin oxide (ZnO) is a wide band gap material with advantages such as large exciton binding energy, high conductivity, high thermal stability in hydrogen plasma atmosphere and high chemical/physical stability [1]. ZnO thin films have been deposited with a number of different techniques such as atom beam sputtering, pulse laser deposition (PLD), radio frequency magnetron sputtering and sol-gel spin coating. Among these techniques, the PLD is preferable and provides unique growth of oxide material due to the oxygen plasma created by the pulsed laser, is very energetic and its density is easily controllable by the oxygen pressure [2]. Doping of ZnO with selective elements has become an important route for enhancing and tuning optical, electrical, and magnetic properties, which are usually crucial for their practical applications. It is well known that rare earth (RE) ions are better candidates as luminescent centres because their special 4f intra-shell transitions usually have rich spectral lines. The density of the oxygen vacancy in ZnO was easily controlled by varying the oxygen partial pressure during film deposition. In this work, we investigated the effect of oxygen partial pressure during PLD on the structural, morphological and optical properties of ZnO:Eu³⁺ thin films. A new approach is reported in this work by controlling the oxygen vacancy in the ZnO and by merging the red emission of Eu³⁺ for white light application.

2. Results

The XRD peaks of ZnO:Eu³⁺ films prepared by the PLD technique at different oxygen partial pressures were found to be oriented along the (002) plane. This is in line with the characteristics of the hexagonal ZnO wurtzite structure where the c-axis is perpendicular to the substrate plane. The three dimension atomic force microscopy (AFM) images of the ZnO:Eu³⁺ films deposited at different oxygen partial pressures on the Si (100) substrates are shown in Fig. 1. The surface roughness of the ZnO:Eu³⁺ thin film changed severely with a change in the partial pressure during the deposition of the films by PLD. The defect related emission due to oxygen vacancy/interstitial varied with oxygen partial pressure during deposition of the films, as confirmed by photoluminescence results. The oxygen partial pressure influenced the structural and optical properties of ZnO due to the oxygen defects in the ZnO thin films and is directly correlated to the deposition partial pressure [3].

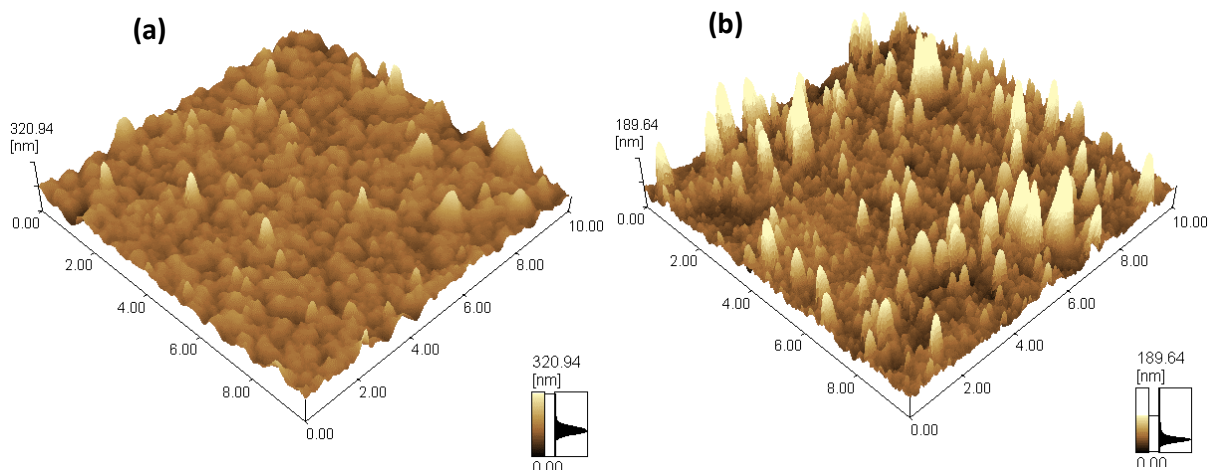


Fig. 29: The effect of oxygen partial pressure on the morphology of ZnO:Eu³⁺ thin films prepared by

3. References

- [1] V. Kumar, O.M. Ntwaeaborwa, T. Soga, V. Dutta and H.C. Swart, *ACS Photonics* **4** (2017) 2613.
- [2] Y.J. Shin, L. Wang, Y. Kim, H.H. Nahm, D. Lee, J. Ra. Kim, Sang, M. Yang, J.G. Yoon, J. S. Chung, M. Kim, S. H. Chang and T. Won Noh, *ACS Appl. Mater. Interfaces* **9** (2017) 27305.
- [3] C.H. Min, S. Cho, S.H. Lee, D.Y. Cho, W.G. Park, J.G. Chung, E. Lee, J.C. Lee, B. Anass, J.H. Lee, C.S. Hwang and S.J. Oh, *Appl. Phys. Lett.* **96** (2010) 201907.

Synthesis and Characterisation of Cadmium-free CuInS/ZnS nanocrystals in combination with a [FeFe]-H₂ase mimic for visible light-driven H₂ production in water

Leandre Brandt^{1,2}, Martin Onani², Ebbe Nordlander²

¹University of the Western Cape 1, Department of Chemistry, Private Bag X17, Bellville, 7535, South Africa.

²Lund university 2, Chemical Physics, PO-Box 124, Lund 221 00.

Corresponding author e-mail address: 2807256@myuwc.ac.za

1. Introduction

The conversion of solar energy of water into clean fuel hydrogen (H₂) is a promising approach for sustainable energy production and storage. Molecular hydrogen (H₂) is considered an ideal candidate as an energy carrier to be used as an alternative to fossil fuels. In nature, natural hydrogenases (H₂ases) have unique active sites with earth abundant elements (such as Fe, Ni) able to catalyze the reversible reduction of protons to H₂ with remarkable catalytic activity. By mimicking nature, scientists have been working hard to develop artificial photosynthetic systems using [FeFe]-H₂ase mimics for photocatalytic H₂ generation. Most photocatalytic systems for the H₂ evolution consist of a photosensitizer, a catalyst, and a sacrificial electron donor to provide electrons. [FeFe] hydrogenases are known to have very high catalytic activity. For these reasons and due to the fact that the synthetic chemistry is relatively well established, we focus on the catalysis process of [FeFe] hydrogenases for sustainable production of hydrogen. The challenge is to overcome the troublesome negative reduction potential of [FeFe]-H₂ase mimics for proton reduction [1]. In addition, typically photosensitizers are based on rare and expensive transition metal complexes with insufficient stability during photocatalysis to achieve high performances [1].

Quantum dots display unique size-dependant optoelectronic properties, high photostability, broad absorption in the visible domain, multiple exciton effects and efficient charge separation,[14-16] have been recently combined with [FeFe]-H₂ase mimics. However, most systems most of these “hybrid” systems use toxic and heavy metal-based quantum dots such as CdS, CdSe and CdTe, limiting their practical utilization. A promising alternative is to replace these molecular photosensitizers with semiconductor nanocrystals and to employ them in combination with noble metal-free H₂-evolving catalysts. CIS QDs are very well-suited for visible light-driven photocatalysis with a band gap of 1.55 eV for the bulk, a broad size-tunable absorption spectrum in the UV-visible range combined with a high absorption coefficient and long-living excitons [2-3].

In this work, we have investigate a hybrid assembly for photocatalytic H₂ evolution in water with CuInS/ZnS QDs as visible-light-absorbing photosensitizers for photocatalytic H₂ generation in combination with a molecular [FeFe]-H₂ase mimics H₂-evolving catalyst.

2. Results

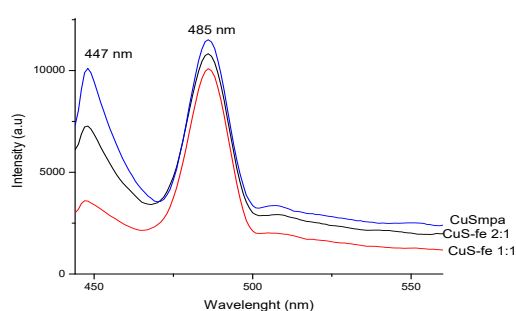


Fig. 30: PL emission spectra of CuInS, and CuInS-Fe assembly nanocrystals, recorded in water/dcm at room

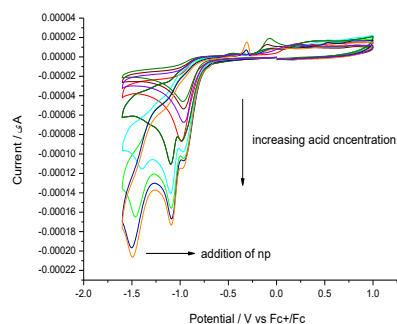


Fig. 2: CVs of a [Fe₂S₂(CO)₆] in the presence of acid of 1–10 molar equivalents, scan rate 0.25 V/s, glassy carbon electrode.

3. References

- [1] W.-J. Liang, F. Wang, M. Wen, J.-X. Jian, X.-Z. Wang, B. Chen, C.-H. Tung, L.-Z. Wu, *Chem. Eur. J.* **21**, (2015), 3187-3192.
- [2] M. D. Regulacio and M.-Y. Han, *Acc. Chem. Res.*, (2016), **49**, 511–519
- [3] A. M. Smith, S. Nie, *Acc. Chem. Res.* (2010), **43**, 190-200.
- [4] S. Kundu, A. Patra, *Chem. Rev.* (2017), **117**, 712-757.

Upconversion emission study of SrWO₄:Er³⁺-Yb³⁺ thin films prepared by radio frequency magnetron sputtering

Anurag Pandey^{1#}, Vinod Kumar^{1,2}, R. E. Kroon¹, H. C. Swart^{1#}

¹Department of Physics, University of the Free State, P. O. Box 339, Bloemfontein 9300, South Africa

²Centre for Energy Studies, Indian Institute of Technology Delhi, New Delhi 110016, India

[#]Corresponding authors e-mail address: anuragpandey439@gmail.com (Anurag Pandey)
swarthc@ufs.ac.za (H. C. Swart)

1. Introduction

Upconversion (UC) films are widely used in photovoltaic cells, optical storage discs and luminescent screens for optically written displays [1]. Several attempts have been made to develop UC luminescence films using different preparation techniques with various lanthanide activated materials. In this study, SrWO₄:Er³⁺-Yb³⁺ thin films were prepared by the radio frequency (RF) magnetron sputtering method. Previously we reported UC emission characteristics of SrWO₄:Er³⁺-Yb³⁺ powder phosphor for optical thermometry [2]. The strong visible emission excited by near infrared (NIR) excitation of this phosphor, prepared by the solid state technique, encouraged the present study. Thin film deposition by RF magnetron sputtering is cost-effective and produces controlled uniform deposition over the entire surface. High purity (99.9-99.99%) precursors WO₃, SrCO₃, Er₂O₃ and Yb₂O₃ (purchased from Sigma Aldrich) were used to prepare SrWO₄:Er³⁺-Yb³⁺ powder which was used to make a target for producing the thin films. The base pressure was 9.6×10^{-6} Torr and the chamber was back filled with argon gas to a pressure of 3.7×10^{-2} Torr. The RF power was varied from 160 to 240 W and the deposition time was fixed.

2. Results

The prepared films were characterized by X-ray diffraction (XRD), atomic force microscopy (AFM) and UC photoluminescence (PL). The XRD study showed the tetragonal phase of SrWO₄ with improved crystallinity at higher RF power. The 3D AFM images of the films prepared at different RF powers are shown in Fig. 1. The images demonstrate the homogeneity of the grains on the surface and the increase of grain size with RF power. The UC emission spectra of the films prepared at different RF powers were measured under identical conditions upon 980 nm laser excitation as shown in Fig. 2. Three emission bands were observed and assigned to the ²H_{11/2}/⁴S_{3/2}→⁴I_{15/2} (two green bands) and ⁴F_{9/2}→⁴I_{15/2} (one red band) transitions of Er³⁺ ions. By comparing the UC spectra, the maximum intensity was observed in the case of the 240 W RF power. The origin of the green and red UC emissions is explained on the basis of pump power dependence and a schematic energy level diagram.

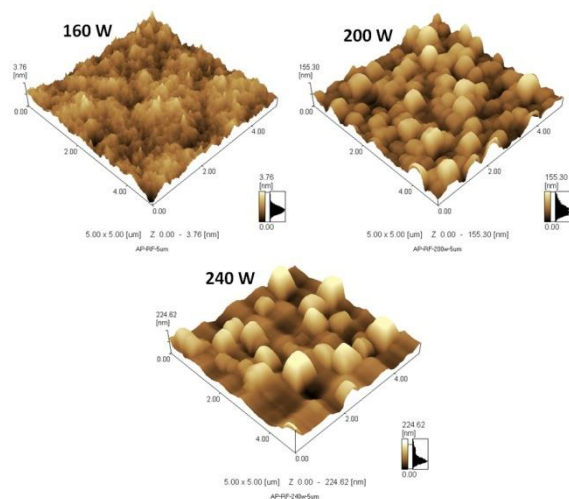


Fig. 31: 3D AFM image of SrWO₄:Er³⁺-Yb³⁺ thin films prepared at 160, 200 and 240 W RF powers.

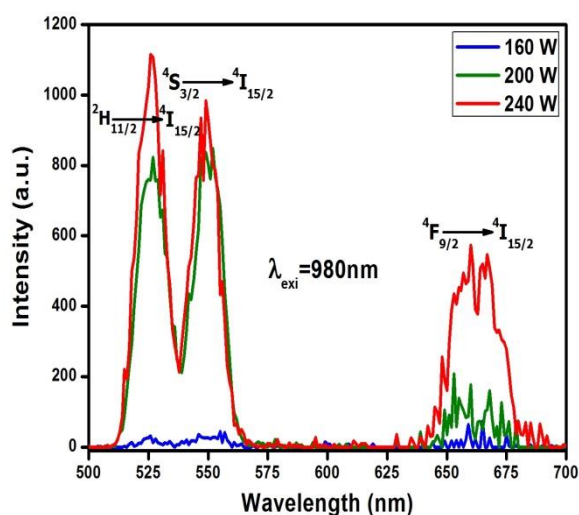


Fig. 2: Comparison of UC emission spectra of SrWO₄:Er³⁺-Yb³⁺ thin films prepared at different RF powers.

3. References

- [1] R. Elleuch, R. Sahli, J.-L. Deschanvres, and R. Maalej. *RSC Adv.* **5** (2015) 60246.
- [2] A. Pandey, V. K. Rai, V. Kumar, V. Kumar and H. C. Swart. *Sensor Actuat. B-Chem.* **209** (2015) 352.

Photoluminescence and thermoluminescence properties of ZnGa₂O₄ prepared by solid-state chemical reaction

Mduduzi Mbongo, Luyanda Noto

University of South Africa, Private Bag X90, Florida, 1710, South Africa

Corresponding author e-mail address: mbongomdu@gmail.com, notoll@unisa.ac.za

1. Introduction

Recently, Zinc Gallate (ZnGa₂O₄) with a cubic spinel structure has been an attractive rare earth free phosphor material, due to its stable luminescent properties in the blue and ultraviolet region. It has a bandgap energy of 4.4–5.0 eV [1]. ZnGa₂O₄ exhibits superior chemical and thermal stability under high electric field and high vacuum conditions, and it is explored for wide applications ranging from vacuum fluorescent display (VFDs), field emission displays (FEDs) to electroluminescent devices (ELDs) [2]. The luminescence of the material, originates from the corner sharing GaO₆ with an appreciable number of defects, which lead to the displayed defect emission [3]

In this work we employed solid-state chemical reaction technique to synthesize ZnGa₂O₄ particles, and they were produced by mixing/milling stoichiometric amounts of ZnO and Ga₂O₃ ingredients followed by thermal treatment at 1200 °C for 8 hours. Optical properties were propped using the UV-vis-NIR absorption, Photoluminescence (PL) and Thermoluminescence (TL) spectroscopic techniques. The band gap of 4.68 eV was approximated from diffuse reflectance spectra using the Kubelka-Munk model. Thermoluminescence measurements were carried out and proved that the electron trapping and detrapping mechanism followed the general-order kinetics. Several methods were used to determine the depth of the electron trapping centres.

2. Results

The X-ray diffraction pattern (Fig. 1) showed that ZnGa₂O₄ was successfully synthesized into a single phase, with the diffraction peaks corresponding to JCPDS 38-140 card number. Fig. 2 presents a 3-D emission spectrum of ZnGa₂O₄ recorded after exciting the sample with several different wavelengths. The spectra show two broad peaks; a strong blue emission centered at 528 nm and a relatively weaker peak centered at 704 nm. The Blue emission originates from self-activation center of Ga-O octahedral group.

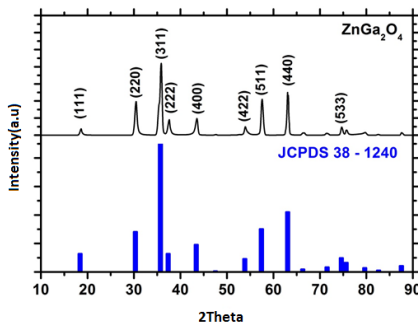


Fig. 32: X-ray diffraction pattern of ZnGa₂O₄ prepared by solid-state chemical reaction at 1200 °C for 8 hrs.

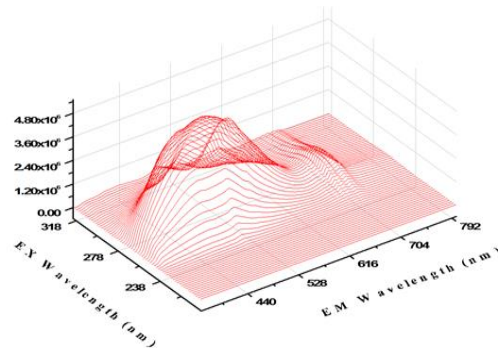


Fig. 2: 3-D Photoluminescence emission spectrum of ZnGa₂O₄.

3. References

- [1] N. Li, P. Zhu, Y. Chen, X. Duan, F. Yu. *Surfaces and Interfaces* 10 (2018) 129-135
- [2] C.S. Kamal, S. Boddu, B. Vishwanadh, K.R. Rao, V. Sudarsan, R.K. Vatsa. *J of Luminescence* 188 (2017) 429-435
- [3] L.L. Noto, D. Poelman, V.R. Orante-Barron, H.C. Swart et al. *Physica B* 535 (2018) 268-271

Photoluminescent and Thermoluminescent properties of $\text{LiBaBO}_3:\text{Dy}^{3+}$ phosphors prepared by solid state reaction method

M.A Lephoto¹, M.S Dhlamini¹, K.G Tshabalala², S.J Motloung² and O.M Ntwaeaborwa³

¹Department of Physics, University of South Africa, Private Bag X90, Florida, 1710, South Africa

²Department of physics, University of the Free State, QwaQwa campus, Private Bag X13, Phuthaditjhaba, 9866, South Africa

³School of physics, University of the Witwatersrand, Private Bag 3, Wits, 2050, South Africa

Corresponding author e-mail address: dunkie86@gmail.com

1. Introduction

Considering the growing importance of energy saving and environmental friendliness, rare-earth ions (RE) and transition metal ions-doped phosphors have attracted extensive research interest. This is because they are efficient luminescent materials and widely used in light-emitting devices such as plasma display panels (PDPs), field emission display (FEDs), fluorescent lamps (FLs) and white light emitting diodes (WLEDs) [1, 2]. WLEDs are considered to be next generation solid state lighting devices owing to their merits of high energy efficiencies, long operation lifetime, lower power consumption and eco-friendliness [2]. This study, is aimed at investigating the luminescent properties (photoluminescence and thermoluminescence) of Dy^{3+} ions in borate host lattices. During the past years, there was an upsurge of using borates as host lattices for phosphors because of their large band gap, high thermal and chemical stability, high luminescence efficiency and low cost [3].

$\text{LiBaBO}_3: x\text{Dy}^{3+}$ ($x = 0.003, 0.005, 0.009, 0.01, 0.03$ and 0.05) powder phosphors were prepared by solid state method at $800 \pm 10^\circ\text{C}$, for ~ 5 hours in air. The resulting powder phosphors were then characterized using different techniques.

2. Results

The PL emission spectra of $\text{LiBaBO}_3: x\text{Dy}^{3+}$ ($x = 0.003, 0.005, 0.009, 0.01, 0.03$ and 0.05) powder phosphors excited at 354 nm are shown in Fig. 1. In addition to the well-known sharp lines peaked at 482 nm (blue) and 575 nm (yellow), a minor line emission at 664 nm (red). These peaks are associated with the transitions of Dy^{3+} from the excited state ${}^4\text{F}_{9/2} - {}^6\text{H}_{15/2}$, ${}^4\text{F}_{9/2} - {}^6\text{H}_{13/2}$ and ${}^4\text{F}_{9/2} - {}^6\text{H}_{11/2}$, respectively. The highest PL intensity was observed from $\text{LiBaBO}_3: x\text{Dy}^{3+}$ ($x = 0.01$) powder phosphor. The TL glow curves of $\text{LiBaBO}_3: x\text{Dy}^{3+}$ ($x = 0.01$) powder phosphor under different heating rates of $2^\circ\text{C}/\text{sec}$, $4^\circ\text{C}/\text{sec}$ and $6^\circ\text{C}/\text{sec}$ at constant UV exposure time of 5 min are shown in Fig. 2. It can be seen that with the increase in the heating rate from $2^\circ\text{C}/\text{sec}$ - $6^\circ\text{C}/\text{sec}$ the peak intensities of the TL glow curves decreases. Also a shift in the peak towards the higher temperature side is observed with the increase in the heating rate. This behaviour in the TL glow curve may be due to the well-known effect of thermal quenching of TL due to the increase in the heating rate.

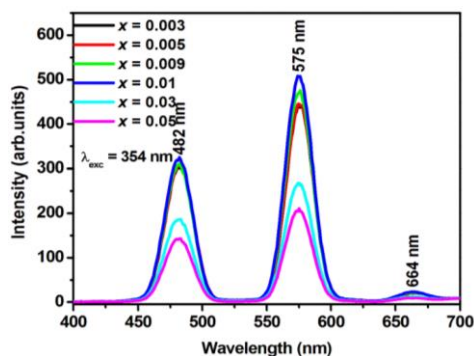


Fig. 33: PL emission spectra of the $\text{LiBaBO}_3: x\text{Dy}^{3+}$ ($x = 0.003, 0.005, 0.009, 0.01, 0.03$ and 0.05) powder phosphors.

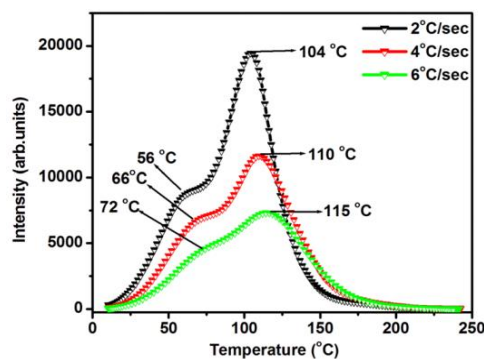


Fig. 2: TL glow curve of $\text{LiBaBO}_3: x\text{Dy}^{3+}$ ($x = 0.01$) powder phosphor for different heating rates.

3. References

- [1] R. Yu, S. Zhong, N. Xue, H. Li and H. Ma. *RSC*, **00** (2013) 1.
- [2] J. Sun, Z. Lian, G. Shen and D. Shen, *RSC*. **3** (2013) 18395.
- [3] Y. Fan, Y. Hu, L. Chen, X. Wang and G. Ju. *Physica B*. **450** (2014) 99.

Synthesis and photoluminescent properties of dysprosium doped BaB₈O₁₃ phosphor

M.A Lephoto¹, M.S Dhlamini¹, K.G Tshabalala² and O.M Ntwaeaborwa³

¹Department of Physics, University of South Africa, Private Bag X90, Florida, 1710, South Africa

²Department of physics, University of the Free State, QwaQwa campus, Private Bag X13, Phuthaditjhaba, 9866, South Africa

³School of physics, University of the Witwatersrand, Private Bag 3, Wits, 2050, South Africa

Corresponding author e-mail address: dunkie86@gmail.com

1. Introduction

In recent years, rare earth ion doped inorganic luminescent materials have been extensively studied in the fields of materials science, physics, chemistry and life sciences due to their various potential applications in light emitting devices [1]. Among these applications, white light emitting diodes (w-LEDs) have been considered to be the next generation illumination sources in the field of solid-state lighting instead of traditional incandescent and fluorescent lamps due to their numerous advantages such as small size, high energy efficiency, robustness, high brightness, fast switching, longer life time (>100000 h) and environmental friendliness [2]. Nowadays, single-phase full-color phosphors are being developed as sources of white in LEDs. White light emission resulting from a single-phase phosphor is expected to obtain high luminous efficacy in comparison with that from two or three phosphors, because it does not show multi-phosphors re-absorption of emission colors. Therefore, single phase white-emitting phosphors are required for UV-pumped w-LEDs to improve the luminescence reproducibility and efficiency [3]. In this work, photoluminescent properties of BaB₈O₁₃ doped dysprosium was studied in order to be used as a potential in single phase white-emitting phosphors.

BaB₈O₁₃: xDy³⁺ powder phosphors were prepared by solution combustion method using urea (CH₄N₂O) as a fuel. The powders were prepared at 600°C and annealed for 5 hours in a muffle furnace at 800°C. The resulting powders were then characterized using different techniques.

2. Results

PL excitation and PL emission spectra of BaB₈O₁₃: xDy³⁺ ($x = 0.005$) powder phosphors are shown in Fig. 1. The excitation spectrum consists of several peaks in the range of 250 – 500 nm obtained by monitoring the emission at 574 nm. The excitation peak at 350 nm corresponding to the ⁶H_{15/2} → ⁶P_{7/2} transition was found to be dominant among the other 4f-4f transition peaks in the excitation spectrum. The emission spectrum of BaB₈O₁₃: xDy³⁺ ($x = 0.005$) powder phosphor under the excitation of 350 nm shows two intense emission peaks at 480 nm and 574 nm, and other less intense peaks at 661 nm and 752 nm. The blue emission at 480 nm and yellow emission at 574 nm are due to ⁴F_{9/2} → ⁶H_{15/2} and ⁴F_{9/2} → ⁶H_{13/2} transitions of Dy³⁺, respectively. The PL emission spectrum of BaB₈O₁₃: xDy³⁺ ($x = 0.005$) powder phosphor excited by 325 nm He-Cd laser is shown in Fig. 2. The spectrum consists of a broad band in the range of 360 – 465 nm, which is attributed to the self-trapped exciton (STE) emission of BaB₈O₁₃ host. Intense emission peaks located at 478 nm and 572 nm together with the less intense peaks located at 660 nm and 751 nm were observed. These observed results indicate that the BaB₈O₁₃: xDy³⁺ phosphor shows potential application in NUV white LEDs.

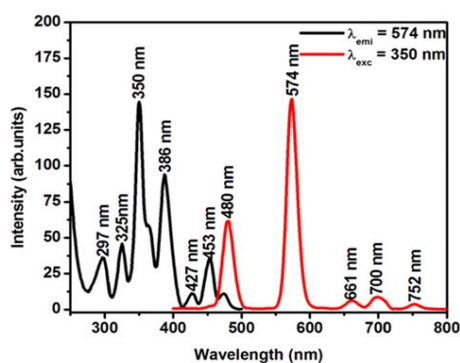


Fig. 34: PL excitation and PL emission spectra of BaB₈O₁₃: xDy³⁺ ($x = 0.005$) powder phosphor.

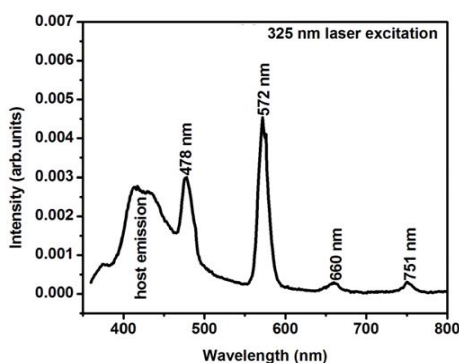


Fig. 2: PL emission spectrum of BaB₈O₁₃: xDy³⁺ ($x = 0.005$) powder phosphor excited by 325 nm He-Cd laser.

3. References

- [1] A. K. Vishwakarma, K. Jha, M. Jayasimhadri, B. Sivaiah, B. Gahtoria, b and D. Haranath. *Dalton Trans.* **44** (2015) 1716.
- [2] S. H. Lee, L. K. Bharat and J. S. Yu. *J. Alloy. Compds.* **726** (2017) 698.
- [3] Z. Zhang, X. Sun, L. Liu, Y. Peng, X. Shen, W. Zhang and D. Wang. *Ceram Int.* **39** (2013) 1723.

Investigation of Ion Migration in Methylammonium Lead Bromide (MAPbBr₃) Perovskite Crystals using Current Deep Level Transient Spectroscopy (I-DLTS)

Nosicelo Mrwetyana¹, Matshisa J. Legodi¹ and Mmantsae Diale¹

¹Department of Physics, University of Pretoria, Private Bag X20, Hatfield 0028, South Africa
Email: mrwetyana.nosicelo@gmail.com

1. Introduction

In recent years, halide perovskites (HAPs) solar cells have seen tremendous improvements in certified power conversion efficiency (PCE) with reported values over 22% [1]. Despite this rapid development, there are many unresolved issues such as the identification and characterization of defects aiding or deleterious to device performance. This dearth of knowledge is inhibiting the commercialization of HAP solar cells. The migration of ionic species in HAPs influences the degradation of perovskite solar cells, and in turn, their PCE, long-term reliability and robustness [2]. Other influences are ferroelectric and charge-trapping effects that produce the switchable photovoltaic effect observed by Xiao et al [3].

We investigated ion migration in methylammonium lead bromide C/MAPbBr₃/Au solar cells in the dark using current-mode Deep Level Transient Spectroscopy (DLTS) in the temperature range 240 K < T < 310 K and for various bias pulse sequences.

2. Results

Figure 1 shows multi-exponential decay curves which we modelled as double-exponentials. We constructed Arrhenius plots from the data and determined ion migration activation energies for the various ion species. We observe an atypical temperature dependency of the current transients: fast transients at low temperature and slower ones at elevated temperatures. In addition, characteristic features typical of ion migration such as light and bias sensitivity, hysteresis accompanying temperature cycling were also observed in the solar cells. The ion transport mechanisms in the C/MAPbBr₃/Au perovskite crystals agree with observations by Eames et al [2] in the MAPbI₃ analogue. We conclude that the fast exponential corresponds to the migration of the negatively charged halide species, Br⁻, with activation energy of 0.44 eV; and, the slower exponential is due to the positively charged methylammonium (MA⁺) species with activation energy of 0.84 eV.

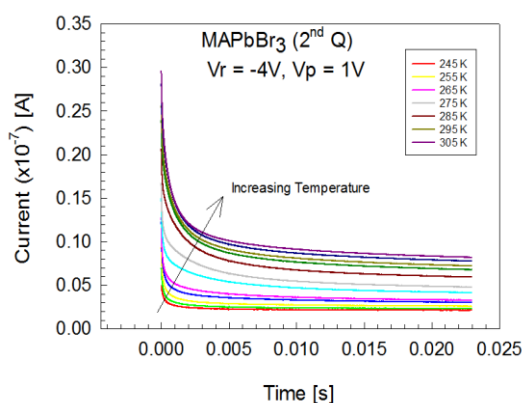


Fig. 1: Typical current transients from MAPbBr₃ (sample 2nd Q) crystals under -4V reverse bias and 1V forward bias for a duration of 10 ms recorded at various temperatures.

3. References

- [1] Nrel.gov. (2019). Photovoltaic Research | NREL. [online] Available at: <https://www.nrel.gov/pv/assets/pdfs/pv-efficiency-chart.20190103.pdf> [Accessed 24 Jan. 2019].
- [2] Eames, C., Frost, J., Barnes, P., O'Regan, B., Walsh, A. and Islam, M. (2015). Ionic transport in hybrid lead iodide perovskite solar cells. *Nature Communications*, 6(1).
- [3] Xiao, Z., Yuan, Y., Shao, Y., Wang, Q., Dong, Q., Bi, C., Sharma, P., Gruverman, A. and Huang, J. (2014). Giant switchable photovoltaic effect in organometal trihalide perovskite devices. *Nature Materials*, 14(2), pp.193-198.

Persistent Luminescence Excitation of BaAl₂O₄:Eu²⁺,Dy³⁺

Marja Malkamäki¹, Adrie J.J. Bos², Pieter Dorenbos², Mika Lastusaari¹, Lucas C.V. Rodrigues³, Hendrik C. Swart⁴, Jorma Hölsä^{4,5,*}

¹ University of Turku, Department of Chemistry, and Turku University Centre for Materials and Surfaces, FI-20014 Turku, Finland

² Delft University of Technology, Faculty of Applied Sciences, 2628 CN Delft, the Netherlands

³ University of São Paulo, Institute of Chemistry, BR-05508-000 São Paulo, SP, Brazil

⁴ University of the Free State, Department of Physics, Bloemfontein ZA-9300, South Africa

⁵ Polish Academy of Sciences, Institute of Low Temperature and Structure Research, PL-50-422 Wrocław, Poland

*Corresponding Author E-mail address: jholsa@utu.fi

1. Introduction

BaAl₂O₄:Eu²⁺,Dy³⁺ is the heaviest but the least efficient persistent luminescent material in the MAAl₂O₄:Eu²⁺,R³⁺ series. Low efficiency may be due to the hygroscopic host material and/or polymorphic structure [1] which may deteriorate the persistent excitation and emission changing the trap structure thus shortening the persistent duration. The 3D persistent excitation spectroscopy may through more light on the persistent properties of BaAl₂O₄:Eu²⁺,Dy³⁺ under β and UV irradiation than the simple thermoluminescence (TL) measurements.

2. Results

Charging of the persistent luminescence of BaAl₂O₄:Eu²⁺,Dy³⁺ is rather fast a process: a steady state can be achieved already after 30 s. Deconvolution of the TL glow curves (Fig. 1) yields a single trap with a depth of 0.8 eV after UV and β irradiation. Results agree well with studies on the BaAl₂O₄:Eu²⁺,Dy³⁺ materials prepared with solid state and combustion methods [2]. The irradiation of BaAl₂O₄:Eu²⁺,Dy³⁺ with 200 to 500 nm UV-vis radiation has no effect on the shape of the TL glow curves consisting still only of a single band centered at 57 °C (Fig. 2). The excitation spectra show little fine structure though at least two bands can be observed at 280 and 330 nm (max) with a shoulder at 380 nm. This structure may be due to the splitting of the ²D excited level of Eu²⁺. The use of free solar energy for excitation in visible is thus limited. The 3D TL emission spectra show only one broad band at 500 nm despite two Ba²⁺ sites. The BaAl₂O₄:Eu²⁺,Dy³⁺ materials are interesting persistent phosphors though UV excitation is required. The relatively shallow trap at 0.8 eV yields weak and short persistent luminescence at room temperature. A stable crystal structure would be an advantage as is the case with the analogous CaAl₂O₄ / SrAl₂O₄ hosts.

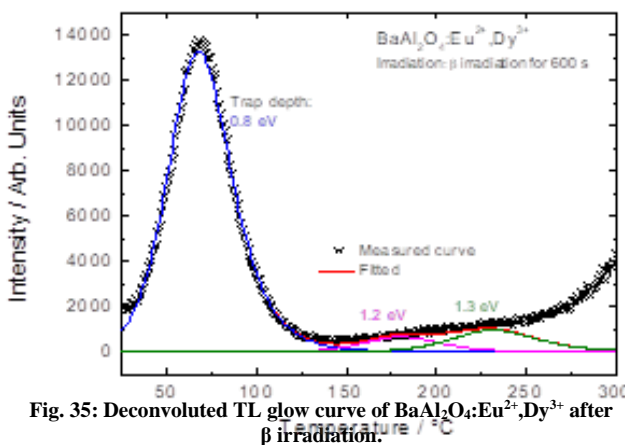


Fig. 35: Deconvoluted TL glow curve of BaAl₂O₄:Eu²⁺,Dy³⁺ after β irradiation.

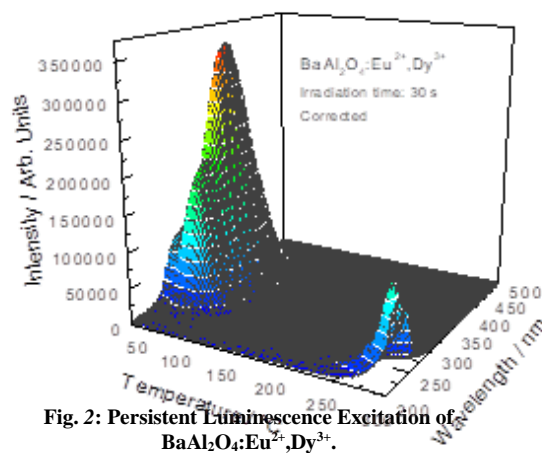


Fig. 2: Persistent Luminescence Excitation of BaAl₂O₄:Eu²⁺,Dy³⁺.

References

- [1] J. Hölsä, H.C. Swart, L.C.V. Rodrigues, H.F. Brito, M. Lahtinen, and M. Lastusaari. ESTAC-11, Aug. 17-21, 2014, Espoo, Finland.
- [2] L.C.V. Rodrigues, R. Stefani, H.F. Brito, M.C.F.C. Felinto, J. Hölsä, M. Lastusaari, T. Laamanen, and M. Malkamäki. *J. Solid State Chem.* **183** (2010) 2365.

Effect of L-arginine concentration on hematite nanostructures synthesized by spray pyrolysis

Justine Nyarige¹, Tjaart P. J. Krüger², Mmantsae Diale¹

^{1,2}Department of Physics, University of Pretoria, Private bag X20, Hatfield, 0028, South Africa

justine.nyarige@gmail.com, mmantsae.diale@up.ac.za

1. Introduction

Hematite has been reported as a good semiconductor photocathode for photoelectrochemical cells used in water splitting. This is because of its small optical band gap of 1.9 eV-2.2 eV, non-toxicity, stability in aqueous solutions, low cost of production and abundance [1]. However, hematite has some limitations which are related to electrical conduction. This includes low conductivity, fast recombination rates and short hole diffusion lengths [2]. Several experiments have been done to address these challenges such as nanostructuring, elemental doping and use of interfacial layers. L-arginine has been reported to improve the efficiency of photocurrent production by altering the shape from nanoparticles to nanocubes, nanorods and nanospheres [3]. The effects of L-arginine on hematite nanostructures were demonstrated. In this study, hematite nanostructures were synthesized by chemical spray pyrolysis[4]. L-arginine was used to transform hematite nanoparticles with no definite shape to hematite nanospheres using chemical bath deposition for 48 hours.

2. Results

Fig. 1 shows the surface morphology of hematite nanoparticles which were evenly distributed on the sample with an average nanoparticle size of 41 nm and Fig. 2 shows the Raman spectrum with all the phonon modes associated with pure hematite. Other optical and electrical properties including photoelectrochemical measurements, transmittance and absorbance will be discussed.

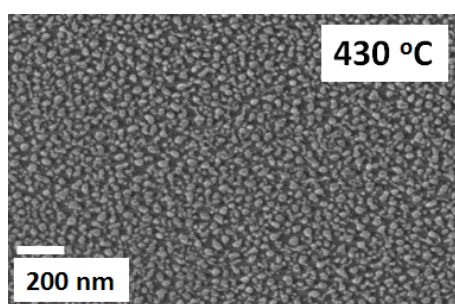


Fig.1: FE-SEM image of hematite nanoparticles prepared by spray pyrolysis

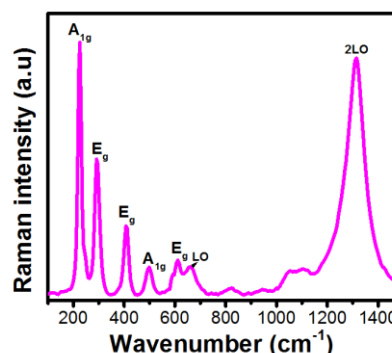


Fig.2: Raman spectrum of hematite nanoparticles with excitation wavelength of 532 nm

3. References

- [1] Abel, A.J. et al. (2015) SILAR-deposited hematite films for photoelectrochemical water splitting: effects of Sn, Ti, thickness, and nanostructuring. *The Journal of Physical Chemistry C* 119 (9), 4454-4465.
- [2] Kazemi, N. et al., Electrochemical preparation of hematite nanostructured films for solar hydrogen production, *EPJ Web of Conferences*, EDP Sciences, 2012, p. 02007.
- [3] Cao, H. et al. (2008) Amino-acid-assisted synthesis and size-dependent magnetic behaviors of hematite nanocubes. *Applied Physics Letters* 92 (1), 013110.
- [4] Abass, K.H. (2015) Fe₂O₃ thin films prepared by spray pyrolysis technique and study the annealing on its optical properties. *Int Lett Chem Phys Astron* 6, 24-31.

Effect of background atmosphere and substrate temperature on SrO:Bi thin films produced using pulsed laser deposition with different lasers

M. H. M. Abdelrehman^{1*}, V. Craciun², R. E. Kroon¹, A. Yousif^{1,3}, H.A.A. Seed Ahmed^{1,3}, H. C. Swart^{1*}

¹Department of Physics, Box 339, University of the Free State, Bloemfontein 9300, South Africa

²Laser Department, National Institute for Laser, Plasma and Radiation Physics, Bucharest-Magurele, Romania

³Department of Physics, Box 321, University of Khartoum, Omdurman 11115, Sudan

*Corresponding author e-mail address: hassamma@ufs.ac.za, SwartHC@ufs.ac.za

1. Introduction

The alkali-earth oxide phosphor SrO:Bi offers a potential low-cost alternative to lanthanide-based blue phosphors. It has been extensively reported in the powder form due to its properties and applicability in several types of optoelectronic devices in different phosphor fields, such as light-emitting diodes and display devices [1]. Pulsed laser deposition (PLD) can be used to grow thin films without a change in the stoichiometry from a multi-component ablation target. Sr_{1-x}O:Bi_{x=0.002} powder optimized for blue luminescence [2] from the ³P₁-¹S₀ transition of Bi³⁺ ions was first prepared by sol-gel combustion synthesis and pressed into a PLD target which was annealed at 200 °C for 2 h in air to remove all adventitious water containing species. Thin films were then successfully fabricated by PLD in vacuum or an O₂ working atmosphere on Si (100) substrates. Films were deposited at different substrate temperatures using a Nd:YAG laser (266 nm) with energy 33.3 mJ/pulse or deposited using different types of excimer lasers i.e. a KrF laser (248 nm) with energy 300 mJ/pulse or a ArF laser (193 nm) with energy 150 mJ/pulse.

2. Results

The X-ray diffraction (XRD) of the films deposited using the Nd:YAG laser in O₂ showed that the crystallinity increased with an increase in the substrate temperature, changing from amorphous to a cubic structure. At the highest temperature of 500 °C, the 111 and 200 SrO peaks were almost the same height, as in the powder. However, for 350 °C and 200 °C, the 200 peak was much smaller, which suggests some preferential orientation for films prepared at lower substrate temperatures. All films deposited in vacuum were amorphous. Atomic force microscopy results showed that the surface roughness decreased as the substrate temperature increased. The optimum substrate temperatures for the maximum luminescence (both photoluminescence (PL) and cathodoluminescence (CL)) were 200 °C and 50 °C for deposition in O₂ and vacuum, respectively. The main PL emission peak position of the thin films showed a shift to shorter wavelengths at 427 nm, when compared to the powder (445 nm). The difference in wavelength was attributed to the Bi³⁺ ions, which are very sensitive towards the environment [3]. Time of flight secondary ion mass spectroscopy depth profiles for the samples deposited in O₂ or vacuum at different substrate temperatures look similar, except for a slight thickness variation. XRD of the thin films obtained with the different types of excimer lasers showed the thin films also had a strong (111) preferential orientation on the cubic phase. PL spectra showed blue emissions at 425 nm with a small shift to shorter wavelength compared with the powder, which was attributed to Si diffusion in the films.

3. References

- [1] Fu, Jipeng, R. Pang, Y. Jia, W. Sun, J. Lihong, S. Zhang and C. Li. *J. Lumin.* **181** (2017) 240.
- [2] M. H. M. Abdelrehman, R. E. Kroon, A. Yousif, H. A. A. Seed Ahmed and H. C. Swart. *J. Vac. Sci. Technol. B* **37** (2019) 011206.
- [3] R. M. Jafer, A. Yousif, V. Kumar, T. K. Pathak, L. P. Purohit, H. C. Swart and E. Coetsee. *Physica B: Condens. Matter* **497** (2016) 39.

Stimulated luminescence study of MgO:Al³⁺,Li⁺ prepared by solution combustion method

Sefako J. Mofokeng¹, Luyanda L. Noto¹, Dumisani V. Mlotswa¹, Bakang M. Mothudi¹, Victor R. Orante-Barron²

¹Department of Physics, CSET, University of South Africa, Johannesburg, 1710, South Africa

²Departamento de investigacion en Polimeros y Materiales de la Universidad de Sonora, Apartado Postal 130, Hermosillo, Sonora 83000, Mexico.

Corresponding author e-mail address: Sefakojmofokeng@gmail.com, notoll@unisa.ac.za

1. Introduction

Recent development of nanocrystalline MgO in modern nanotechnology created comprehensive applications, particularly as a base catalyst in organic reactions, electronic and optical devices, medicine, toxic waste remediation, etc [1, 2]. In this research, we report the investigations on the thermoluminescence (TL) and structural properties of MgO nano-particles co-doped with Al³⁺ and Li⁺ ions, prepared by microwave-assisted solution combustion synthesis using glycine as fuel. The sample was studied for dosimetry applications.

2. Results

The XRD pattern revealed that MgO:Al³⁺,Li⁺ nano-particles were obtained. The TL glow curve of MgO:Al³⁺,Li⁺ showed the main peak at ~50°C under beta irradiation, and further studies on the dose response and sensitivity were carried out (Fig. 1&2). The involved electron kinetics were investigated and the corresponding depth of the electron trapping centers was determined.

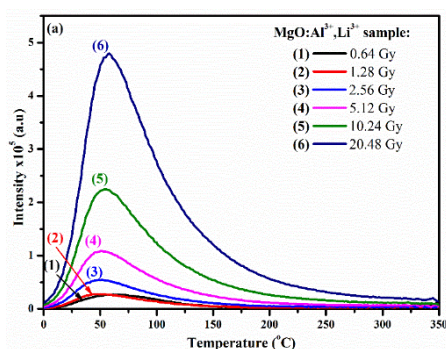


Fig. 36: The TL glow curve of MgO:Al³⁺,Li⁺.

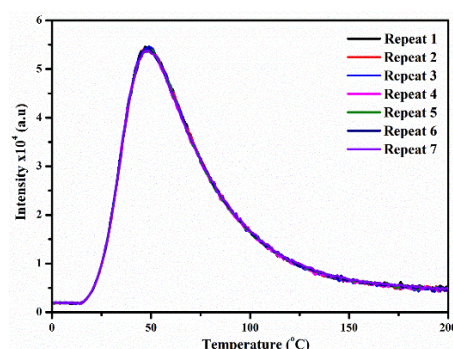


Fig. 2: TL glow curves showing the signal repeatability.

3. References

- [1] V.S. Cvetkovic, N.M. Vukicevic, N.D. Nikolic, G. Brankovic, T.S. Barudzija, and J.N. Jovicevic, *Electrochimica Acta*, (2018), **268**, 1494502.
- [2] X. Tang, Y. Nie, Q. Jin, L. Guo, J. Zhao, T. Li and Y. Zhu, *Ultrasonics – Sonochemistry*, (2018), **40**, 995–1002.

Synthesis of Methyl Ammonium Lead Tribromide Perovskite by Sequential Physical Vapour Deposition for Solar Cell Applications

Juvet N. Fru¹, Nolwazi Nombona², Mmantsae M. Diale¹

¹Department of Physics, University of Pretoria, Private Bag X20, Hatfield 0028, South Africa
(South African Research Chair in Clean and green energy, University of Pretoria)

²Department of Chemistry, University of Pretoria, Private Bag X20, Hatfield 0028, South Africa
Corresponding authors e-mails: juvet.fru@up.ac.za, mmantsae.diale@up.ac.za

1. Introduction

Methyl ammonium lead tribromide ($\text{CH}_3\text{NH}_3\text{Br}_3$) perovskite was synthesized by sequential physical vapour deposition of lead (II) bromide and methyl ammonium bromide. The structural, optical, morphological, and topological properties were found to be highly dependent on the thickness of methyl ammonium bromide. X-ray diffraction patterns confirmed that the cubic methyl ammonium lead tribromide crystals were successfully synthesized [1], and the sample with 100 nm thickness of lead (II) bromide and 300 nm thickness of methyl ammonium bromide contained the smallest amount of impurities as presented in fig. 1. UV-visible spectra revealed broad absorption bands with absorption onset at about 550 nm as shown in fig. 2, giving a large bandgap of 2.3 eV which is suitable for tandem solar cell application. Scanning electron microscopy images showed densely packed, randomly distributed grains with large coverage and without pinhole-like defects. Atomic force microscopy validated that the films were smooth with root mean square roughness less than 4 nm, indicating better quality of vapour deposited films as opposed to solution processed films [2]. This method simple and can be applied in large scale synthesis of quality halide perovskites thin films for solar cell applications.

2. Results

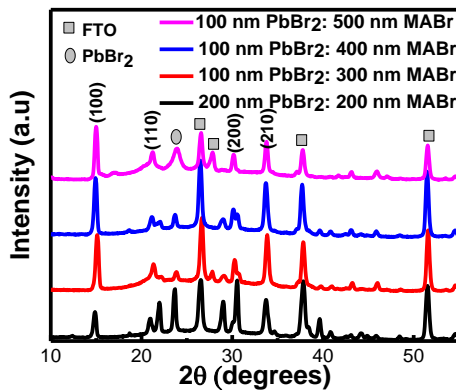


Fig. 1: XRD Patterns of $\text{CH}_3\text{NH}_3\text{Br}_3$ film for different thicknesses

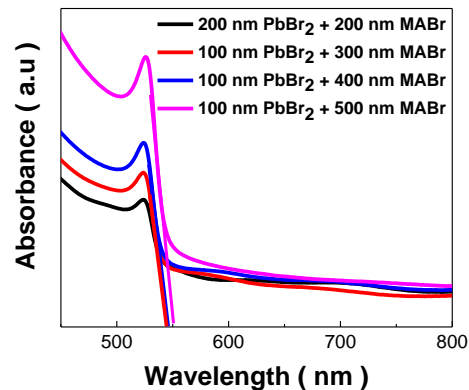


Fig. 2: UV-vis spectra of $\text{CH}_3\text{NH}_3\text{Br}_3$ for different thicknesses

3. Reference

- [1] R. Sheng, A.Ho-Baillie, S.Huang et al. *J.Phys. Chem C*. 199 (2015) 3345
[2] J. Ávila, C. Momblona, P. P. Boix, M. Sessolo, and H. J. Bolink, *Joule*, (2017) 431

Effect of Er and Yb doping on morphology, optical and Schottky diode properties of ZnO thin films prepared by sol-gel spin coating

Mohammed Ahmed^{1,2}, Jackie Nel¹, Walter Mayer¹

¹ Department of Physics, University of Pretoria, Private Bag X20, Hatfield 0028, South Africa.

²Department of Scientific Laboratories-Physics, Sudan University of Science and Technology, P.O Box 407, Khartoum, Sudan.
U17401918@tuks.co.za

1. Introduction

- ZnO is one of the II-VI group semiconductor materials with a wide direct band gap of approximately 3.4 eV and large exciton binding energy of 60 meV at room temperature.
- ZnO as a very attractive host lattice for doping of different kinds of dopants, due to having excellent physical and chemical stability.

Recently, there have been extensive studies on rare earth doped semiconductors for using in optoelectronic devices such as visible and infrared luminescent devices.

- Undoped, Er⁺³(3 at%) and Yb⁺³(3 at%) doped ZnO thin films were prepared using the sol-gel spin coating after annealing at 600 °c. The morphology was investigated using scanning electron microscopy (SEM). The optical properties studied using photoluminescence (PL) spectroscopy. The Schottky barrier diodes were fabricated on the synthesized undoped, Er⁺³ and Yb⁺³ doped ZnO thin films. The Schottky barrier height (SBH) calculated from current-voltage (*I-V*) measurements were 0.73 eV, 0.95 eV and 1.06 eV for undoped, Er⁺³ and Yb⁺³ doped ZnO thin films respectively. The optical and electrical properties will be discussed.

2. Results

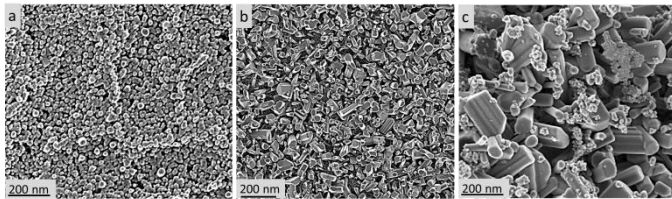


Figure 37: SEM images of (a) undoped ZnO (b) Er⁺³ doped ZnO and (c) Yb⁺³ doped ZnO thin films deposited on glass substrate showing significant differences in the morphologies.

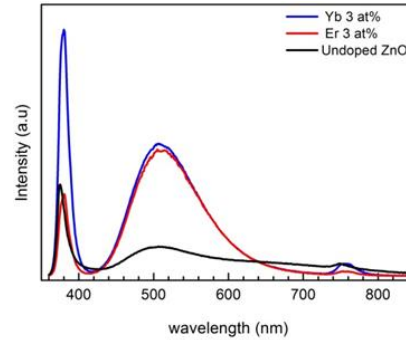


Figure 2: PL spectra for doped and undoped ZnO thin films at room temperature. A strong UV emission around 379 nm and green emission centers at 506 nm are observed in all samples, with the undoped ZnO sample showing weaker green emission.

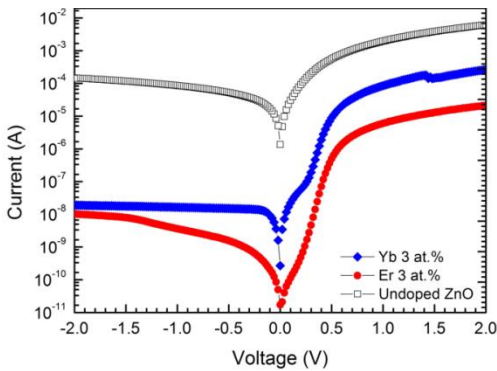


Figure 3: Room temperature semi-logarithmic plot of *I-V* measurements of Pd/doped ZnO/n-Si/AuSb Schottky diode. The rectification were 1.5, 3 and 4 orders of magnitude for undoped, Er⁺³ and Yb⁺³ doped ZnO thin films respectively. Er⁺³ and Yb⁺³ doped ZnO result in an increase in the SBH as well as decreased in ideality factor.

Table 38: The Schottky diodes parameters from *I-V*

Events	SBH (eV)	Ideality factor (<i>n</i>)	Saturation current (<i>I_s</i>) (A)	Series resistance ×10 ³ (Ω)
Undoped ZnO	0.73	2.69	5.0 ×10 ⁻⁶	0.19
Er	1.06	1.88	9.0×10 ⁻¹²	54
Yb	0.95	2.11	706×10 ⁻¹²	3.0

The diodes parameters shown in Table 1 were calculated by performing a linear fit in forward bias region using thermionic emission theory [1].

3. References

[1] E. Rhoderick, R. Williams, Metal-semiconductor Contacts, Second Edition, Clarendon Press, 1988.

An investigation of defects introduced in Si during sputter-deposition using deep-level transient spectroscopy

Helga Tariro Danga, Shandirai Malven Tunhuma, Francois Danie Auret and Walter Ernst Meyer

Department of Physics, University of Pretoria, Pretoria 0002
Corresponding author e-mail address: helga.dang@up.ac.za

1. Introduction

Sputter deposition is a widely used technique to deposit thin films on substrates. The technique is based on ion bombardment of a source material known as the target. Ion bombardment results in a vapour due to a purely physical process, that is, the sputtering of the target material. This technique is part of the class of physical vapour deposition techniques, which includes thermal evaporation and pulsed laser deposition. The most common method of depositing thin films by sputter deposition is the use of a magnetron source in which positive ions present in the plasma of a magnetically enhanced glow discharge bombard the target. The target can be powered in different ways, ranging from direct current (DC) for conductive targets to radio frequency (RF) for nonconductive targets [1].

Process induced damage occurring during the deposition of Schottky barrier diodes (SBDs) has been shown to intensely influence the quality and characteristics of these devices. The introduction of electrically active defects in the substrate at and near the metal-semiconductor interface has been reported for contacts deposited by DC, ion beam sputtering and RF sputtering. The effect of these defects changes the barrier properties of the SBDs [2].

In this work, we investigate the damage induced in the substrate when Ti Schottky barrier diodes (SBD's) are sputter deposited. The effect of the damage on the properties of the rectifying junctions is obtained from current-voltage (I - V) measurements, while deep-level transient spectroscopy (DLTS) is employed to characterise the nature of the defects, and the extent to which they increase recombination [3].

2. Results

Soon after metallisation DLTS was employed and the defect level observed was H(0.40). The apparent capture cross-section was $1.4 \times 10^{-17} \text{ cm}^2$. This defect was observed by Chabane-Sari *et.al* [4] in boron-doped silicon after rapid thermal annealing between 900 and 1100 °C.

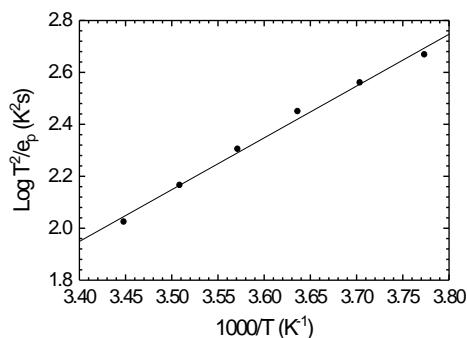


Fig. 39: Arrhenius plot of Ti SBD soon after sputter-deposition

3. References

- [1] D. Depla, J.E. Greene. *Sputter Deposition Processes* (Elsevier Inc,2010),Chap. 5.
- [2] F D Auret, G M Matusiewicz. *J. Electrochem. Soc* **131** (1984) 1712.
- [3] O. Paz; F. D. Auret, J. F. White. *Vacuum* **35** (1985) 195.
- [4] N.E. Chabane-Sari, L. Thibaud, S. Kaddour, M. Berenguier, and D. Barbier *J. Appl. Phys.* **71** (1992) 3320

Green Synthesis of Metal Nanoparticles using Phycocyanin

Theophilus Selepe^{1,2}, Michal Gwizdala², Tjaart P.J. Krüger², Nolwazi Nombona³, Mmantsae Diale²

¹Department of Physics, Sefako Makgatho Health Science University, MEDUNSA, 0204, South Africa.

²Department of Physics, University of Pretoria, Pretoria, 0002, South Africa.

³Department of Chemistry, University of Pretoria, Pretoria, 0002, South Africa.

Corresponding author: E-mail: theophilus.selepe@smu.ac.za; Mmantsae.diale@up.ac.za

1. Introduction

Metal nanoparticles (MNPs) were synthesized via a bio-reduction method using phycocyanin (PC), an extract of cyanobacterium *Synechocystis* sp. PCC 6803. The formation of the synthesized MNPs was first confirmed by visual inspection as the colour changed to yellowish and purple for both silver (Ag) and gold (Au) nanoparticles (NPs), respectively. The structural characterization of synthesized MNPs was done using transmission electron microscopy (TEM), X-ray diffraction (XRD) and Fourier transform infrared (FTIR) spectroscopy. The optical properties were studied using UV-Visible spectrophotometry (UV-Vis) and Photoluminescence (PL) spectroscopy.

TEM analysis revealed spherical MNPs and XRD revealed peaks which were related to crystallographic planes (111), (200), (220), and (311). FTIR spectra indicated interactions between the MNPs and phycocyanin due to the presence of amines, alcohol and carbonyl functional groups which acted as capping and stabilizing agents during the synthesis of MNPs. UV-Vis analysis showed strong surface plasmon resonance absorption peaks of both AgNPs and AuNPs. Photoluminescence emission spectra from PC overlap with the MNPs' absorption spectra, which may suggest that there is energy transfer from the protein to the MNPs. The biosynthesized MNPs may be useful in making optical devices as well as for other applications.

2. Results

Figure 1 shows the absorption and emission spectra of fluorescent phycocyanin (PC) with absorption spectra of Au and Ag MNPs. The overlap between the absorption spectra of biosynthesized MNPs and the emission spectra of PC may suggest energy transfer from the protein to MNPs.

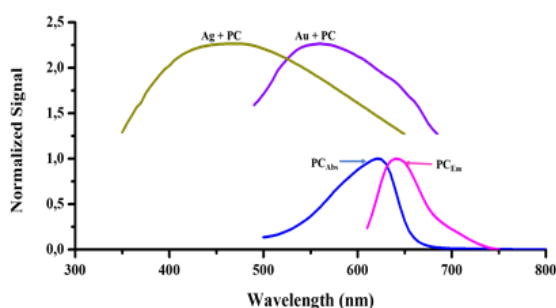


Fig. 40: Absorption and emission spectra of fluorescent phycocyanin (PC) with absorption spectra of Au and Ag metal nanoparticles.

Thermal Conductivity of Ultra-Wide Bandgap Thin Layers: High-Al Content AlGa_N and β -Ga₂O₃

Dat Q. Tran^{1,2}, Pitsiri Sukkaew^{1,2}, Alysa Mock³, Hengfang Zhang^{1,2}, Nikolas Blumenschein⁴, John F. Muth⁴, Plamen P. Paskov^{1,2}, Vanya Darackchieva^{1,2,3}

¹ Department of Physics, Chemistry and Biology, Linköping University, 581 83 Linköping, Sweden

² Center for III-Nitride Technology, C3NiT-Janzen, Linköping University, 581 83 Linköping, Sweden

³ THz Materials Analysis Center (TheMAC), Linköping University, 581 83 Linköping, Sweden

⁴ Department of Electrical and Computer Engineering, North Carolina State University, Raleigh, NC 27695, USA

Corresponding author e-mail address: dat.tran@liu.se

1. Introduction

Ultra-high bandgap semiconductors have been increasingly important for high-power and high-frequency device applications. SiC and GaN have emerged as interesting materials offering very high breakdown voltage, almost one order larger than the commonly used semiconductors like Si or GaAs. A lot of efforts have also been spent on exploring new materials aiming at enhancing breakdown voltage of the power devices. Adding aluminum (Al) into GaN to make high-Al AlGa_N alloy or switch to completely new materials such as β -Ga₂O₃ is already proved to increase the device breakdown voltage [1, 2]. However, there are several unsolved problems that raise a question about the possibility for practical devices applications. Alloy scattering in AlGa_N due to the incorporation of Al element strongly degrades thermal conductivity of AlGa_N. Very low thermal conductivity was found for β -Ga₂O₃ even it possesses relatively high phonon velocity which is comparable to GaN. Our study is aiming at determining and shedding the light on the physics behind the thermal conductivity of high-Al AlGa_N and β -Ga₂O₃.

2. Results

Our study on AlGa_N [0001] and β -Ga₂O₃ [-201] thin films using time-domain thermoreflectance (TDTR) technique with the assistance of modeling based on Callaway-Debye formalism [3] found that AlGa_N becomes more heat-resistive and its thermal conductivity is minimized at high-Al content ([Al] = 0.5-0.8) (Fig. 1a). The thermal conductivity value is reduced more than 10 times for sub-micrometer high-Al AlGa_N film compared with GaN film of the same thickness. β -Ga₂O₃ layers show comparable value to high-Al AlGa_N (Fig. 1b). Our analysis points out high thermal boundary resistance at heterojunctions of AlGa_N and β -Ga₂O₃ with other materials (Au transducer in our sample structure). Phonon mismatch model cannot explain for the thermal boundary resistance of these two materials. Because of strong alloy scattering in high-Al AlGa_N and strong normal scattering in β -Ga₂O₃, their phonon mean-free paths get closed to 10 nm comparable to surface roughness that might be the reason of remarkably increasing thermal boundary resistance.

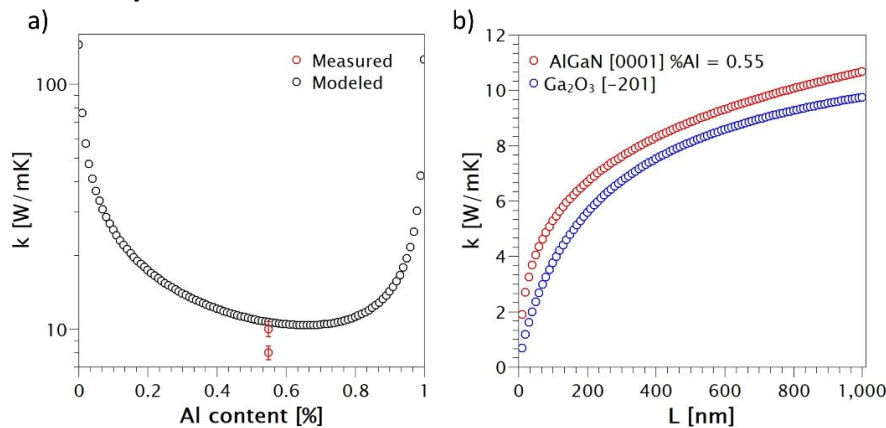


Figure 1. a) The measured and modeled data for Al composition dependent thermal conductivity of AlGa_N, the thickness of 1 μ m is used. b) A comparison of modeled thickness-dependent thermal conductivities between Al_{0.55}Ga_{0.45}N [0001] and β -Ga₂O₃ [-201].

3. References

- [1] R. J. Kaplar et al., *ECS J. Solid State Sci. Technol.* **6**, Q3061 (2017).
- [2] K. Sasaki et al., *J. Cryst. Growth* **378**, 591 (2017).
- [3] M. Asen-Palmer et al., *Phys. Rev. B* **56**, 9431 (1997).

Effect of Er^{3+} on Structural and optical properties of microwave synthesized $\alpha\text{-Fe}_2\text{O}_3$ nanoparticles

L. Mathevula, B. M Mothudi, M.S Dhlamini

Department of Physics, University of South Africa, P. O. Box 392, 0003, south Africa
langutanimathevula755@gmail.com

1. Introduction

$\alpha\text{-Fe}_2\text{O}_3$ is an environmentally friendly n-type semiconductor with the band gap of ~ 2.1 eV. It is the most stable iron oxide under ambient conditions. It is widely used in gas sensing, high density magnetic recording media, clinical therapy, Magnetic resonance imaging and diagnosis [1-2]. Rare earth (RE) atoms recently have been introduced into the iron oxide matrix which leads to a material that shows multiple interesting effects. Recently, the design of nanostructured materials containing RE elements, either as major or as dopant, has paved a way for the development of new applications. There are some desirable requirement that the nanoparticles intended for bioimaging applications should fulfill. Thus, uniform size, shape, composition and surface chemistry are essential [3].

2. Results

Er^{3+} doped $\alpha\text{-Fe}_2\text{O}_3$ nanoparticles were successfully synthesized by microwave synthwave using PEG as polymerizing agent. The powders were doped with different concentrations of the Er^{3+} . The structural, size, optical and luminescence studies of the synthesized powder were characterized by XRD, SEM, UV-Vis and PL spectral techniques. Fig 1 shows and enhancement of luminescence emission as Er^{3+} is added into the matrix and quench as the concentration of Er^{3+} is increased.

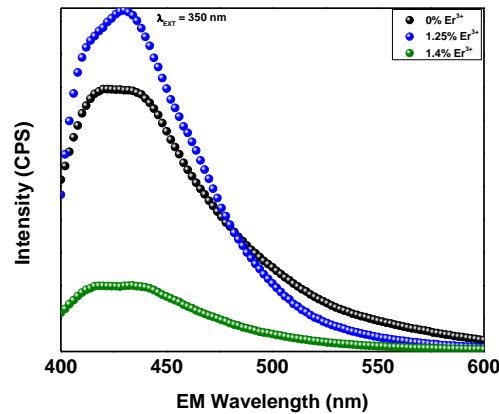


Fig. 1: Photoluminescence spectra of un-doped and $\text{Fe}_2\text{O}_3:\text{Er}^{3+}$ nanoparticles at different doping concentration annealed at 600°C . The insert is the magnified region of (116) peak

3. References

- [1] M. N Batin and V. Popesca, *optoelectronics and advanced materials-rapid communications*, 6 (2012) 727-729
- [2] Libor Machala, Radek Zboril, and Aharon Gedanken, *J. Phys. Chem.*, 111 (2007) 4003-4018
- [3] Alberto Escudero*, Ana I. Becerro, Carolina Carrillo-Carrión, Nuria O. Núñez, Mikhail V. Zyuzin, Mariano Laguna, Daniel González-Mancebo, Manuel Ocaña and Wolfgang J. Parak, *Nanophotonics* 6 (2017) (5) 881–921

Luminescence properties of P3HT-ZnO: RE ions nanoparticles: A photon up-conversion materials for organic solar cell application

Qotso A.S, Mbule P.S, Mothudi B.M.

Department of Physics, CSET, University of South Africa, Johannesburg, 1710, South Africa

**Corresponding author email-address: qotsoas@gmail.com, mbuleps1@unisa.ac.za*

1. Introduction

Organic-inorganic semiconductors are the main focus of tremendous research activities due to their promising prospective in optoelectronic device application [1]. Hybrid heterostructure based on pristine P3HT-conjugated polymer with an inorganic ZnO:RE nanoparticles are said to enhance optoelectronic properties owing to the advantages offered by the high electron mobility of ZnO [2].

In this work, we incorporated ZnO:RE nanoparticles in the pristine P3HT-conjugated polymer and systematically studied the effect of the ZnO:RE nanoparticles on the structure, morphology and optical properties for organic solar cells application. Rare-earth ions doped zinc oxide (ZnO:RE) up-conversion materials were prepared using sol-gel method at room temperature. Thioglycerol was used as capping agent during the synthesis and its concentration was varied to control the nanoparticles uniformity. Different doping concentrations (1 – 9 mol%) of ytterbium (Yb^{3+}) were varied while keeping erbium (Sm^{3+}) concentration at 3% to investigate the up-conversion luminescence. The synthesized ZnO:RE nanoparticles were characterized using field emission scanning electron microscopy (FESEM), X-ray diffraction (XRD), photoluminescence (PL), ultra violet to visible (UV-Vis) techniques. FESEM showed uniform well dispersed spherical nanoparticles while the XRD data revealed that ZnO has the hexagonal wurtzite structure. PL and UV-Vis showed that 1 mol% of Yb^{3+} has the higher intensity and absorption, respectively. These particular heterostructures are of interest as absorbing layers in organic-inorganic bulk heterojunction solar cells, thus opening perspectives for applications in various optoelectronic devices, including solar cells.

2. Reference

- [1] Ikrama M, Murray R, Hussainc A, Ali S, Shaha S. I, *Mater, Sci. Eng. B* **189** (2014) 64 – 69.
- [2] Arias J. J. R, Marques M. F. V, *React. Funct. Polym*, **113** (2017) 58 – 69.

Morphology, structural and luminescent properties of sol-gel synthesized SiO₂:Sr:xTb nanopowders.

R.G. Moji¹, L.F. Koao², J.P. Mofokeng¹, R.E. Kroon³, S.V. Motloutung⁴ and T.E. Motaung⁵

¹Department of Chemistry, University of the Free State (Qwaqwa Campus), Private Bag X13, Phuthaditjhaba, 9866, South Africa.

²Department of Physics, University of the Free State (Qwaqwa Campus), Private Bag X13, Phuthaditjhaba, 9866, South Africa.

³Department of Physics, University of the Free State, P.O. Box 339, Bloemfontein, 9300, South Africa.

⁴Department of Physics, Nelson Mandela University (NMU), P. O. Box 77000, Port Elizabeth 6031, South Africa

⁵Department of Chemistry, University of Zululand, KwaDlangezwa, 3886, South Africa

Corresponding author e-mail address: mojirg@ufs.ac.za/koalof@ufs.ac.za

1. Introduction

Phosphors or luminescent materials are mostly solid inorganic materials consisting of a host lattice that is intentionally doped with “impurities” [1]. The host lattice in this instance was amorphous SiO₂ that was used because of its chemical stability, non-hygroscopic nature, the possibility of incorporating larger amounts of luminescent ions and the opportunity of cost reduction [2]. The sol-gel was the preferred method of preparation since it is considered as an efficient technique for the synthesis of phosphors due to the good mixing of starting materials and relatively low reaction temperature [3]. Tb³⁺ ions exhibit a characteristic green luminescence (due to the ⁵D₄ – ⁷F₅ transition at 540 nm) which is important in the LEDs. Thus, in this study, a series of SiO₂ doped with 0.4 mol% Sr²⁺ and co-doped with different mol percentages of Tb³⁺ was synthesized using sol-gel method. All the samples were annealed under N₂ at 800°C for 2 hours. X-ray diffraction, scanning electron microscopy, Uv-vis absorption and photoluminescence were used to determine the morphology, structural and luminescent properties of the nanopowders.

2. Results

The XRD patterns for all the nanopowders show a broad amorphous peak typical of SiO₂, which show that the dopants concentration did not have any effect of the structural properties of the nanoparticles. The PL-results on the other hand indicate that the luminescent intensity (for the strongest emission peak around 540 nm) increases with increasing mol percentage Tb³⁺ concentration.

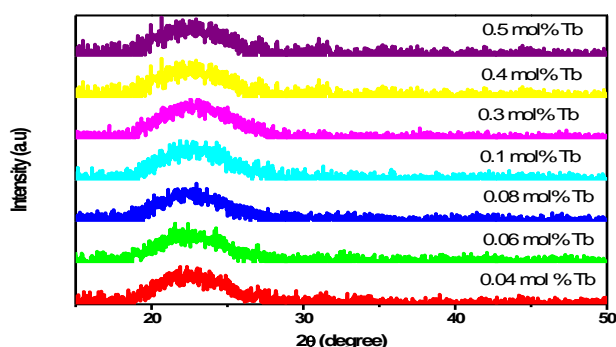


Fig. 1: XRD patterns of SiO₂:Sr²⁺:Tb³⁺

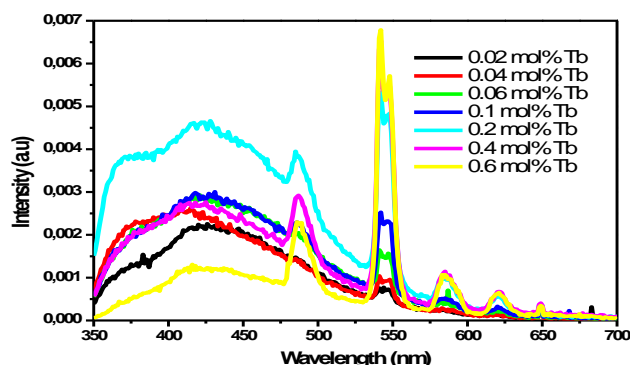


Fig. 2: Emission spectra of SiO₂:Sr²⁺:Tb³⁺

3. References

- [1] C.R. Ronda, T. Justel, H. Nikol, J. Alloys and Comps. **275** (1998) 669.
- [2] R.E. Kroon, H.A.A. Seed Ahmed, O. M. Ntwaeaborwa, L.F. Koao, I.M. Nagpure, M.A. Gusowski, J.R. Botha, H.C. Swart, Physica B., **407** (2012) 1595.
- [3] J.M. Nedelec, L. Courtheoux, E. Jallot, C. Kinowski, J. Lao, P. Laquerriere, C. Mansuy, G. Renaudin, S. Turrell, J Sol-Gel Sci. Technol., **46** (2008) 259.

Temperature dependence of opto-electric response of Si PV cells

Ross Dix-Peek, Ernest van Dyk, Frederik Vorster, Daniel Janse van Rensburg

*Nelson Mandela University, Physics Department
University Way, Summerstrand, Port Elizabeth, South Africa
Corresponding author e-mail address: s212286552@mandela.ac.za*

1. Introduction

Photovoltaic (PV) devices operate at a variety of different temperatures. Semiconductor parameters are often assumed to be homogeneous and one dimensional but, this assumption can be particularly problematic when applied to large area devices such as solar cells. Spatial device inhomogeneities have been well documented; using techniques such as Electroluminescence (EL) imaging [1], Lock-in Thermography (LIT) [2] and Light Beam Induced Current (LBIC) measurements [3].

The general assumption that the temperature dependence of device parameters is homogeneous in nature has recently become a topic of interest [4]. The effect of local temperature dependencies of specific parameters on the global temperature dependencies is not well documented or studied. In this paper, LBIC is used to study the basic linear temperature dependence of opto-electric parameters such as light beam induced photo-potential and photo-current.

2. Results

The preliminary results shown in fig 1 and 2 show the temperature dependent LBIC (T-LBIC) measurements of a mono-crystalline back contact Si PV cell designed for highly concentrated light. The light beam probe consisted of a 660nm laser probe with beam diameter of 50 μ m and intensity of 1000 W/m². The data was collected at seven temperatures, ranging from 303 K to 363 K. At each point the photo induced current at various temperatures were collected. A temperature coefficient for each point was calculated using simple linear regression. Fig. 1 is the map of the temperature coefficient of the photo induced current for the device. Fig. 2 contains the data used in the linear regression to determine the temperature coefficients of the local sites indicated in Fig. 1.

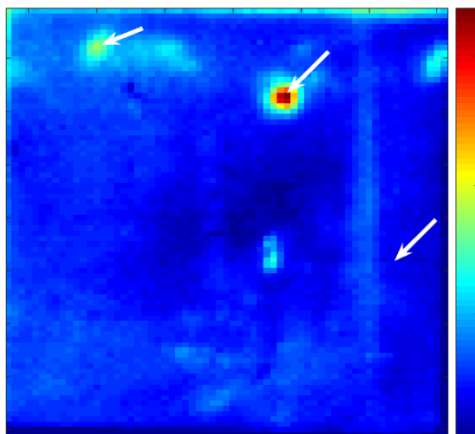


Fig. 41: Temperature Coefficient of Photocurrent map across Back-contact concentrator Si PV cell (0.005..0.219 μ A/K)

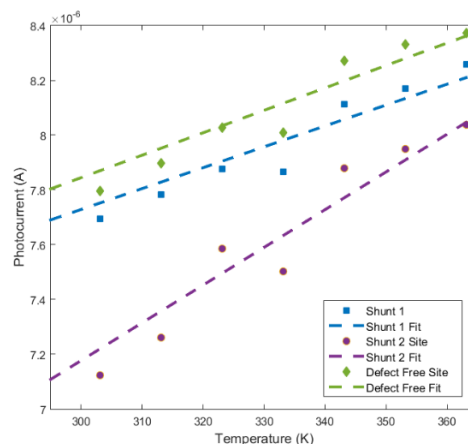


Fig. 2: Temperature dependence of photocurrent of selected regions

3. References

- [1] Dix-Peek, R., van Dyk, E., Vorster, F. and Pretorius, C. (2018). Breakdown voltage mapping through voltage dependent ReBEL intensity imaging of multi-crystalline Si solar cells. *Physica B: Condensed Matter*, 535, pp.63-66.
- [2] Breitenstein, O. (2011). Nondestructive local analysis of current-voltage characteristics of solar cells by lock-in thermography. *Solar Energy Materials and Solar Cells*, 95(10), pp.2933-2936.
- [3] Fuyuki, T. and Kitiyanan, A. (2008). Photographic diagnosis of crystalline silicon solar cells utilizing electroluminescence. *Applied Physics A*, 96(1), pp.189-196.
- [4] Eberle, R., Kwopil, W. and Schubert, M. (2018). Temperature Coefficient Imaging for Silicon Solar Cells. In: *SiliconPV 2018*. [online] AIP Conference Proceedings. Available at: <https://aip.scitation.org/doi/abs/10.1063/1.5049244> [Accessed 14 Jan. 2019].

LaBO₃ (B= Fe, CO) nanofibers and their structural, optical and gas sensing characteristics

Katekani Shingange^{1,2}, Hendrik Swart², Gugu Mhlongo^{1,2*}

¹ DST/CSIR National Centre for Nanostructured Materials, Council for Scientific and Industrial Research, Pretoria 0001, South Africa

² Department of Physics, University of Free State, Bloemfontein 9300, South Africa
Corresponding author e-mail address: gmhlongo@csir.co.za

1. Introduction

Due to the importance of monitoring and control of hazardous gases in our living spaces, gas sensors have become vital in our life. The need to develop affordable and high performance gas sensors has triggered the focus of research into enhancing the performance of these sensors mostly with regard to sensitivity and selectivity. One common technique is morphology engineering where different morphologies have been reported for enhancing sensor performance [1]. Of particular interest is one-dimensional (1D) nanofibers as they possess high surface area for adsorption-desorption reactions and the presence of nanograins provide large grain boundary areas, ensuring high sensitivity in the sensors [2]. Amongst many of the sensing materials used for gas sensing, perovskite oxides (ABO₃) have emerged as excellent candidates due to their catalytic activity and chemical and thermal stability [3]. The gas sensing properties of the perovskite materials are strongly dependent on the choice of the B-site cation, which can significantly affect the electronic conductivity of the perovskite oxide [4].

In this work; 1D nanofiber lanthanum - based perovskite oxides LaBO₃ (B= Fe, CO) were synthesized through electrospinning followed by calcination at 600 °C. X-ray diffraction (XRD) was used to determine the crystalline phases of the LaBO₃ samples. The morphology of the samples was determined through scanning electron microscopy (SEM) studies. Nitrogen adsorption-desorption analysis was performed to determine the surface area and pore volume of the samples. Ultraviolet–visible absorption spectroscopy (UV-Vis) and photoluminescence (PL) were used to examine the optical properties. X-ray photoelectron spectroscopy (XPS) was employed to examine the chemical composition and valence state of the elements in the LaBO₃ samples. Further characterization includes testing the LaBO₃ nanofibers for gas sensing performance under different concentrations of NH₃, CO, CH₄, CO₂, NO₂ and C₃H₆O in operating temperatures ranging from room temperature to 200 °C and in different humidity conditions. Selectivity, reproducibility and stability measurements of the sensors were also carried out.

2. Results

Fig. 1 displays the SEM images which revealed nanofibers composed of loosely packed nanograins ranging from ~20-60 nm in grain size for (a) LaFeO₃ and (b) LaCoO₃, respectively.

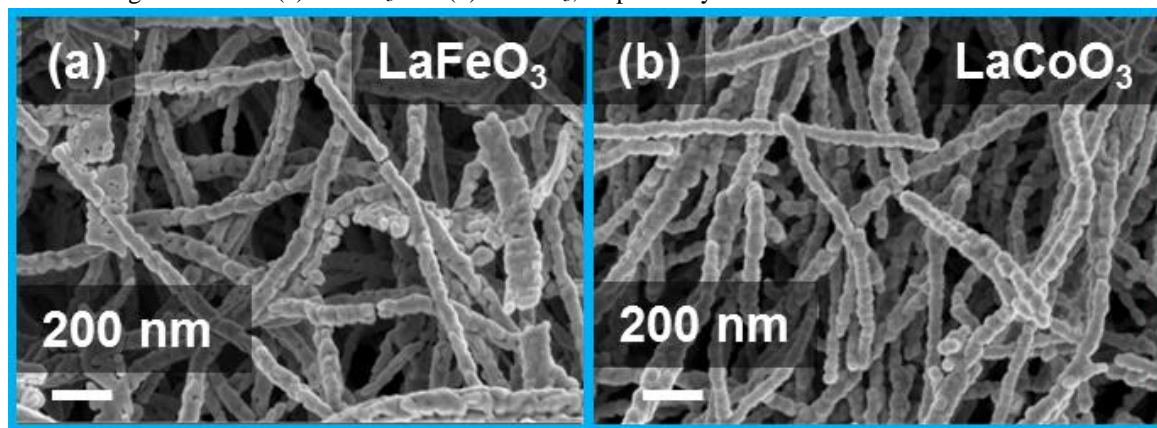


Fig. 1: SEM images of (a) LaFeO₃ and (b) LaCoO₃ nanofibers

3. References

- [1] K. Shingange, Z. P. Tshabalala, B. P. Dhonge, O. M. Ntwaeaborwa, D. E. Motaung and G.H.Mhlongo. *Mater. Res. Bull.* **85** (2017) 52-63.
- [2] K. Hayat, S. S. Shah, M. Yousaf, M. J. Iqbal, M. Ali, S. Ali, M. Ajmal and Y. Iqbal. *Mater. Sci. Semicond. Process.* **41**(2016) 364-369.
- [3] H. Zhang, P. Song, D. Han and Q. Wang. *Physica E.* **63** (2014) 21-26.
- [4] W. Haron, A. Wisitsoraat and S. Wongnawa. *Ceram. Int.* **43** (2017) 5032-5040.

Investigations of Pd diffusion through ZrC thin films

J.J. Terblans¹, H.C. Swart¹, E Coetsee¹, M.M. Duvenhage¹, D. Craciun², G. Dorcioman², V. Craciun^{2, 3*}

¹Department of Physics, University of the Free State, Bloemfontein, South Africa

²National Institute for Lasers, Plasma and Radiation Physics, Măgurele, Romania

³Extreme Light Infrastructure-Nuclear Physics, Magurele, Romania

Corresponding author: valentinrcr5@gmail.com

1. Introduction

Thin films used for nuclear fuel encapsulation applications in advanced nuclear reactors should exhibit a good radiation tolerance and retention of fission products. We have shown that nanocrystalline ZrC films maintained their structure and chemical composition when irradiated with 800 keV Ar or 1 MeV Au ions up to fluences of $1 \times 10^{15}/\text{cm}^2$. We investigated Pd diffusion, one of the most radioactive fission products through thin films of ZrC. A film of Pd was deposited using magnetron rf sputtering at room temperature on a Si wafer. Without breaking the vacuum, a thin ZrC film was then deposited using pulsed laser deposition on top of the Pd film. The structure and density of the deposited films were investigated using X-ray reflectivity and grazing incidence X-ray diffraction. After deposition, the sample was transferred to a Time of Flight Secondary Ion Mass Spectroscopy (ToF SIMS) system. The sample was mounted on the heating stage of the ToF SIMS. A depth profile was obtained at room temperature, where after the sample was heated to 400 °C at a rate of 1 K/s. The temperature was maintained at 400 °C for 10, 20, 40, 80 and 160 minutes, respectively. In between each heating cycle, a depth profile was obtained. The ToF SIMS analysis was performed with a pulsed Bi⁺ primary ion beam and its energy was 30 keV and the beam current was 1 pA. All the analyses were performed in the positive spectroscopy mode. A Cs⁺ sputter gun (1 kV, 75 nA) was used together with the Bi⁺ gun in the non-interlaced mode for depth profiling and the sputter interval was 10 s. The analysis area was $100 \times 100 \mu\text{m}$ (with 512×512 analysis points) and the sputtering area was $450 \times 450 \mu\text{m}$. The base pressure was $\sim 1 \times 10^{-9}$ mbar. Upon heating the sample the surface of the sample changed from a uniform surface to a surface covered with black and white spots. Using the selective region of interest (ROI) mode of the analysis software depth profiles were extracted from both the smooth part and the black and white spot parts of the heated films. Interdiffusion between the Pd and Si occurred during annealing. From the depth profiles, it was clear that the ZrC formed a diffusion barrier that prevented the Pd to diffuse towards surface. The diffusion rate was different in the areas that appeared as black and white spots. The Si diffused up to the ZrC diffusion barrier and was blocked by the ZrC layer.

2. Results

Examples of the ToF SIMS depth profiles are shown in fig. 1(a) and (b). The profile in fig. 1(a) was obtained from the unannealed ZrC/Pd/Si layer and the profile in fig 1(b) of the thin film after annealing at 400°C for 160 min. It is clear from the intermixing of the Si and Pd signal at the Pd/Si interface that diffusion has taken place during the annealing process and a silicide formed during the interdiffusion. The profiles obtained at the other annealing times clearly showed that the diffusion and silicide formation were a function of annealing time. Also clear is that no diffusion took place between the Pd and ZrC. The different diffusion rates in the different areas and silicide formation will be discussed in detail.

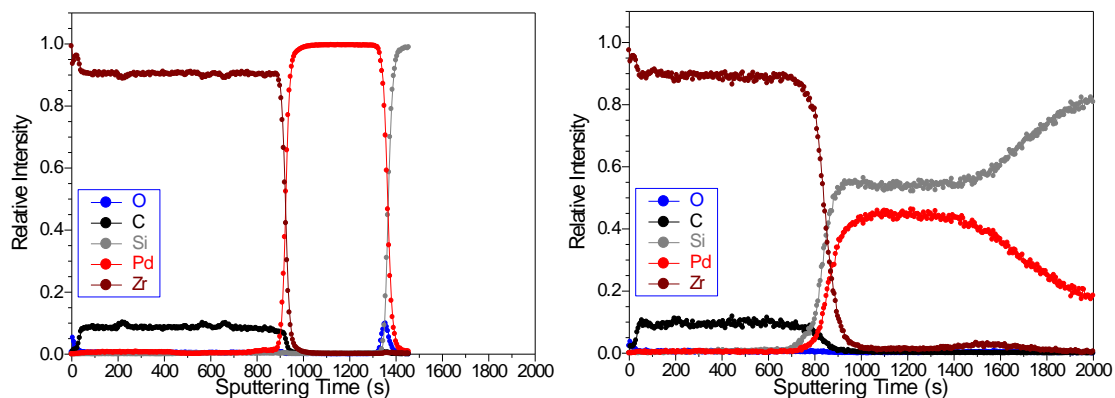


Figure 1: ToF SIMS profiles of (a) unannealed ZrC/Pd/Si film and (b) 160 min annealed film at 400 °C.

Acknowledgment The Romanian team work was funded by Nucleu –INFLPR program, STAR 161/2017 and ELI 17/2017 project

CdX (X=S, Se, Te) Quantum Dots and a Bi-Iron Chalcogenide for Hydrogen Generation

Zuraan Paulsen¹, Leandre` Bianca Brandt

¹ University of the Western Cape
Robert Sobukwe Road
Bellville, 7535
Republic of South Africa

Corresponding author e-mail address: monani@uwc.ac.za

1. Introduction

Since the beginning of the 21st century there has been a growing global need for energy. The worlds energy supply for electricity and transportation, primary comes from fossil fuel resources. Fossil fuels are limited and their use causes the release of environmentally harmful greenhouse gas (GHG) emissions.

While using renewable forms of energy is good for the environment, there are two major drawbacks namely: it is difficult to provide similar volumes of electricity that are generated by fossil fuels, and the sources of the energy aren't reliable [1]. The most promising candidate currently is to use hydrogen as an alternative energy carrier. Hydrogen is, easily accessible, it produces zero GHG emissions when implemented in hydrogen fuel cells (HFC), it has a high energy yield, and has fuel efficiency of 40-60% [2]. Hydrogen however is, hard to store in its pure form, HFCs have been reported to release nitrogen dioxide emissions, and to produce hydrogen on a large scale will require the use of fossil fuels [3]. At present, hydrogen is mainly produced from fossil fuels such as natural gas by steam reforming. Considering the environmental and energy issues, hydrogen needs to be produced using natural energies such as sunlight and water. There are several ways of solar hydrogen production; however a powdered photocatalyst system will be advantageous for large-scale application.

The research I am conducting will be looking into creating a powdered photocatalyst system, in the hopes of creating a fossil-fuel-free way to produce hydrogen on a large scale. I will be attempting to split water using artificial photosynthesis. Artificial photosynthesis systems usually consist of a photosensitizer, coupled with an inorganic, organometallic or enzymatic catalyst. Water splitting can be achieved when a photocatalyst is modified with a suitable cocatalyst; it is therefore important to develop both photocatalysts and cocatalysts. The photocatalysis system will consist of a CdX quantum dots and a bi-iron chalcogenide.

2. Results

The UV-Vis absorption spectra of the Oleic Acid capped CdS (Fig.1) shows a peak at around 450nm, while the stripped QDs peak has moved to around 440nm. For the CdSe (Fig.2) you will notice to peaks at approximately 425nm and 524nm for the Oleic Acid capped QDs, while the stripped QDs shifts to 450nm and 550nm. The shifts imply that the nanoparticles size have changed, confirming that the ligand stripping has occurred.

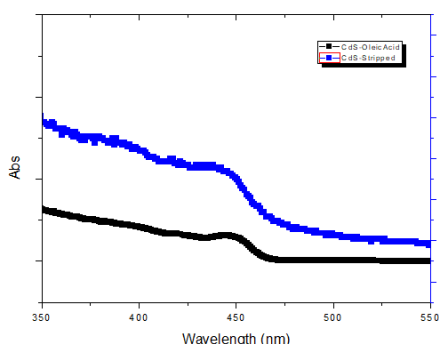


Fig. 42: Solution phase UV-Vis absorption spectra CdS QDs

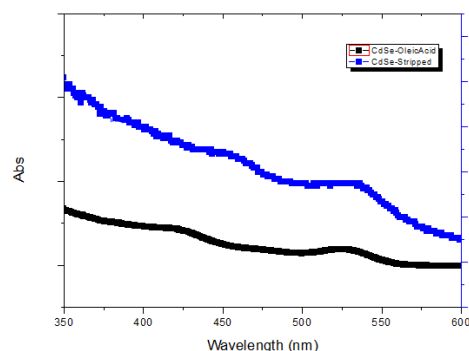


Fig. 2: Solution phase UV-Vis absorption spectra of CdSe QDs

3. References

- [1] Panwar N.L, Kaushik S.C, Surendra Kothari S., *Renewable and Sustainable Energy Reviews*, **15** (2011) 1513–1524.
- [2] Karapinar I. and Kargi F., *Enzyme and Microbial Technology*, **38** (2006) 569–582.
- [3] Züttel A., Remhof A., Borgschulte A., Friedrichs O., *Phil. Trans. R. Soc. A.*, **368** (2010) 3329–3342.

Electronic properties of vacancies in hydrogenated bilayer graphene

Edwin Mapasha¹, Felana Andriambelaza¹, Emmanuel Igumbor², Nithaya Chetty^{1,3}

¹Department of Physics, University of Pretoria, Private bag X 20, Hatfield 0002, Pretoria, South Africa

²School of Interdisciplinary Research and Graduate Studies, University of South Africa,

UNISA 0003, Preller Street, Pretoria, South Africa

³National Institute for Theoretical Physics, Johannesburg 2000, South Africa

Corresponding author e-mail address: edwin.mapasha@up.ac.za

1. Introduction

In search for the new two-dimensional (2D) materials competitive to graphene for future electronics, hydrogenated bilayer graphene (bilayer *graphane*) attracted a lot of research attention owing to its unique structural arrangement and wide band gap[1]. This composite in any case has a potential of being used in a wide range of nanotechnological devices such as optoelectronic, photovoltaic and spintronic. The electronic characters of bilayer *graphane* are similar to those of experimentally synthesised single layer *graphane*,[2] in which the magnitude of the band gap depends on the exchange correlation functional used. There are defects noted in a single layer *graphane* mostly vacancies occurred during synthesis. Defects can improve or deteriorate the performance of a material during the electronic operation. In this work, various vacancies such as the hydrogen V_H , carbon V_C and hydrogen-carbon pair V_{CH} vacancies, as well as the nearest neighbour carbon-carbon pair V_{C-C} divacancy are investigated using the density functional theory approach. These vacancies usually leave dangling bonds on the nearest neighbour atoms that induce states within the band gap which mainly affect the electronic and magnetic characters of the material. We further alter the vacancy induced electronic properties through the charge states modulation.

2. Results

To examine the electronic properties, the density of states plot of V_{CH} vacancy shows the induced spin polarised defect states within the bilayer *graphane* band gap suggesting a transition from semiconducting to metallic. The V_{CH} vacancy is ferromagnetic having the magnetic moment of $1 \mu_B$. We find that the injection of charge states -1 or +1 alters the electronic character and fine tunes the magnetic moment of the vacancies, suitable for application in electronic and optical devices.

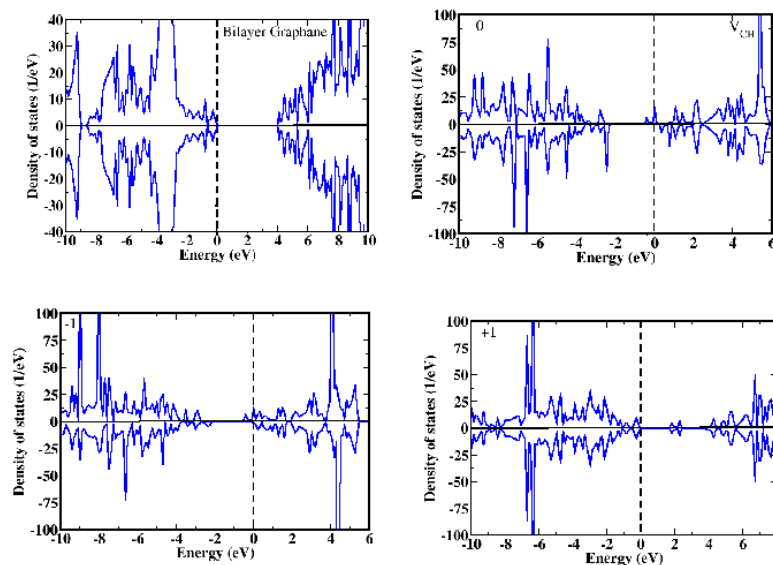


Fig.1: The density of states of bilayer *graphane*, V_{CH} vacancy in bilayer *graphane*, -1 charge V_{CH} vacancy and +1 charge V_{CH} vacancy in bilayer *graphane*. The dashed line represents the Fermi level.

3. References

[1] Elias *et al. Sci.*, **323** (2009) 610 – 613

[2] H. Sahin, O. Leenaerts, S. K. Singh and F. M. Peeters, *WIREs Comput Mol Sci.* **5** (2015).

Transformation of 1D to 0D nickel oxide nanostructures induced by ramping rate during heat treatment: Gas sensing and luminescence properties

Teboho P. Mokoena^{1,2}, Hendrik C. Swart², David E. Motaung^{1,2}

¹ DST/CSIR National Centre for Nanostructured Materials, Council for Scientific Industrial Research, Pretoria, 0001, South Africa

² Department of Physics, University of the Free State, Bloemfontein, ZA9300, South Africa

Corresponding author e-mail address: TMokoena2@csir.co.za

1. Introduction

Over the last couple of decades, as a result of rapid growth in industrialization, vehicle usage, and high energy demands, understanding the gases released to the environment from these sources has become more important. Therefore, designing the nanostructure-based gas sensors which possess a relatively high sensitivity, selectivity, stability, and enhanced response and recovery times is one of the most important branches of nanotechnology [1]. Among them, p-type NiO based gas sensors display morphology and structure-dependent gas sensing properties, which urge the researchers to exhaust other facile routes to synthesize NiO nanostructures with novel morphologies and unique structures. Luminescent properties verified the existence of defects on nanostructures, and NiO with more presence of nickel vacancies and oxygen interstitials and/or vacancies displayed a relatively high gas sensing characteristics. The role of these defects they act as adsorption active sites towards target gases.

Herein, we report on gas sensing characteristics of transformation of 1D to 0D NiO nanostructures induced by ramping rate during heat treatment. Structural analyses revealed that the nanostructures were polycrystalline, displaying average crystallite sizes of 10 ± 4 nm. Brunauer, Emmett and Teller (BET) revealed the surface area in the range of 20.98 to 67.89 m²/g. Scanning electron microscopy images revealed the nanorods and agglomerated nanoparticles, before and after heat treatment, respectively. The photoluminescence studies showed blue broad emission due to nickel vacancies and oxygen interstitials and/or vacancies. The effects of morphology on the luminescence and gas sensing characteristics of NiO based sensors have been investigated towards various gases at various working temperatures and relative humidity.

2. Results

Fig. 1 shows a transformation of morphology from smooth behaviour to nanorods surrounded with nanoparticles. This supported by the BET surface area (see Fig. 2), which increased with transformation of morphology with an increase in ramping time. According to the studies, a higher BET surface area resulted to an improvement in the sensing response.

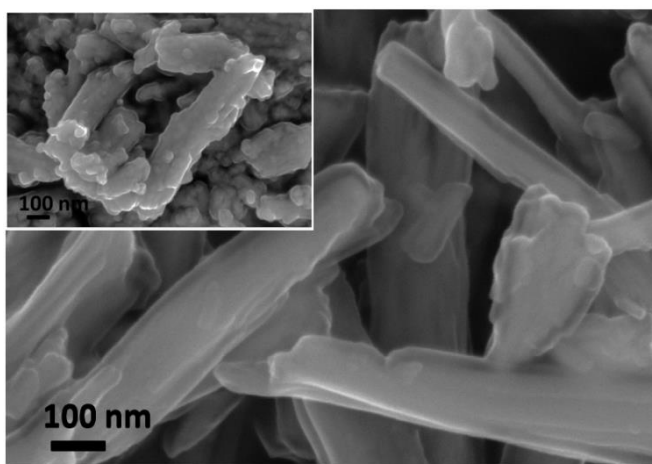


Fig 1: SEM micrographs of NiO as-prepared and the inset shows NiO nanostructure after heat treatment.

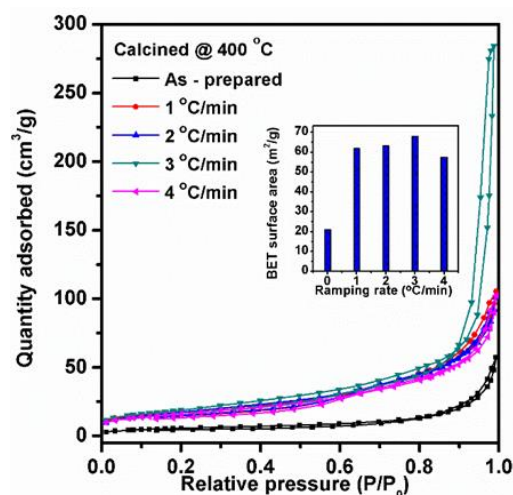


Fig 2: BET isotherms of NiO nanostructures calcined at 400 °C with various ramping rates and the inset shows bar graph of BET surface area against ramping rate.

3. References

- [1]. F. Qu, Y. Wang, J. Liu, S. Wen, Y. Cen, S. Ruan, *Materials Letters*, 132 (2014) 167 -170.
- [2]. J. Cao, H. Zhang, X. Yan, *Materials Letters*, 185 (2016) 40 - 42.
- [3]. Y. Yu, Y. Xia, W. Zeng, R. Liu, *Materials Letters*, 206 (2017) 80 - 83.

Electrical characterization of swift heavy ion irradiated GaN by DLTS

P.N.M. Ngoepe¹, W.E. Meyer¹, F.D. Auret¹, E. Omotoso¹, T.T. Hlatshwayo¹, V.V. Skuratov² and M. Diale¹

¹Department of Physics, University of Pretoria, Private bag X20, Hatfield, 0028

²Joint Institute for Nuclear Research, Joliot-Curie 6, 141980 Dubna, Moscow region, Russia

Corresponding author e-mail address: phuti.ngoepe@up.ac.za

1. Introduction

Gallium nitride (GaN) is a wideband gap semiconductor on which devices can be fabricated for space, military and industrial applications. It is a strong contender for optoelectronic devices as it can operate at high temperature, voltage and frequency [1]. It also operates well in caustic environments due to its high mechanical strength and relative resistance to radiation from particles [2]. The bombardment of particles on a semiconductor device can have a detrimental or beneficial effect on the characteristics of the device. In particular, defects can be induced in the device due to exposure to this radiation. In this study, the electrically active defects related to the exposure of GaN to Kr ion irradiation are investigated. The GaN sample was irradiated with Kr ions at room temperature with energy of 107 MeV to a fluence of 10^{10} cm⁻². Deep level transient spectroscopy (DLTS) measurements were then performed to characterize the defects before and after irradiation.

2. Results

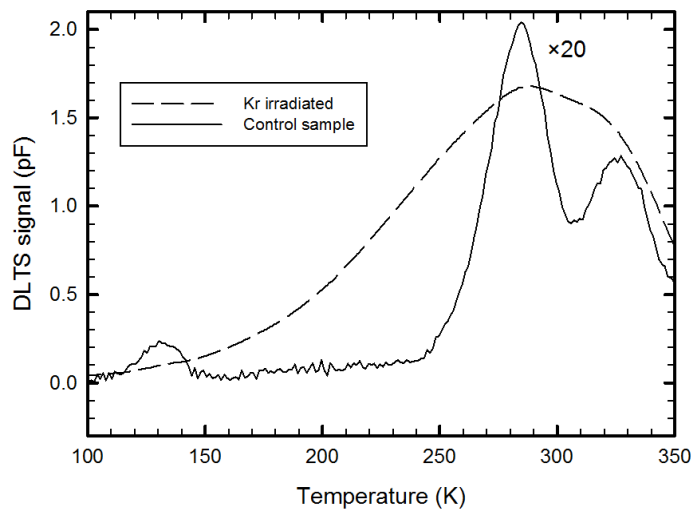


Fig. 1: DLTS spectra of Ni/Au Schottky diodes fabricated on GaN. One sample was irradiated with Kr while the other was used as a control sample.

The DLTS spectra before and after Kr irradiation are compared in Fig.1. The spectra were measured at a rate window of 80 s⁻¹. The DLTS spectrum of the Kr irradiated sample exhibit a broad peak. This broad peak is due to extended defects [3].

3. References

- [1] S.N. Mohammad, A.A. Salvador and H. Morkoç, *Proceedings of the IEEE* **83**, (1995) 1306.
- [2] A. Ionascut-Nedelcescu, C. Carlone, A. Houdayer, H.J. Von Bardeleben, J.L. Cantin, and S. Raymond, *IEEE Trans. Nucl. Sci.* **49** (2002) 2733. doi:10.1109/TNS.2002.805363.
- [3] L. Gelczuk, M. Dabrowska-Szata, G Jozwaik, *Materilas Science-Poland* **23** (2005) 625.

4f^N Energy Level Schemes for the Di-, Tri-, and Tetravalent Lanthanides

Lucas C.V. Rodrigues¹, Mika Lastusaari², Hendrik C. Swart³ Jorma Hölsä^{1,2,4*}

¹ University of São Paulo, Institute of Chemistry, BR-05508-000 São Paulo, SP, Brazil

² University of Turku, Department of Chemistry, and Turku University Centre for Materials and Surfaces, FI-20014 Turku, Finland

³ University of the Free State, Department of Physics, Bloemfontein ZA-9300, South Africa

⁴ Polish Academy of Sciences, Institute of Low Temperature and Structure Research, PL-50-422 Wrocław, Poland

*Corresponding Author E-mail address: jholsa@utu.fi

1. Introduction

Since the refinement of the famous Dieke diagram (DD) [1] to include all higher energy levels, not much progress has been made in this field. It is now clear, though, that the purely theoretical methods have still a long way to go to yield the 4f^N (or 5f^N) energy levels in any accuracy. This is necessary because new applications, *e.g.* up- and down-conversion, require energy levels that are ever more accurate. In fact, these processes are the most efficient when quasi-resonant condition is reached. The proven phenomenological methods to calculate the energy level schemes (and wave functions required by many applications) are still the most reliable, accurate and fastest way. Unfortunately, some of the published data [2] is so inaccurate that it is of little or no use.

2. Results

The energy level schemes (Figs. 1 & 2) for the di-, tri-, and tetravalent lanthanides were calculated taking into account the crystal field effects as well. The effect of the host was synchronised for both the R²⁺ and R³⁺ series by the use of isomorphic crystal structures (BaFCl and ROCl, respectively) facilitating the comparison between them. Utmost care was taken to compare the calculated data with the experimental one which was easy for the R³⁺ but much more scarce for the R²⁺ series. For the R^{IV} series, experimental data is virtually inexistent. The energy level schemes for the R³⁺ are the most useful ones whilst the 4f^N levels of the R²⁺ series are often masked in practice by the low-energy 4f^{N-1}5d¹ configuration. The 4f^N levels of the R^{IV} series are practically inaccessible because of the low-energy charge transfer transitions and the initial low-energy positions of the 4f^N levels of R^{IV} species.

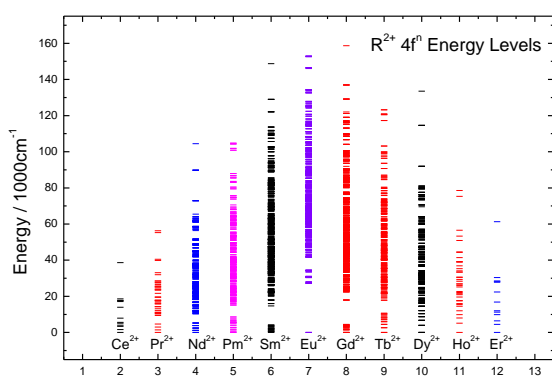


Fig. 43: Calculated 4fⁿ energy levels of the R²⁺ ions.

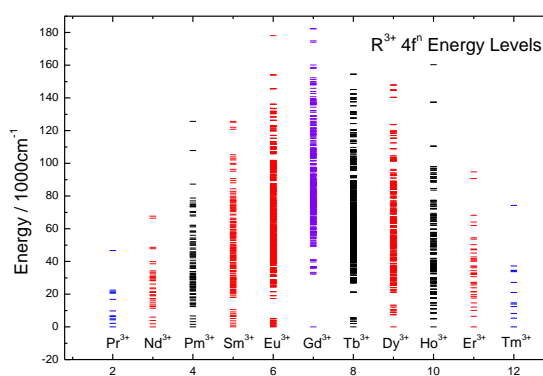
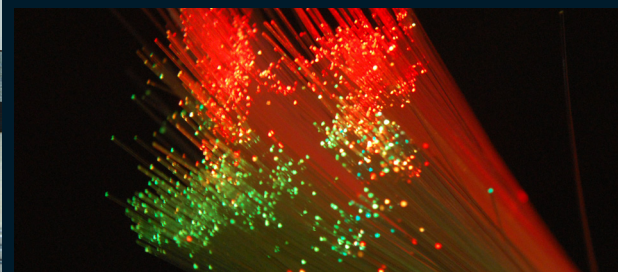
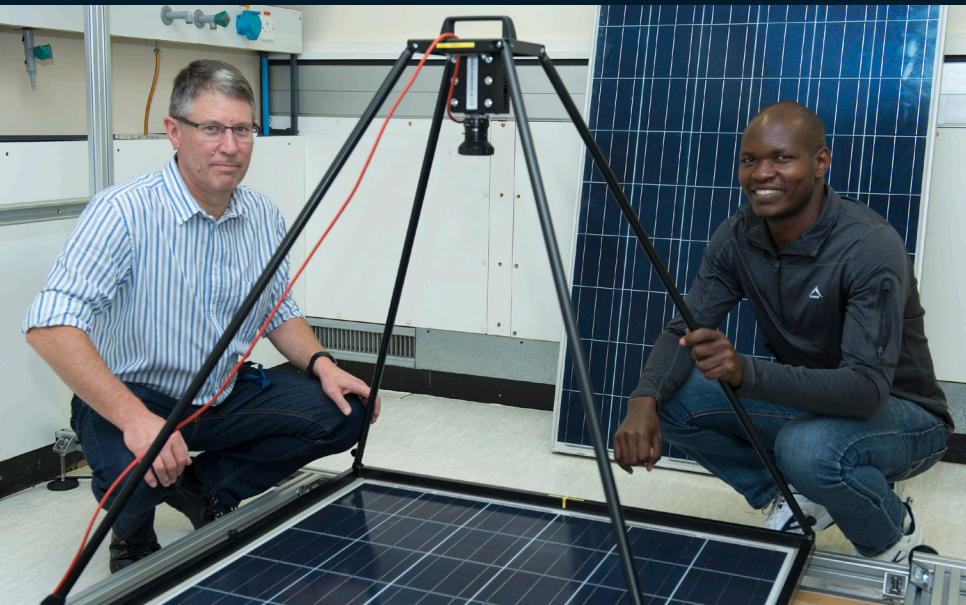


Fig. 2: Calculated 4fⁿ energy levels of the R³⁺ ions.

References

- [1] R.H.T. Wegh, A. Meijerink, R.-J. Lamminmäki, and J. Hölsä. *J. Lumin.* **87-89** (2000) 1002.
- [2] C.-G. Ma, M.G. Brik, D.-X. Liu, B. Feng, Ya Tian, and A. Suchocki, *J. Lumin.* **170** (2016) 369.

NELSON MANDELA UNIVERSITY



Department of Physics

Photovoltaics

Sustainable Energy for the Future

The Photovoltaics Research Group focusses on the characterisation of Photovoltaics (PV) materials, devices and systems. The facilities include:

- » Photovoltaic Research Laboratory (PV Lab) for advance solar cell and PV module characterisation
- » Outdoor Research Facility (ORF) for PV module and system monitoring and characterisation
- » ISO17025 accredited Photovoltaic Test Laboratory (PVTL) – PVinsight (Pty) Ltd

The following Applied Physics skills are also acquired:

- » Advance solar cell and PV module characterisation and evaluation
- » Data acquisition and analysis, including curve fitting and parameter optimisation
- » LabView programming and computer interfacing
- » Data acquisition system design

For further information on student projects please contact the PVRG.

Prof Ernest van Dyk

E ernest.vandyk@mandela.ac.za

Optical Fibre Telecommunication Research

Escalating bandwidth demands fuelled by smartphones, tablet computers, social media and cloud computing makes Telecommunications an extremely challenging and rewarding field.

Nelson Mandela University has one of the best equipped Optical Fibre Research laboratories in Africa.

We offer an exciting range of MSc and PhD projects featuring:

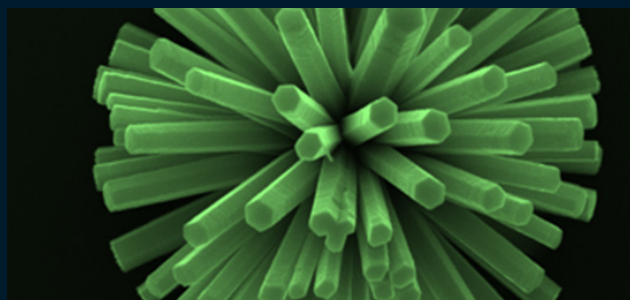
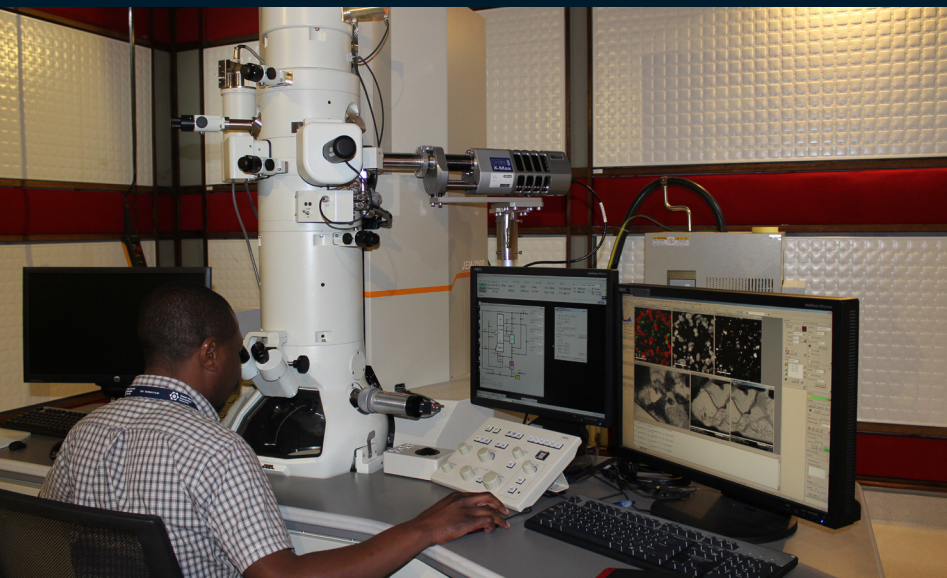
- » Dispersion measurement, compensation and emulation
- » Fibre-to-the-home (FTTH) technologies
- » Square Kilometer Array related optical fibre topics
- » Polarization effects, wavelength division multiplexing, non-linear effects
- » Modelling and simulation, OTDR, fusion splicing, bit error rate testing

The Optical Fibre Research Unit is part of the Telkom-sponsored Centre of Excellence.

Scholarship opportunities are available for good, motivated students.

Prof Tim Gibbon

E tim.gibbon@mandela.ac.za



Department of Physics

Electron Microscopy for Materials Research

The Centre for High Resolution Transmission Electron Microscopy (Centre for HRTEM) at Nelson Mandela University houses four state-of-the-art electron microscopes including the only aberration-corrected atomic resolution electron microscope in Africa. The wide range of research projects and MSc and PhD topics include:

- » HRTEM and in situ HRTEM investigation of nanoparticle catalysts
- » Irradiation damage and fission product transport in nuclear reactor materials
- » Corrosion resistant nuclear reactor materials
- » Refining of weldability limits of creep-aged power plant stainless steel
- » Lifetime assessment of high value power plant components
- » Characterisation of diamond, Pt, Ti and Al alloys, compound semiconductor structures and gold and platinum bearing ores

Prof Jan Neethling

E jan.neethling@mandela.ac.za

Semiconductor Materials Development

This research focuses on vapour phase and solution-based deposition of semiconductors for opto-electronic devices.

The Physics Department has unique equipment for the synthesis and characterization of semiconductor thin films and nano-structures, including a state-of-the-art reactor for compound semiconductor deposition.

We currently develop:

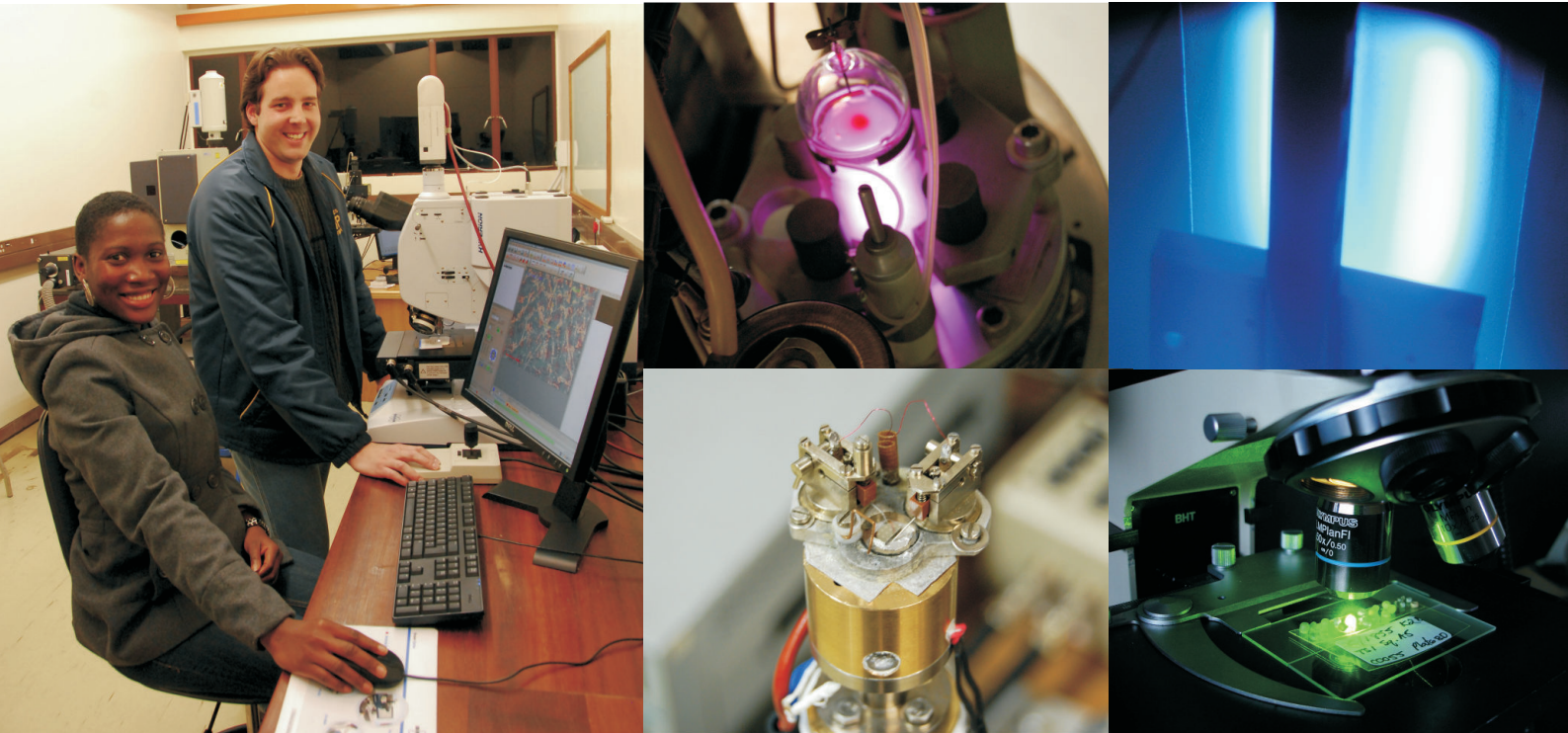
- » Epitaxial InAsSb and related compounds for infrared detectors
- » ZnO nanorods for high efficiency white LEDs and hybrid solar cells
- » Nanostructured TiO₂ for solar water splitting

Our active collaborations with several local and overseas universities over many years, including groups in Sweden, Germany and the UK, have forged excellent academic links.

For information on these exciting research topics contact:

Prof Reinhardt Botha

E reinhardt.botha@mandela.ac.za



We offer postgraduate opportunities in the following research focus areas

Materials

- Nuclear applications
- Under irradiation
- Solar cells
- Opto-electronics
- Carbon-based
- Nano-magnetism

Theoretical Physics

- Mathematical physics
- High energy theory
- Quantum resonances theory
- Quantum information theory
- Computational solid state physics
- Symmetries and group theory

Astronomy

Biophysics

Physics Education

Enquiries about postgraduate studies

Head: Department of Physics
University of Pretoria
Private Bag X20, Hatfield, 0028

Email: Chris.Theron@up.ac.za

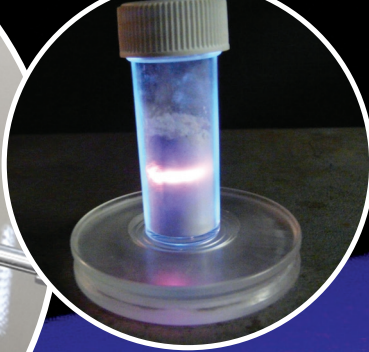
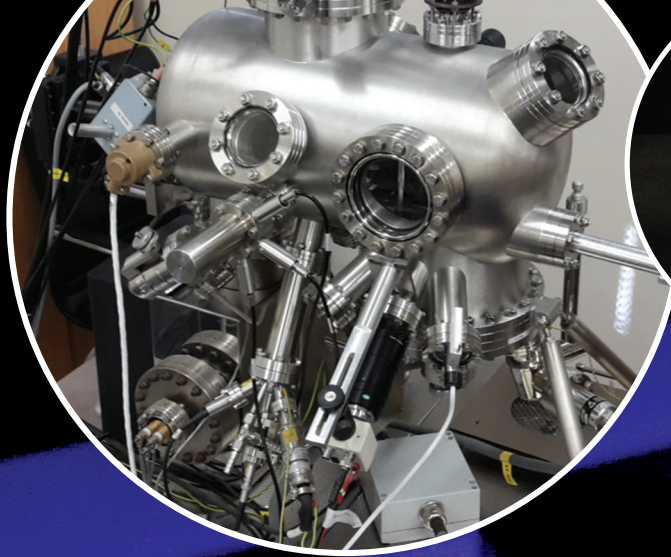
Tel: +27 12 420 2455

Fax: +27 12 362 5288

Web: <http://www.up.ac.za/physics>



UNIVERSITEIT VAN PRETORIA
UNIVERSITY OF PRETORIA
YUNIBESITHI YA PRETORIA
Faculty of Natural and Agricultural Sciences



Don't stop dreaming.

Department of Physics



T: +27(0)51-401 2531 | natagri@ufs.ac.za | www.ufs.ac.za/natagri

 UFSUV |  UFSweb |  UFSweb

*Inspiring excellence.
Transforming lives.*

UNIVERSITY OF THE
FREE STATE
UNIVERSITEIT VAN DIE
VRYSTAAT
YUNIVESITHI YA
FREISTATA



UFS·UV

NATURAL AND
AGRICULTURAL SCIENCES
NATUUR- EN
LANDBOUWETENSAPPE